論文 / 著書情報
Article / Book Information

題目(和文)	アンチモン酸チタン陽イオン交換体における3価金属イオンのイオン交換特性に関する研究
Title(English)	Ion Exchange Properties of Titanium Antimonate Cation Exchanger for Trivalent Metal Ions
著者(和文)	金子宏
Author(English)	Hiroshi Kaneko
出典(和文)	学位:理学博士, 学位授与機関:東京工業大学, 報告番号:甲第2548号, 授与年月日:1993年3月26日, 学位の種別:課程博士, 審査員:
Citation(English)	Degree:Doctor of Science, Conferring organization: Tokyo Institute of Technology, Report number:甲第2548号, Conferred date:1993/3/26, Degree Type:Course doctor, Examiner:
学位種別(和文)	博士論文
Type(English)	Doctoral Thesis

ION EXCHANGE PROPERTIES OF TITANIUM ANTIMONATE CATION EXCHANGER FOR TRIVALENT METAL IONS

Hiroshi KANEKO

1993

Department of Chemistry
Faculty of Science
Tokyo Institute of Technology

Supervisor Professor Yutaka TAMAURA

CONTENTS

Chapter 5. SELECTIVE EXCHANGE OF Am^{3+} and Pu^{4+} ON SYNTHETIC INORGANIC ION EXCHANGERS

CHAPTER 1
GENERAL ASPECTS OF ION EXCHANGE

1. INTRODUCTION

1-1 Ion-exchange and exchangers

Ion-exchange is a stoichiometric process in which reversible exchange of ions takes place between a solid phase and solution without affecting the solid structure. Ion exchangers are usually insoluble solid materials which contain exchangable cations or anions. However liquid ion exchangers immiscible with water are also known.

The exchangable cations or anions on an ion exchanger (insoluble solid materials) can be exchanged stoichiometrically with an equivalent amount of other ions of same charge when the exchanger is in contact with an electrolyte solution. The cation exchange reaction on a cation exchanger can be represent as,

$$n\,\overline{X_m A^{m+}} + mB^{n+} \rightleftarrows m\,\overline{X_n B^{n+}} + nA^{m+}$$

and a typical anion exchange on anion exchanger is,

$$n\,\overline{X_m C^{m-}} + mD^{n-} \rightleftarrows m\,\overline{X_n D^{n-}} + nC^{m-}$$

where bar denotes the solid exchanger phase; A, B represent cations and C, D as anions with their valency number m or n. Certain materials are capable of exchanging both cations and anions. These are called amphoteric ion exchangers.

The charactairstic properties of ion exchangers owe to the peculiarity of their structure. They are composed of a framework (skeleton) formed by chemical bonds or lattice energy. The framework possess positive or negative charges which are compensated by ionsof opposite charge called counter ions. The counter ions responsible for ion-exchange and can be replaced by other ions of the same charge preserving the electroneutrality of the exchanger framework. The counter ion content of an exchanger (i.e. ion-exchange capacity) is constant and corresponding to the magnitude of the framework charge and is independent of the nature of the counter ions. The

electroneutrality condition renders the ion-exchange a stoichiometric process and hence, is independent of the nature of counter ions. The interstices in the framework are known as pores which may make channels or capillaries in the framework depending on their inter-connections.

The concentration ratio of the competing ions in exchanger and in solution are not same in an ion-exchange equilibrium for the reason that a particular exchanger prefers one species over the other. This property of an exchanger is called the ion-exchange selectivity and is dependent on

a) Nature and type of exchanger.

b) The size and valence of the competing ions.

c) Interactions other than the electrostatic influencing the uptake of an ion.

d) Steric hindrance by the large ions or for the larger ions due to pore size of the exchanger.

The ion-Exchange phenomenon have been discussed in more details by Helfferich.[1)]

1-2 Types of exchangers

Ion Exchangers are of different types,

1) Liquid exchangers

2) Solid exchangers

(i) Organic exchangers

a) organic resines or macroreticular exchangers

b) Gels or microreticular exchangers

(ii) Membranes and Papers

(iii) Inorganic exchangers

The discussion on these exchangers are as follows,

1-2-1 Liquid exchangers

The ion-exchange phenomenon between two immiscible liquid phases is performed on liquids with ion-exchange properties. This type of exchanger is prepared usually by dissolving an ionogenic compound (with hydrophobic groups) in organic solvent e.g. chloroform xylene etc. which are immiscible with H_2O. The ionogenic compounds (containing functional or exchangeable groups) are commonly fatty acids[2)] and dialkalyphosphates used for the preparation of cation exchanger[3-5)] whereas long chain

aliphatic amines for making anion exchangers.[6-9] These types of exchangers are used for ion-exchange in aqueous electrolytes and for liquid-liquid extraction of electrolytes from aqueous solution.

1-2-2 Organic exchangers

The framework is formed of organic polymers e.g. cellulose, dextran etc.. Crosslinking bonds (methylene or divinylbenzene bridges, ionic bonds etc.) between the polymer chains form a three dimentional framework. Swelling of the framework occur when in contact with the inorganic solvent and extent of swelling depends on the content of crosslinking bonds. The ionogenic (functional or exchangeable) groups are commonly $-SO_3H$, -COOH, $-PO(OH)_2$, $-NH_2$, $-N^+R_3$ etc. Acidic ionogenic groups in the H^+ form dissociate with the release of the H^+,

$$-SO_3H \rightleftarrows -SO_3^- + H^+$$

$$-COOH \rightleftarrows -COO^- + H^+$$

similarly the basic groups in the OH^- form release OH^-,

$$-NR_3OH \rightleftarrows -N^+R_3 + OH^-$$

$$-NH_2 + HOH \rightleftarrows -N^+H_3 + OH^-$$

More comprehensive discussion has been reported by Marhol.[10]

1-2-3 Resins or macroreticular exchangers

The macroreticular (macroporous) organic resins are composed of styrene-divinylbenzene (DVB) framework of sufficiently large pores which are statistically distributed throughout the whole framework volume. These types of exchangers are commonly obtained by the addition of an appropriate solvent (to dissolve the organic monomer completely) during the polymerization of monomers. This type of resin is a solid aggregate with large macropores and inner surface. These are more resistant to osmotic pressures and accomodate large number of ionogenic groups.

1-2-4 Gels or microreticular exchangers

The gel-like or microporous resins are usually composed of DVB in a gel-like framework. This type of framework is composed of mutually penetrating networks formed by the individual chains. The sieve size is considerably heterogeneous and porosity is very low. From many soluble ionogenic compounds, insoluble ion exchanger gels can be obtained simply by crosslinking with formaldehyde or epichlorohydrine.[11)]

1-2-5 Exchanger membranes and papers

The membranes are solid (or liquid) ion exchanger films or layers with a greater surface area than their thickness. It include any ion-exchange material which can be used as a separation/partition wall between two solutions irrespective of its geometrical forms. The membranes are permeable for counter ions, co-ions and neutral molecules and their electric conductivity. When membranes are in contact with electrolyte solutions, uptake the counter ions which in turn can pass through from one solution to another. The inselectivity of a particular exchanger for co-ions make it difficult to pass through.

The first exchanger membrane was synthesized in 1950.[12)] The membranes can be homogeneous. These may be cylindrical plugs,[7,13)] single beads in a frame or ribbons of ion-exchange material[14,15)] in contact with solutions at an end.

The permselective (permselectivity = characteristic difference in permeability for counter ions and co-ions) inorganic membranes have considerable advantage over those based on organic exchange resins[16)] e.g. in fuel cells employing these for the transport of hydrogen ions. Such membranes are also employed for the selectivity exchange of Na ions in the production of NaOH and NaCl. The widely used zirconium phosphate membranes have been developed by different workers.[17,18)]

The ion-exchange reaction or paper chromatography can be performed on the papers impregnated with the dissolved poly electrolytes or liquid ion exchangers.[1)]

1-2-6 Inorganic exchangers

The framework of the exchanger is of inorganic origin e.g. complex cyanide of some elements and compounds of phosphate type,[19)] arsenate, tungstate and molybdate of quadrivalent elements (Zr, Ti, Sn etc.), insoluble heteropoly acids and their salts[19)] and aluminosilicates etc. The inorganic groups attached to the framework are also of inorganic nature and the exchanging ions or counter ions are commonly H^+, NH_4^+ alkali or

alkaline earth metal ions. Inorganic exchangers possess rigid structure and undergo less or no swelling in constract to the organic exchangers. These can withstand higher temperatures and ionizing radiation.

The inorganic ion exchangers as a main subject of this dissertation is discussed in more details under section 3 of this chapter.

2. HISTORICAL

Ion-exchange and exchangers have an interesting historical background. In 1850 H. S. Thomson and J. T. Way two English chemists discovered the cation exchange phenomenon in soils. The materials responsible for such an exchange phenomenon were identified[21,22] as clays, glauconites, zeolites and humic acids. It was found that when soils were treated with solution of NH_4^+, it is taken up by the soil and an equivalent quantity of Ca^{2+} released. This property was observed to be reversible and was held for number of other cations besided NH_4^+.

Even though the first synthetic industrial ion exchanger was prepared in 1903 by Harm and Rumpler,[23] the pioneer study of ion-exchange phenomenon was carried out on synthetic inorganic ion exchanger by Guns.[24] The first inorganic exchanger prepared by Gans were sodium alumino-silicates[13] containing exchangeable sodium ions. The sodium ions of the exchanger could reversibly be exchanged with calcium and magnesium ions in hard water. The exhausted exchanger could also be regenerated with sodium chloride solution. These were mainly used for water softening and in sugar industry. Other types of exchangers known atn that time were the permutites. Two types of permutites were known i.e. fusion permutites and gel permutites. The former was prepared by fusion of soda, potash, feldspar and kaolin mixture, while the latter by adding alkali solution to an acidic solution of aluminum sulfate and sodium sulfate mixture. The crystalline zeolites were also prepared by the hydrothermal crystallization from alkalie solutions of silica and alumina at elevated temperature.

The relationship between ion-exchange and crystal structure was first understood by work of Pauling[25,26] and Bragg[27] on crystalline structure of mica and clay. During the period 1925-45, the field of development of ion-exchange materials showed decline compare to the synthetic organic resins. Adams and Holmes discovered synthetic ion-exchange resins in 1935.[28] They prepared sulfonic acid resins with high cation-exchange capacity and polyamine type resin having anion-exchange properties.

Even though the organic resins were considered to have better applications due to fast exchange rate, exchange capacity and physical and chemical stability in contact with the aqueous electolyte solutions at certain temperature range (more efficient at room temperature), could not withstand higher temperatures and ionizing radiation. Whereas the research and development of ion exchangers has been increased with the need for

separation of ionic components in wastes at high temperatures. The organic resins proved to be inefficient due to their degradation at high temperature and change in selectivity and capacity on exposure to radiations.

3. INORGANIC EXCHANGERS

Inorganic ion exchangers have attracted the attention of researchers owing to their remarkably high selectivity for certain ions or groups of ions as well as their profound thermal and radiation stability. The specific characteristics of inorganic ion exchangers arise partly from their rigid structure which undergo little swelling or shrinking in the aqueous phase. This brings about a strong steric effect or an ion sieve effect for various ions depending on the effective or hydrated ionic radii of the adsorbing ions. Inorganic exchangers (natural or synthetic) can be classified as shown in Table 1-1. The adsorption properties of these materials have been studied extensively with regard to their adsorption mechanism as well as their different applications. Several reviews on inorganic exchangers have been published in the last decades.[16,29-32] Various types of inorganic exchangers have been synthesized and their ion-exchange properties have been studied since the pioneering work by Kraus.[33,34] However the contributions of Amphlett,[16] Abe,[35] Clearfield,[36] Rees,[37,38] Fuller,[29] Veselý and Pekárek[30,39] and De and Sen[40] are worth mentioned. The details of type and nature of different exchangers of the main groups indicated in Table 1-1 are discussed hereafter.

3-1 Clays and clay minerals

Clays are the complex aluminosilicates. Some of the groups of clay minerals are listed in Table 1-2. The aluminosilicate clay is composed of alternating two dimentional layers formed from aluminate octahedra and silicate tetrahedra.[41] The formula of Kaolinite, a simplest type of clay can be represented as $Si_4Al_4O_{10}(OH)_8$. The basic unit is a double layer consisting of a silicate and an aluminate layer. The units (of layers) are pilled up along the c-axis of the crystal perpendicular to the layer planes. At the edges and corners of which are free hydroxl groups capable of ion-exchange. More complex type of clay mineralsare composed of repeated units of one aluminate layer sandwiched between two silicate layers, the basic formula of the type being $Si_4Al_4O_{20}(OH)_4 \cdot nH_2O$.

The ion-exchange in clay minerals is non-stoichiometric and amphoteric, exchanging both OH^- and H^+ (as are weak acids). The exchange capacity depends on the nature and composition of a particular clay. For cations the decreasing order of capacity is montmorillonite > Illite > Kaolinite. The selectivity sequence for alkali metal ions Li < Na < K < Rb < Cs was observed to increase with the decrease in hydrated ionic radii

Table 1-1 Classification of Inorganic Ion-exchange Materials.

i) Clays and clay minerals

Kaolinite, Montmorillonite, etc.

ii) Natural and synthetic zeolites

Sodalite [$Na_6Al_6Si_6O_{24} \cdot 2NaCl$],

Type-A [$(Na_{12}Al_{12}Si1_2O_{48} \cdot 27H_2O)_8$],

Faujasite [$(Na_2CaMg)_{29}Al_{58}Si_{134}O_{384} \cdot 240H_2O$], etc.

iii) Oxides and hydrous oxides of multivalent metals

Al_2O_3, $ZrO_2 \cdot nH_2O$, $TiO_2 \cdot nH_2O$, $Sb_2O_5 \cdot nH_2O$,

$MoO_3 \cdot nH_2O$, $WO_3 \cdot nH_2O$, etc.

iv) Acid salts of multivalent metals

$Zr(HPO_4)_2 \cdot nH_2O$, $Ti(HPO_4)_2 \cdot nH_2O$, Tin antimonate,

Titanium antimonate, Stannic tungstate, etc.

v) Salts of Herteropolyacids

$(NH_4)_3PMo_{12}O_{40} \cdot 2H_2O$, ammonium molybdoarsenate,

ammonium tungstophosphate, etc.

vi) Insoluble hexacyanoferrate

$KCu[Fe(CN)_6]$, $Sn[Fe(CN)_6] \cdot nH_2O$, etc.

vii) Other Exchangers

Tobermorites [$Ca_5Si_6O_{18} \cdot 4H_2O$], Hydroxyapatite,

Hydrotalcite, Metal sulfide, etc.

Table 1-2 Main Groups of some Clay Minerals.[16]

GROUPS	MINERALS
1) Kaolinites	Kaolinite
2) Illites	Illite
	Muscovite
3) Fibrous clays	Attapulgite
4) Montmorillonites	Montmorillonite
	Saponite
	Nontronite
5) Mica derivatives	Vermiculite
	Biotite

of the ions on some clays.[16)]

3-2 Natural and synthetic zeolites

Zeolites are a well defined class of highly cross-linked crystalline porous aluminosilicates. Their three dimentional framework is made of $[SiO_4]^{4-}$ and $[AlO_4]^{5-}$ polyhedra. The basic unit of polymeric macromolecules are $Si(O/2)_4$ and $Al(O/2)_4$ tetrahedra, where O/2 stands for the bridging oxygen atoms. Their geometric arrangement is such that to avoid Al-O-Al bonds as much as possible.[42)] Their frameworks are generally very open and contain channels and cavities in which cations and water molecules are located. The negative charge on each tetrahedron is compensated by a monovalent or multivalent cations present in the interstices of the aluminosilicate framework. These cations are usually mobile and exhibits the ion-exchange properties of zeolites. The rest of the space in interstices is occupied by H_2O or solvent molecules.[16)] The general formula of zeolite is presented by,

$$M_xD_y[Al_{x+2y}Si_{n-(x+2y)}O_{2n}]mH_2O$$

where M stands for a monovalent cation e.g. H^+, Na^+, K^+ and D for divalent cation e.g. Ba^{2+}, Ca^{2+}, Mg^{2+}, etc., M_xD_y represent exchangeable cations located at so called exchange sites. $Al_{x+2y}Si_{n-(x+2y)}O_{2n}$ corresponds to zeolitic framework which include well defined pores, channels and cages, whereas mH_2O are the zeolitic water molecules. These zeolitic water molecules are easily removed, sometimes reversibly.

The word "Zeolite" has Greek origin which means Boiling Stones, an allusion to the visible loss of water noted when the natural zeolites were heated.[43)] When the water molecules are removed, the voids created can take other molecules. The zeolites are usually synthesized hydrothermally from alkaline solution. The type and concentration of the alkali are important structure directing matters. At present, 39 naturally occuring zeolites have been recorded and their structures are determined.[44)] In addition, over 150 zeolites have been synthesized hydrothermally.[45)] Some of these resemble naturally occuring zeolites whereas others have no natural analog.

The zeolitic framework show profound ion-sieve character for the uptake of metal ions and are named as molecular sieves giving rise to very selective adsorption.[46)] The synthetic zeolites due to their molecular- and ion-sieve properties, gas adsorption and catalytic capabilities, have attracted the attention of scientists in recent developments of inorganic ion-exchange materials. The ion-exchange and ion-sieve characteristics of both

natural and synthetic zeolites have been reported by Barrer and Sherry.[47-51)]

3-3 Metal oxides and hydrous oxides

The most commonly used metals for the preparation of respective oxides or hydrous oxides (extensively studied for their ion-exchange behavior) are listed below,

Divalent	Mg, Be etc.
Trivalent	Al, Fe etc.
Quadrivalent	Si, Ti, Mn, Zr, Sn, Hf etc.
Pentavalent	Sb, Nb, Ta, V etc.
Hexavalent	Mo, W, Te etc.

The hydrous oxides of multivalent metals are generally synthesized by adding excess alkali to solution of their salts at room or moderately higher temperature or at higher temperature under reflux or by simple hydrolysis of their salts in large quantity of water or acid solutions at high temperature. They are either amorphous or crystalline materials with high surface area. Their ion-exchange behavior is strongly dependent on their physicochemical properties i.e. crystal structure and pore size. In addition to the conventional oxides, new types of hydrous oxides with layer or tunnel structures,[52,53)] or with an ion memory effect[54,55)] have recently been developed. These oxides show superiority over the conventional oxides due to their peculiar ion-selectivities.

The hydrous oxides of multivalent metals behave as either cation exchangers or anion exchangers depending on the basicity of central metal atom and the strength of the metal-oxygen bond relative to that of the hydrogen-oxygen bond in the hydroxyl group.[16)] The strength of an acid increase with the electronegativity of the central metal atom and with the number of oxygen atoms per replaceable hydrogen.[56)]

Abe[57)] has classified various oxides and hydrous oxides of different metals in view of the polarizing power of the metals as, cation, amphoteric and anion exchangers. The presence of additional oxygen attached to M (central metal atom) increases the acid strength of the exchanger. The series $MO < M_2O_3 < MO_2 < M_2O_5 < MO_3$ represents the probable order of increasing acidity and cation exchange character for insoluble hydrous oxides.[57,58)] The higher oxides e.g. Sb(V) and Mo(VI) exhibit no anion exchange properties whereas Mg(II) and La(III) are practically anion exchangers even at high pH.[59)] The acidities of the hydrous oxides of quadrivalent metals depend on the electronegativity of M and decrease in the order $MnO_2 > SiO_2 > SnO_2 > TiO_2 > ZrO_2 > CeO_2 >$

ThO_2.[58]

If the central metal atom M of an oxide has a small radius and is highly electronegative element, will exhibit acidic properties. The increase in the size of M or decrease in its electronegativity results in amphoteric character followed by basic behavior.

The ion-exchange behavior of hydrous oxides such as alumina and silica are known since long time. Most of these behave as amphoteric exchangers and their exchange reaction can be described as fol

lows,

a cation exchange reaction in basic medium,

$$\overline{ROH} \rightleftarrows \overline{RO^-} + H^+$$

an anion exchange in acidic medium,

$$\overline{ROH} \rightleftarrows \overline{R^+} + OH^-$$

or

$$\overline{ROH} + H^+ \rightleftarrows \overline{R\text{-}OH_2^+}$$

Abe and Ito[58] have reported the uptake of K^+ and Cl^- on various hydrous oxides as a function of pH. The pH value at which both cations and anions are exchanged, is known as equiadsorption point (EAP) and varies with the type and composition of a particular exchanger. The EAP and relative ion-exchange behavior of an exchanger depend on the acidities of the oxides. Different values of EAP ranging from 4~11 are available in the literature.[60] This large difference may result from preparation methods and impurities present in the exchanger. The details of some of the oxides and hydrous oxides of multivalent metals are given below.

3-3-1 Oxides of divalent metals

The amorphous hydrous beryllium oxide $BeO \cdot 1.7H_2O$ and magnesium hydroxide (prepared by the reaction of aqueous ammonia and beryllium or magnesium chloride) behave as amphoteric and anion exchangers respectively.[59] The adsorption of Zn^{2+} on $Mg(OH)_2$ has also been reported in an adsorption co-precipitation experimental

observations.[61] However that can be more a co-precipitation than an ion-exchange reaction.

3-3-2 Oxides of trivalent metals

The hydrous oxides of Fe^{3+} and Al^{3+} as ion-exchangers have been extensively studied. Hydrous oxides of Fe^{3+} exist as amorphous, α-FeOOH (goethite), β-FeOOH and γ-FeOOH (lepidocrocite). The amorphous materials behave as amphoteric ion exchangers whereas γ-FeOOH shows only anion exchange properties.[59] The adsorption of VO_3^-, WO_4^{2-}, $Cr_2O_7^{2-}$ and MnO_4^{2-} anions have been studied on ferric oxides.[62] The Aluminum oxide hydroxide (AlOOH) is known to exist in diaspore and boehmite {$(Al_2O_3 \cdot H_2O)$ anion exchanger}. Other common modifications are gibbsite, bayerite {$(Al_2O_3 \cdot 3H_2O)$ amphoteric exchanger} and norstrandite. Amorphous aluminum oxide is observed to be very selective for Cs ion.[63]

3-3-3 Oxides of quadrivalent metals

Generally the hydrous oxides of quadrivalent metals are obtained by the addition of excess alkali to solutions of their salts. Amorphous as well as crystalline materials could be obtained by the use of same procedure. A few examples of these oxides are discussed below,

(a) Hydrous Silicates: Silica gel has been used as ion exchanger for many years. It behaves as cation exchanger.[58] However the isoelectric point has also been determined at pH below 3.[60]

(b) Manganese Dioxide: The characteristic feature of hydrous manganese(IV) oxide compared to other hydrous metal oxides is their precipitation in many polymorphic forms (α, β, γ, ε or λ -MnO_2, etc.) depending on the preparation methods. A recent study of these oxides showed that the [MnO_6] octahedra share edges and vertices to form the framework of different complexities which can accommodate a variety of cations and/or ligands.[64] Their structure can be either chain and tunnel or layer and sheet like.[64] The chain structure is characterized by the size of tunnels in the [MnO_6] octahedral chains. The tunnel sizes in pyrolusite (β-MnO_2), ramsdellite, hollandite (α-MnO_2) and cryptomelane are reported to be, 1 × 1, 1 × 2, 2 × 2 and 2 × 3, respectively. The layer

structure contain infinite two dimentional sheets of edge shared octahedra with a usual separation of 0.7 nm (chalcophanite, birnessite, etc.) or 1.0 nm (lithiophorite or buserite, etc.).

Recently ion-sieve or so called ion-memory type manganese oxides are also reported with their peculiar adsorption behavior.[65-68] The selectivity order of different metal ions on various types of hydrous manganese oxides is reviewed by Ooi.[69] Cryptomelane (α-type) MnO_2 has been reported[70] with high selectivities for metal ions having crystal radii of about 1.4. Recently λ-MnO_2 with spinal structure was prepared by topotactic extraction of Li^+ from Li_2MnO_4 with an acid by Hunter.[71] The product was observed to be selective for Li^+.[72]

(c) Stannic Oxide: α-type hydrous stannic oxide could be prepared by acidification of sodium stannate solution and β-type by dissolving tin metal in HNO_3.[58,73] The difference in two types is the distinct particle size. Both exchangers are amphoteric in nature. However the selectivity series,[74] $Mn^{2+} < Ni^{2+} < Fe^{2+} < Co^{2+} < Zn^{2+} < Cu^{2+}$ was closely related with the order of the equilibrium constants of the hydrolytic reaction,

$$M^{2+} + H_2O \rightleftarrows MOH^+ + H^+ \quad \text{(where M = metal)}$$

The exchangers were also selective for Al^{3+} and Cr^{3+} with a selectivity sequence $Cr^{3+} > Al^{3+}$.

(d) Titanium Oxide: Four different types of hydrous titanium oxides such as amorphous, anatase, rutile and brookite have been reported so far. Amorphous titanium dioxide hydrate could be obtained by the addition of NaOH solution to titanyl oxalate or $TiCl_4$ solution.[58,75,76] The acidity order from pH titration curves was found to be rutile < anatase < amorphous.[58] These exchangers showed low capacities for cations at high pH. Recently amorphous and layered structure titanium oxides with high exchange capacity have been obtained.[77-80] Am-HTDO was observed to be useful for the radiochemical separation of ^{77}Br from As(V) compounds used as target material bombarded by an α-particle.[81]

(e) Zirconium oxide: The gelatinous white precipitate (hydrous zirconia) is formed by

adding an excess of alkali to a solution of Zr(IV) salt. When freshly prepared precipitate of zirconium oxide was boiled with alkali, the exchange of anion from the solid phase with hydroxyl group of aqueous phase took place leading to formation of crystalline zirconium oxide.[82] Transformation from cubic to monoclinic phase was obtained from mild to extensive boiling. These oxides behave as amphoteric exchangers.

3-3-4 Oxides of pentavalent metals

Different types of hydrous oxides of pentavalent metals are discussed below,

(a) Niobium Oxide: Amorphous material could be obtained by the hydrolysis of niobium pentachloride solution with water.[58,83] The material showed only cation exchange properties with K^+ uptake of 3.3 meq g^{-1} at pH 12.5. Recently crystalline niobic acid $HNbO_3$ with pervoskite structure has been prepared by topotactic extraction of Li^+ from $LiNbO_3$.[84]

(b) Tantalum Oxide: Hydrolysis of tantalum pentachloride solution with an excess of water or by addition of ammonia gives amorphous product. The exchanger is most stable as compared to niobium oxide towards most chemical reagents.[58] It proved to be cation exchanger with K^+ uptake of 2 meq g^{-1} at pH 12. Recently crystalline tantalum oxide $HTaO_3$ with perovskite structure has been prepared in a similar manner to that adopted for $HNbO_3$.[84]

(c) Antimony Oxide: Three types of antimony oxide (antimonic acid), amorphous (A-SbA), glassy (G-SbA) and crystalline (C-SbA) materials have been reported so far.[85] Amorphous antimonic acid is prepared by the hydrolysis of antimony pentachloride solution with excess water and aging at low temperature. Glassy type is obtained when freshly prepared antimonic acid is dispersed in hot water and then evaporated. Whereas crystalline material is obtained by the prolonged aging of amorphous antimonic acid in acid solution. Crystalline material has been reported to be cubic (a = 1.034 nm) with zeolitic water.[36] The selectivity sequence of micro amount of alkali metal ions was Li < Na < K < Rb < Cs on A-SbA and G-SbA whereas Li << K < Cs < Rb < Na on C-SbA.[86,87] The C-SbA was found to be very selective for the ions having crystal radii of about 0.1nm.

3-3-5 Oxides of hexavalent metals

The hydrous molybdenum (VI) oxides, e.g. $MoO_3 \cdot H_2O$ and $MoO_3 \cdot 2H_2O$ are obtained by the slow acidification of a molybdenum(VI) solution at optimum temperatures. The NMR spectra of these compounds indicated that all of the hydrogen present are water-molecule-type.[88]

Two types of hydrous tungsten(VI) oxides, $WO_3 \cdot 2H_2O$ (white tungstic acid) and $WO_3 \cdot H_2O$ (yellow tungstic acid) are known.[89] The white tungstic acid is obtained by the acidification of ammonium tungstate solution with HCl at lower than room temperature (0-10°C). Both $MoO_3 \cdot 2H_2O$ and $WO_3 \cdot 2H_2O$ have dibasic acid properties,[58] however soluble at pH > 4 and > 7, respectively.

3-4 Acid salts of multivalent metals

Various types of acid salts such as phosphates, arsenates, molybdates or tungstates of multivalent metals e.g. Zr, Ti, Ce, Th, Sn etc. are well known. A few examples of these materials are described below.

3-4-1 Zirconium phosphate, arsenate and antimonates:

The earlier studies on zirconium phosphates were carried out mostly on amorphous materials.[90] These materials are prepared from a suitable salt of Zr(IV) and phosphoric acid. Recently the interest has been focused on the crystalline forms.[30,91-94] Refluxing the amorphous materials with > 2.5 mol dm^{-3} phosphoric acid give rise to semicrystalline or crystalline phase. These material have been extensively studied for their ion-exchange properties with special interest to alkali metal ions.[36]

Amorphous zirconium arsenate was prepared with arsenic acid (H_3AsO_4) and then converted to the crystalline material by prolonged refluxing.[95,96]

Zirconium antimonate was prepared as an amorphous material from $ZrOCl_2$ solution and excess Sb_2O_5 dissolved in HCl or aqueous solution of $K[Sb(OH)_6]$.[97]

3-4-2 Titanium phosphate, arsenate and antimonates:

The preparation methods for amorphous or crystalline phosphates of titanium have been reported by Clearfield.[36] Crystalline titanium phosphate has been used for separation of radioactive Cs from strongly acidic nuclear fuel-processing solutions.[98]

Amorphous titanium arsenate could be obtained from sodium arsenate and $TiCl_4$

solutions,[99] Whereas crystalline form was obtained[100] by refluxing (for 45 h) the solution of freshly prepared amorphous material in 8 mol dm^{-3}.

The titanium antimonate could be prepared by mixing $TiCl_4$ and $SbCl_5$ and subsequent hydrolysis with water or neutralization with ammonia.[101,102] This material proved to be unselective for Li^+ as compared to other alkali metal ions. The Li^+ selective, semicrystalline titanium antimonate (with almost rutile structure) could be prepared by the hydrolysis of Ti and Sb chlorides.[103] The selectivity sequence was observed to be Na < K < Rb < Li < Cs in acid medium.

3-4-3 Stannic phosphate, arsenate and antimonate:

These materials have been prepared from solutions of $SnCl_4$ and NaH_2PO_4.[104,105] Crystalline $Sn(HPO_4)_2 \cdot H_2O$ was obtained by refluxing mixture of $SnCl_4$, HNO_3 and H_3PO_4.[106]

Details of preparation procedure for both amorphous and crystalline stannic arsenate are well reported in the literature.[107-109] The pioneer study on the preparation and ion-exchange properties of tin antimonate was reported by Abe and Ito.[110-112] The exchanger was semi-crystalline/amorphous material with extremely high selectivity for micro amount of Li^+. The selectivity sequence for alkali metal ions was in the order Na < K < Rb < Cs << Li.

3-4-4 Thorium arsenate:

This type of exchanger was synthesized[113] by refluxing thorium nitrate solution in arsenic acid at 110°C. The crystalline material $Th(HAsO_4)_2 \cdot H_2O$ was selective for Li^+ only with no adsorption of other alkali metal ions which proved to be a better ionic-sieve inorganic ion exchanger.

3-5 Heteropoly acid salts

The general formula of heteropoly acid salt can be represented as $H_{3\text{-}5}XY_{12}O_{40} \cdot nH_2O$ where X may be phosphorous, arsenic silicon etc., and Y as molybdenum or tungsten etc.. The first systematic study of ion-exchange was carried out on ammonium phosphomolybdate.[39] Several reviews on the molybdo- and tungsto-heteropoly complexes are available in the literature.[114-115] The synthetic chemistry of heteropoly complexes had been extensively studied and methods for the preparation of a wide variety of these

compounds are reported.[116-119] Generaly these insoluble acid salts are prepared by mixing water soluble ammonium molybdate or tungstate, ammonium nitrate and nitric acid. Keggin and many other workers had determined the essential features of the crystal structure of these acids.[118,120-123]

The ion-exchange, thermodynamics and kinetics of ion-exchange reactions on ammonium 12-molybdophosphate has been reported by Smit et al.[124] These acid salts are well known for their selective adsorption of Cs^+.

3-6 Insoluble Hexacyanoferrate

Quite a large number of insoluble ferrocyanides have been prepared by mixing metal (Zn, Cd, Cu, Ni, Co, Pb, etc.) salt solutions with $H_4Fe(CN)_6$ or $Na_4Fe(CN)_6$ solution.[39] These exchangers were found to be selective for Cs ion.

4. INCENTIVE FOR THE PRESENT WORK

The synthetic inorganic ion-exchangers have attached the interest of chemists in the field of inorganic, analytical, environmental and radiochemistry, especially separation science and technology for the last two dxecades. These exchangers are quite stable towards high temperature and ionizing radiation, therefore, possess a significant superiority over the natual inorganic or commercially available organic exchangers. Owing to high stability and ion-exchange capacity, these exchangers are suitable for use in nuclear industry, hydrometallurgy, water softening, preparation of analytical grade (extra pure) reagents and recovery of valuable materials from industrial wastes and sea water, etc. These exchangers can fulfill the recent demands of world research community for the disposal and treatment of nuclear wastes. The work done in the field of inorganic ion-exchangers has been reviewed by a number of authors.[16,37,38,40,125,126)]

Most investigations with insoluble acid salts of quadrivalent metals have been carried out on zirconium and titanium phosphates of various types.[1)] It is known that the acid salts of multivalent metals as ion-exchange matelials classified according to the valency of multivalent metals. Quadrivalent metal antimonate ion exchangers were studied first by Abe and Ito.[111)] The titanium antimonate showed a high selsctivity for lithium ion was prepared by Abe et al.[103)], and was achieved removal of lithium ion from sea water and hydrothermal water successfully.

The TiSbA behaves cation exchanger with relatively high capacity, and has been several investigators.[101,102,103)] However, the systematic study on the ion exchange property of trivalent metal ions on TiSbA has not been reported. TiSbA are prepared at differrent Sb/Ti ratios, and the unusual selectivity were observed on rutile-type TiSbA. TiSbA show different ion exchange property according to different Sb/Ti ratios. But their structual study has not been reported on TiSbA with different Sb/Ti ratios.

This study, therefore, describes the systematic ion-exchange property of trivalent metal ions on TiSbA and their structure. In order to study the structure of TiSbA several methods were used, e.g. X-ray diffraction, thermogravimetric-differencial thermo analysis (TG-DTA), infrared spectra (IR), nuclear magnetic resonance (NMR) and extended X-ray absorption fine structure (EXAFS). In addition a developement of TiSbA on nuclear waste solution is described.

5. REFERENCES

1. F. Helfferich, Ion Exchange, McGraw Hill, N. Y., 1962.
2. L. M. Gindin, P. I. Bobikov, E. F. Kouba and A. V. Bugaeva, Zhur Neorg. Khim., *5,* 1868 (1960).
3. C. A. Blake, C. F. Baes Jr., K. B. Brown, C. F. Coleman and J. C. White, "Proc. 2nd Intern. Conff. Peaceful Uses of Atomic Energy., Geneva", *28,* 289 (1958).
4. H. Irving and D. N. Edgington, Proc. Chem. Soc., 360 (1959).
5. C. J. Lewis, Ind. Wastes, *2,* 137 (1957).
6. J. A. Brothers, R. G. Hart and W. G. Mathers,J. Inorg. Nucl. Chem., *7,* 85 (1958).
7. J. Y. Ellenburg, G. W. Leddicotte and F. L. Moore, Anal.Chem., *26,* 1045 (1954); H. A. Mahlman, G. W. Leddicotte and F. L. Moore, 1939, ibid.
8. F. L. Moore, Anal. Chem., *29,* 1660 (1957); *30,* 908 (1958).
9. U. Schindewolf, Z. Elektrochem., *62,* 335 (1958).
10. M.Marhol, Ion Exchangers in Analytical Chemistry Their Property and Use in Inorganic Chemistry, Wilsonand Wilson's Comprehensive Anal. Chem., G. Svehla (ed.), Vol. XIV, Elsevier Sci. Pub. Co., N. Y., 1982.
11. H. Deuel, Helv. Chim. Acta, *30,* 1269 (1947); H. Deuel, K. Huutschneker and J. Solms, Z. Elektrochem., *57,* 172 (1953); H. Deuel and H. Neukom, Advn. Chem. Ser., *11,* 51, (1954).
12. C. B. Amphlett, "Proc. 2nd Intern. Conf. Peaceful uses ofatomic energy, Geneva", *28,* 63 (1958).
13. R. Gans, Ger. Patent 174097, 1906.
14. G. Scatchard in Ion Transport Across Membranes, H. T. Clarke (ed.), p.128, Academic Press, Inc., New York, 1954.
15. G. Scatchard, J. S. Coleman and A. L. Shen, J. Am. Chem. Soc., *79,* 12 (1957).
16. C. B. Amphlett, Inorganic Ion Exchangers, Elsevier Pub. Co., 1964.
17. A. Dravnieks and J. Bregman, Chem. Eng. News, *39,* 40 (1961).
18. R. P. Hamlen, J. Electrochem. Soc., *109,* 746 (1962).
19. Y. Inoue, J. Inorg. Nucl. Chem., *26,* 2241 (1964).
20. N. Nonaka, K. Sato, H. Higuchi and H. Hamaguchi, Radioisotopes, *25,* 599 (1975).
21. J. Lemberg, Z. Deut. Geol. Ges., *22,* 355 (1870); *28,* 519 (1876).
22. G. Wiegner, J. Landwirtsch., *60,* 111, 197 (1912).

23. F. Harm and Rumpler, "Proc.5th Intern. Congr. Pure Appl. Chem.", 59, 1903.
24. R. Gans, Jahrb. Preuss. Geol. Landesantalt (Berlin), *26,* 179 (1905).
25. L. Pauling, J. Am. Chem. Soc., *49,* 765 (1927).
26. L. Pauling, Proc. Nat. Acad. Sci., U. S., *16,* 123 (1930).
27. W. L. Bragg, Atomic Structure of Minerals, Cornell Univ. Press, 1937.
28. B. A. Adams and E. L. Holmes, J. Soc. Chem. Ind., *54,* 1T (1935).
29. M. J. Fuller, Chromatogr. Rev., *14,* 45 (1971).
30. V. Veselý and V. Pekárek, Talanta, *19,* 219 (1972).
31. M. Abe, Bunseki Kagaku, *23,* 1245, 1561 (1974).
32. A. Clearfield, Inorganic Ion Exchange Materials, CRC Press, Boca Raton, Fl. 1982.
33. K. A. Kraus and H. O. Phillips, J. Am. Chem. Soc., *78,* 249 (1956).
34. K. A. Kraus, H. O. Phillips, T. A. Carlson and J. S Johnson, "Proc. 2nd Intern. Conf. Peaceful Uses of Atomic Energy", 28, 15/P/1832, United Nations, Geneva, 3, 1958.
35. M. Abe, Bunseki Kagaku, *23,* 1254, 1561 (1974).
36. A. Clearfield, Inorganic Ion Exchange Materials, CRC Press, Boca Raton, Fl. 1982, Chapt. 1, 2, 6.
37. L. V. C. Rees, Rep. Progr. App. Chem., *54,* 655 (1969).
38. L. V. C. Rees, Ann. Rep. Progr. Chem. Sect. A, *67,* 191 (1970).
39. V. Pekárek and V. Veselý, Talanta, 19, 1245 (1972).
40. A. K. De and A. K. Sen, Sep. Sci. Technol. 13, 517 (1978).
41. R. E. Grim, Clay Minerology, McGraw Hill, London (1953).
42. W. M. Meier, Molecular sieves, Soc. Chem. Ind., London, 1969, p.10.
43. A. F. Cronstedt, Akad. Handl. Stockholm, *17,* 120 (1756).
44. A. Dyer, An Introduction to Zeolite Molecular Sieves, John Wiley and sons, N. Y., 1988, p.12.
45. R. Szostak, Molecular Sieves, Van Nostrand Reinhold, N. Y., 1989, p.51.
46. A. P. Bolton, Experimental Methods in Catalytic Research, vol 2, Academic Press N. Y., 1976, p.1.
47. R. M. Barrer, Endeavour, 122 (1964).
48. R. M. Barrer, Ber. Busenges. Physik. Chem., *69,* 786 (1965).
49. R. M. Barrer, Proc. Rrit. Ceram. Soc., 145 (1964).

50. R. M. Barrer, Chem. Brit., 380 (1966).
51. H. S. Sherry, in Ion Exchange, J. A. Marinsky (Ed.), 2, 89-133, Dekker, N. Y., 1969.
52. Y. Fujiki, Y. Komatsu and T. Sasaki, IONICS, Japan, No.120, 131 (1985).
53. B. Raveau, Rev. Chim. Miner., *21,* 391 (1984).
54. V. V. Vol'khin, S. A. Onorin, G. V. Leont'eva, and N. B.Khodyashev, Z. Prikl. Khim., *50,* 749 (1977); P. G. Kudryavtsev, S. A. Onorin and V. V. Vol'khin, Izv. Vyssh. Uchebn. Zaved., Tsvetn. Metall., 50, 1977.
55. R. Chitrakar and M. Abe, Mat. Res. Bull., *23,* 1231 (1988).
56. M. Abe in Inorganic Ion Exchange Materials, A. Clearfield (Ed.), CRC Press, Boca Raton, Fl. 1982, Chapt. 6.
57. M. Abe and T. Ito, Nippon Kagaku Zasshi, *87,* 417 (1966).
58. M. Abe and T. Ito, Nippon Kagaku Zasshi, *86,* 1259 (1965).
59. M. Abe and T. Ito, Nippon Kagaku Zasshi, *86,* 817 (1965).
60. G. A. Parks, Chem. Rev., *65,* 177 (1965).
61. Ya. I. Korenman, Tr. po Khim. i Khim. Tekhnol., 124 (1964).
62. D. Kyriacou, Surface Soil, *8,* 370 (1967).
63. S. C. Churns, J. S. Afr. Chem. Inst., *19,* 108 (1966).
64. R. G. Burns and V. M. Burns, "Manganese Dioxide Symposium Vol.2, Tokyo, 1980", B. Schumm Jr., H. M. Joseph and A. Kozawa (Eds.), I. C. MnO_2 Sample office, Cleaveland, Ohio, 1981, p.97.
65. G. V. Leont'eva, and V. V. Vol'khin, Z. Prikl. Khim., *44,* 2615 (1971); G. V. Leont'eva, L. G. Chirkova and V. V. Vol'khin, ibid., *53,* 1229 (1980); G. V. Leont'eva, V. V. Vol'khin, L. G. Chirkova and E. A. Mironova, ibid., *55,* 1306 (1982); V. V. Vol'khin and G. V. Leont'eva, Izv. Akad. Nauk SSSR, Neorg. Mater., *9,* 1041 (1973); G. V. Leont'eva, V. V. Vol'khin and S. A. Onorin, ibid., *11,* 1110 (1975).
66. M. Tsuji and M. Abe, Solvent Extr. Ion Exch., *2,* 253 (1984); idem, Bull. Chem. Soc. Jpn., *58,* 1109 (1985); idem, Radioisotopes, *33,* 218 (1984).
67. Y. Miyai, K. Ooi and S. Katoh. Sep. Sci. Technol., *23,* 179 (1988); idem, Bull. Soc. Sea Water Sci. Jpn., *42,* 114 (1988), idem, J. Colloid Interface Sci., *130,* 535, (1989).

68. Xiang-Mu Shen and Xue-Yuan Wang, Acta Chim. Sin., *39,* 711 (1981); Xiang-Mu Shen and A. Clearfield, J. Solid State Chem., *64,* 270 (1986).
69. K. Ooi," Studies on Specific Adsorption of Li ions onto Spinel Type Manganese Oxide", Ph.D. Thesis, 1989, Govt. Ind. Res. Inst. Shikoku, Takamatsu, Japan.
70. M. Tsuji and M. Abe, Solvent Extr. Ion Exch., *2,* 253 (1984).
71. J. C. Hunter, J. Solid State Chem., *39,* 142 (1981).
72. K. Ooi, Y. Miyai and S. Katoh, Solvent Extr. Ion Exch., *5,* 561 (1987).
73. J. D. Donaldson and M. J. Fuller, J. Inorg. Nucl. Chem., *30,* 1083 (1968).
74. J. D. Donaldson and M. J. Fuller, J. Inorg. Nucl. Chem., *32,* 1703 (1970).
75. C. Heitner-Wirguin and A. Albu-yaron, J. Appl. Chem. (London), *15,* 445 (1965).
76. C. Heitner-Wirguin and A. Albu-Yaron, J. Inorg. Nucl. Chem., *28,* 2379 (1966).
77. Y. Inoue and M. Tsuji, J. Nucl. Sci. Technol., *13,* 85 (1976).
78. H. Izawa, S. Kikkawa and M. Koizumi, J. Solid State Chem., *60,* 264 (1985).
79. T. Sasaki, Y. Komatsu and Y. Fujiki, Solvent Extr. Ion Exch., *1,* 775 (1983).
80. A. Clearfield and J. Lehto, J. Solid State Chem., *73,* 98 (1988).
81. M. Tsuji and M. Abe, J. Radioanal. Nucl. Chem. Article, *102,,* 283 (1986).
82. A. Clearfield, Inorg. Chem., *3,* 146 (1964).
83. Y. Inoue and H. Yamazaki, Bull. Chem. Soc. Jpn, *58,* 2481 (1985).
84. C. E. Rice and J. L. Jackel, J. Solid State Chem., *41,* 308 (1982).
85. M. Abe and T. Ito, Bull. Chem. Soc. Jpn, *41,* 333 (1968).
86. M. Abe, Bull. Chem. Soc. Jpn, *42,* 2683 (1969).
87. M. Abe and T. Ito, Bull. Chem. Soc. Jpn, *40,* 1013 (1967).
88. F. A. Cotton and G. Wilkinson, Advanced Inorganic Chemistry, 2nd ed., Interscience, N. Y., 1966, p.937.
89. L. M. Mellor, A Comprehensive Treatise on Inorganic and Theoretical Chemistry, vol. 11, Longmans, London, 1954, p.762.
90. G. H. Nancollas and V. Pekárek, J. Inorg. Nucl. Chem., *27,* 1409 (1965).
91. A. Clearfield and J. A. Stynes, J. Inorg. Nucl. Chem., *40,* 117 (1964).
92. G. Alberti and E. Torracca, Talanta, *30,* 317 (1968).
93. A. Clearfield and G. D. Smith, Inorg. Chem. *8,* 431 (1969).
94. A. Clearfield and G. D. Smith, J. Inorg. Nucl. Chem., *30,* 327 (1968).
95. A. Clearfield, G. D. Smith and B. Hammond, J. Inorg. Nucl. Chem., *30,* 277

(1968).
96. E. Torracca, U. Costantino and M. A. Massucci, J. Chromatogr. *30,* 584 (1967).
97. R. F. Brigevich and R. A. Kuznetsov, Vestn. Leningr. Univ., Fiz., Khim., 145 (1969).
98. G. Balon, C. Beaudet, J. Piret and W. R. Ruston, Kerntech. Isotopentech. Chem., Z. Ing. Aller. Fachrichtungen, *9,* 258 (1967).
99. M. Qureshi and S. A. Nabi, J. Inorg. Nucl. Chem., *32,* 2059 (1970).
100. G. Alberti and E. Torracca, J. Inorg. Nucl. Chem., *30,* 3075 (1968).
101. M. Qureshi and V. Kumar, J. Chem. Soc. A, 1488 (1970).
102. S. N. Tandon and J. S. Gill, J. Radioanal. Chem., *20,* 5 (1974).
103. M. Abe and M. Tsuji, Chem. Lett., 1561 (1983).
104. Y. Inoue, Bull. Chem. Soc. Jpn, *36,* 1316 (1963).
105. Y. Inoue, J. Inorg.Nucl. Chem., *26,* 2241 (1964).
106. U. Costantino and A. Gasperoni, J. Chromatogr., *51,* 289 (1970).
107. M. Qureshi, R. Kumar and H. S. Rathore, J. Chem. Soc. A, 272 (1970).
108. M. Qureshi, H. S. Rathore and R. Kumar, J. Chem. Soc. A, 1986 (1970).
109. U. Costantino and A. Gasperoni, J. Chromatogr., *51,* 289 (1970).
110. M. Abe, T. Kenjo and T. Ito, Kogyo Kagaku Zasshi, *70,* 291 (1967).
111. M. Abe and T. Ito, Kogyo Kagaku Zasshi, *70,* 440 (1967).
112. M. Abe and K. Hayashi, Solvent Extr. Ion Exch., *1,* 97 (1983).
113. G. Alberti and M. A. Massucci, J. Inorg. Nucl. Chem., *32,* 1719 (1970).
114. D. L. Keppert, Inorg. Chem., *8,* 1556 (1969).
115. L. C. W. Baker and J. S. Figgis, J. Am. Chem. Soc., *92,* 3794 (1970).
116. H. Wu, J. Biol. Chem., *43,* 189 (1920).
117. P. Cannon, J. Inorg. Nuc. Chem., *13,* 261 (1960) and references cited therein.
118. J. W. Illingworth and J. F. Keggin, J. Chem. Soc., 575 (1935).
119. J. Van R. Smit, J. J. Jacobs and W. Robb, J. Inorg. Nucl. Chem. *12,* 95 (1959).
120. J. F. Keggin, Nature, *131,* 908; ibid., *132,* 351 (1933).
121. J. F. Keggin, Proc. Roy. Soc. London, A., *144,* 75 (1933).
122. J. A. Santos, Proc. Roy. Soc. London, A., *150,* 309 (1935).
123. A. J. Bradly and J. W. Illingworth, Proc. Roy. Soc. London, A. *157,* 113 (1936).
124. J. C. A. Boeyens, G. J. Mcdougall and J. Van R. Smit. p.291; G. J. Mcdougall and

J. Van R. Smit. p.348; B. Bisnath, H. S. Govinden and J. Van R. Smit, p.357, in Recent Developments In Ion Exchange, P. A. Williams and M. J. Hudson (eds.), Elsevier Applied Science, London, 1987.

125. I. S. C. Churms, S. Afr. Ind. Chem., 19 (1965).

126. V. Veselý, and V. Pekárek, Talanta, *19,* 219, 1245 (1972).

CHAPTER 2
SYNTHESIS AND CHARACTALIZATION OF TITANIUM ANTIMONATE

1 INTRODUCTION

It is known that the inorganic ion exchangers have the selectivity for particular ions, and the ion exchange property of an inorganic ion exchanger varies with conditions of preparations. The preparation of inorganic ion exchangers are classiffied into solid state method or wet method.

(a) solid state method

Two or more starting substances weighed to equal to the chemical composition of product are mixed, heated for the reaction of decomposition, and then the product is done conditioning. In this reaction, usually, metal oxide is mixed with alkali metal carbonate, hydroxide or acetate. The reaction can be performed at relatively low temperature for some combination of metal oxide and alkali metal salt.

(b) wet method

In this method the exchanger is obtained by hydrolysis of the aqueous solution of metal salt or the alchol solution of metal alchoxide. The one metal salt (alchoxide) or some metal salts (alchoxides) are used as starting substance, and they are chloride sulfate or nitrate. The exchanger prepared by hydrolysis at low temperature is ussually low crystallized material.

(c) sol-gel method

The product prepared from metal alchoxide is mixed with alkali metal salt and treated hydrothermally at 100-300°C. The clay mineral and zeolite are obtained in this method.

Three type of antimonic acids such as amorphous (A-SbA), glassy (G-SbA) and crystalline (C-SbA), have been prepared by the different wet methods. C-SbA belongs to cubic phase and its selectivity is $Li^+ < K^+ < Cs^+ < Rb^+ < Na^+$, while A-SbA and G-SbA are amorphous materials and their selectivity is $Li^+ < Na^+ < K^+ < Rb^+ < Cs^+$.[1] On the oter hand, the antimonic acid prepared by the solid state method belongs to monoclinic crystal system, and its selectivity is $K^+ < Rb^+ < Cs^+ < Na^+ < Li^+$.[2] In these

way, the ion exchange property depends on the condition in preparation of ion exchanger.

Also, the inorganic ion exchangers can be classified in the crystal structure as shown in Table 2-1. And the typical compounds are given in Table 2-1, the ion exchange property depends on the crystal structure of ion exchanger.

The fiber and membrane compounds are obtained by the preparation with different physical and chemical conditions.

The ion in the exchanger is generally hydrated state, so interlayer distance of layer structure compound can be enlarged with the size of the ions in interlayer. Using this property, the high qualitative catalyst can be prepared by introduction of host molecule (e.g. complex) in interlayer space. On the other hand, because the crystal lattice can not be changed in tunnel or cage structure compound, these exchangers might show the steric effect and have high selectivity.

In recently, the new preparation is attempted as follows; the precursor prepared by the above methods is performed some treatments to substitute exchangeable metal ions from hydrogen ions without changing the structure, and that compound is utilized the H^+-form ion exchanger.[3,4)]

Titanium or titanic antimonate (they have been referred as different names) cation exchangers were prepsred by the several investigators with the different starting materials etc. Titanic antimonate was prepared by metathesis of Ti^{4+} and $[Sb(OH)_6]^-$ with using $TiCl_4$ and $K[Sb(OH)_6]$ by J. S. Gill and S. N. Tandon.[5)] And, titanium antimonate was prepared by precipitation reaction of $TiCl_4$ and $SbCl_5$ with NH_3 solution by M. Qureshi and V. Kumar.[6)]

The titanium antimonate (TiSbA) were prepared by the wet method of hydrolysis $TiCl_4$ and $SbCl_5$ without other reagent under different mole ratios of antimony and titanium (Sb/Ti), and charactarized by chemical analysis, X-ray diffraction and thermal analysis by M. Abe et al.[7)] It is known the TiSbA with Sb/Ti ratios of 0.27~0.86 show the X-ray diffraction pattern similar to rutile type TiO_2.[7)] But the detailed structure of TiSbA has not been reported because of its low crystallinity.

The oscillations in the Extended X-ray Absorption Fine Structure (EXAFS) region result from scattering of photoelectron on the surrounding coordination sphere. They contain information about the type and number of nearest hneighbors, their distance to to the absorbing atom.[8)] EXAFS has some advantages, e.g. EXAFS is independent of the

Table 2-1 Inorganic Ion-exchangers Classified in the Structure.

(a) amorphous compounds

hydrous oxides of multivalent metals (hydrous aluminate, hydrous zirconate etc.)

(b) tunnel structure compounds

aluminate (β-Al_2O_3 etc.), titanate, silicate, manganate (cryptomelane etc.),

tungstate ($K_2W_4O_{13}$ etc.), β-FeOOH, hydroxyapatite

(c) layer structure compounds

clay mineral (alumino silicate etc.), calsium silicate,

acid salt of tetravalent metal (phosphate, arsenate etc.),

tungstate ($Na_2W_4O_{13}$ etc.), titanate ($Na_2Ti_3O_7$, $K_2Ti_2O_5$ etc.),

silicate (tobermorite etc.), manganate (birnessite etc.), molibdate ($Mg_2Mo_2O_7$ etc.),

niobate ($KNbO_3$), hydrotalcite

(d) cage structure compounds

zeolite (Zeolite A, ZSM-5, chabazite, mordenite etc.), antimonate ($Sb_2O_5 \cdot 4H_2O$ etc.),

transition metal cyanoferrate

---

condition of a target materials, EXAFS can select the absorption atoms in multi composition and determine the neighbouring local structure around the absorbing atoms. Thus, EXAFS are widely applied for solutions and amorphous compounds which could not be determined their structure by X-ray structure analysis. It seems the interatomic distance in TiSbA can be determined by EXAFS.

Recently, FT-NMR techniques have been applied with good results in solid-state chemistry and are also expected to become a powerful means to understand the state of coordination water in inorganic ion exchangers. In view of this point FT-NMR is expected to approach the behavior of water in the ion-exchange matelials.

In the present work, TiSbA was prepared at different chemical composition and subjected to the chemical analysis, X-ray diffractometry, thermal analysis, and the measurement of IR, EXAFS and NMR spectra. And the crystal structure of TiSbA was described about the configuration of Sb and Ti atoms.

2 EXPERIMENTAL

2-1 Chemicals

Chemical grade of Antimony pentachloride supplied by Yotsuhata Co. Ltd. (>99% as metal), and titanium tetrachloride supplied by Wako Chemical Co. Ltd. (>99% as metal), were used without further purification.

2-2 Preparation of TiSbA.

The TiSbA was prepared as described previously[7]; A 4M (1M = 1 mol dm^{-3}) antimony pentachloride solution was obtained by hydrolysis of antimony pentachloride with H_2O (1+1), a 4M titanium tetrachloride solution was obtained by hydrolysis of titanium tetrachloride with H_2O (1+1.2). A 4M antimony pentachloride solution was mixed with a 4M titanium tetrachloride solution at different molar ratios of:

(A) 0.1, 0.3, 0.5, 0.7, 1, 1.5, 3

(B) 0.3, 0.5, 0.7, 0.9

at 60°C. The mixed solutions were immediately hydrolyzed in demineralized water (1+25) at the same temperature. The total volume of (A) is $1dm^3$ and that of (B) is $5dm^3$. The white precipitate obtained was allowed to stand in the mother solution overnight at 60°C, filtered and then washed with demineralized water with the aid of centrifuge operated about 10,000 rpm until the pH of the supernatant solution was higher than 1.5. The white product obtaied was dried at 60°C for 2 days, ground and sieved 100~200 mesh size.

The samples prepared were rewashed with demineralized water in order to remove adherent fine particles. A demineralized water was percolated through the samples until free from chloride ions, and then 1M HNO_3 solution was percolated until free from sodium ions. Finally, the samples were rewashed with demineralized water and air dried at room temperature.

2-3 Determination of Antimony and Titanium

A (0.1g) sample of TiSbA was dissolved in hot concentrated sulfuric acid ($50cm^3$) and diluted to 0.4M in sulfuric acid solution with water. The contents of antimony and titanium were determined using a Seiko Instruments Inc. SPS 7000 inductively coupled plasma atomic emission spectrometer (ICP-AES).

2-4 X-ray diffraction and thermal analysis

For X-ray studies, a JEOL X-ray diffractmeter model JDX-7E and Rigaku Denki RINT 1100 X-ray diffractmeter were used with Ni-filtered Cu-K_α radiation.
A Rigaku Denki Thermoflex Model 8001 was used for the study of the thermal analysis at a heating rate of 10^0C/min. by using α-Al_2O_3 as the reference material.

2-5 IR spectra

IR spectra were measured by the KBr disc (1cm i.d., 1mm thick) method with a Japan Spectroscopic Co., LTD. infrared spectrometer model FT/IR-8900.

2-6 EXAFS Study

For EXAFS study, the samples were mixed with polyethelene powder and pressed at 500 kg/cm^2 for the measuremeants (1cm i.d., 2mm thick). The X-ray absorption around Sb K-edge was measured with BL-10B beam line at Photon Factory of National Laboratory for High Energy Physics. The spectra were recorded at room temperature with a channel-cut Si(311) monochromator. The EXAFS data were analyzed by using a program EXAFS4 (N. Kosugi and H. Kuroda, Research Center for Spectrochemistry, the University of Tokyo).

2-7 NMR Study

The NMR spectra were obtained by employing JEOL FT-NMR spectrometer model GSX-270 and α-500. The observed frequency were 270MHz and 500MHz for ^{1}H, respectively. The NMR spectra were obtained by using nonedecouplig single-pulse mode. The spin-lattice relaxation time, T_1, was measured by means of inversion recovery method and the spin-spin relaxation time, T_2, by Carr-Purcell-Meiboom-Gill (CPMG) method.

3 THEORITICAL

3-1 EXAFS Spectroscopy[9,10)]

EXAFS ascribes to oscillations of the X-ray absorption coefficient on the high energy side of an absorption edge. Such oscillations can extend up to 1000eV above the edge and may have a magnitude of 1~20% of the edge jump. EXAFS spectroscopy refers to the measurement of the X-ray absorption coefficient μ as a function of photon energy E above the threshold of an absorption edge. Fig.2-1(a) shows schematically one edge of an absorber. In a transmission experiment, μ or μx (x is the sample thickness) is calculated by

$$\mu x = \ln I_0/I$$

where I_0 and I are the intensities of the incident and transmitted beams, respectively. EXAFS spectra generally refer to the region 40~1000 eV above the absorption edge. Near or below the edge, there generally appear absorption peaks due to excitation of core electrons to some bond states (1s to nd, (n+1)s, or (n+1)p orbitals for K edge, and 2s for L_I edge, 2p for L_{II}, L_{III} edges to the same set of vacant orbitals, etc.). This pre-edge region contains valuable bonding information such as the energetics of virtual orbitals, the electoronic configuration, and the site symmetry. The edge position also contains information about the charge on the absorber. In fact, a shift of various edga features to higher energy of with increasing absorber valence has been observed. [11,12)]

EXAFS is a final state interference effect involving scattering of the outgoing photoelectron from the neighboring atoms. Fig.2-1(b) attempts to convey the current view of EXAFS. In the presence of neighboring atoms, the outgoing photoelectron can be backscattered from the neighboring atoms thereby producing an incoming wave which can interfere either constractively or destructively with the outgoing wave near the origin, resulting oscillatory behavior of the absorption rate. The amplitude and frequency of this sinusoidal modulation of μ vs E depend on the type of neighboring atoms and their distances away from the absorbor, respectively.

This simple picture of EXAFS has been formulated the generally accepted short-range single-electron single-scattering theory. The modulation of the absorption rate in EXAFS, normalized to the "background" absorption (μ_0) is given by

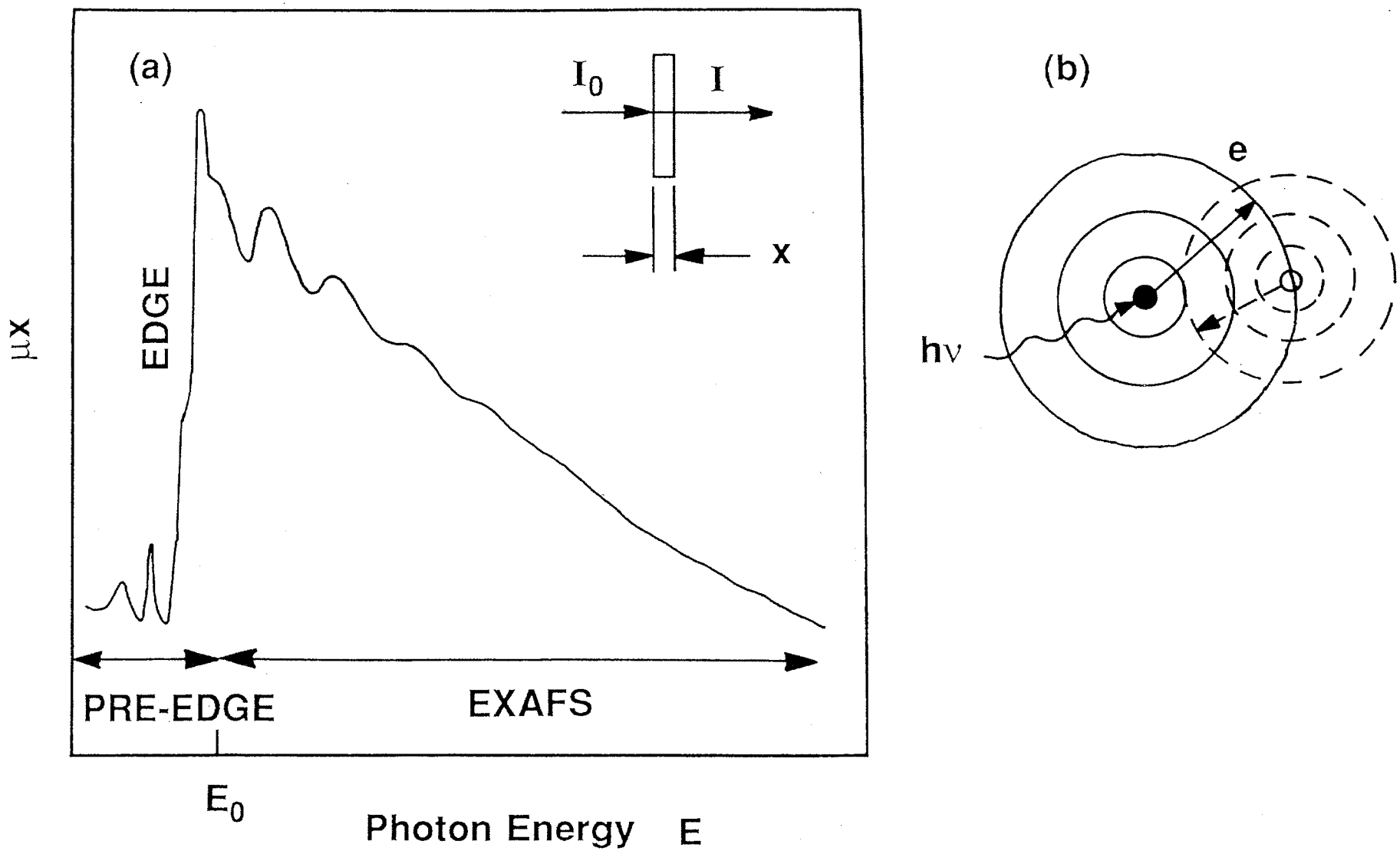

Fig.2-1 Schematic Representation of the Transmission Experiment and the Resulting X-ray Absorption Spectrum μx vs E (a) and the Principle of EXAFS (b)

$$\chi(E) = \frac{\mu(E) - \mu_0(E)}{\mu_0(E)}$$

In order to relate to structural parameters, it is necessary to convert the energy E into the photoelectron wavevector k via

$$k = \sqrt{\frac{2m}{\hbar^2}(E-E_0)} = \sqrt{0.2626\ (E-E_0)}$$

This transformation of χ(E) in E space gives use to χ(k) in space where

$$\chi(k) = \sum_j N_j F_j(k) e^{-2\sigma_j^2 k^2} e^{-2r_j/\lambda_j(k)} \frac{\sin(2kr_j + \Phi_j(k))}{kr_j^2}$$

Here $F_j(k)$ is the backscattering amplitude from each of the N_j neighboring atoms of the jth type with a Debye-Waller factor σ_j to account for thermal vibration and static disorder and at a distance r_j away. $\phi_j(k)$ is the total phase shift experimental by the photoelectron. The term $\exp(-2r_j/\lambda_j)$ is due to inelastic loses in the scattering process with λ_j being the electron mean free path.

$F_j(k)$ and $\Phi_j(k)$ are specific values which are dependent on the atom and pair of atoms, so they are evaluated from the theoretical calculation or the analysis for spectrum of the material with well known structure. N_j, r_j, σ_j and λ are structural constant deviated from EXAFS experimental.

3-2 NMR Spectroscopy

When we put a sample in a magnetic field, the induced field which we expect to arise does not spring instantaneously into exitence, but will appear over some interval. Calculating how long this should take, and what form the approach to equilibrium adopts, is a whole area of physics, and cannot be achieved without extensive approximation. In the Bloch theory of NMR, the problem vastly simplified by assuming that the equilibrium will be approached exponentially, and treating the time constant of this exponential as a parameter which one might set out to measure. That exponential relaxation is a hypothesis, not a universal fact. Putting this idea formally, the hypothesis is that the induced field will biulding up according to the equation:

$$\frac{dM_z}{dt} = \frac{M_0 - M_z}{T_1}$$

where M_0 is the magnetisation at thermal equlibrium, so that if the magnetisation is initially 0:

$$M_z = M_0 (1 - e^{-t/T_1})$$

The time constant T_1 is known as the longitudinal or spin-lattice relaxation time. The latter term arose because much of the original theory of relaxation was worked out for solid samples, where the interaction of the magnetic moments with the rigid lattice was of interest. One popular method is illustsrated in Fig.2-2. The idea is to invert the z magnetisation with a π pulse, then wait a while for it to relax back towards the +z axis, and finally apply a $\pi/2$ pulse and measure the signal. Note that when the interval τ is less than $T_1/\ln 2$ the sampled signal arrives along -y axis; we already know that this corresponds to an apparent negative peak if we phase-correct so that +y is positive. The result of such an experiment with varying τ can be extracted the T_1 graphically from the varying peak heights.

Think of the sample being subdivided down into small regions, small enough that the field is perfectly uniform within each region. The total magnetisation is the sum of the contributions from these regions; each region contributes a vector precessing in the static frame with perfectly well defined frequency, but the frequency may vary from one region to another. In the rotating frame, this corresponds with the vector initially aligned along the y axis gradually becoming blurred as some of the contributing isochromats precess a little faster than the frame, some a little slower. Thus the total magnetisation does decay, even without longitudinal relaxation. The process is not changing the energy of the sample, as no transitions between levels are occurring, but the amount of order present is decreasing. In other words, the enthalpy remains constant but the entropy increases. This too is a form of relaxation, referred to as transverse or spin-spin; again the second term is sometimes a little misleading, however we will see how it arises momentarily. Transverse reminds us that the process occurs in the x-y plane and does not necessarily involve the z magnetisation. We assume once more that the process takes place exponentially, and call the time constant T_2. $(\pi/2)_x$-τ-τ_x-2τ-π_x-2τ-π_x-..... (the carr-

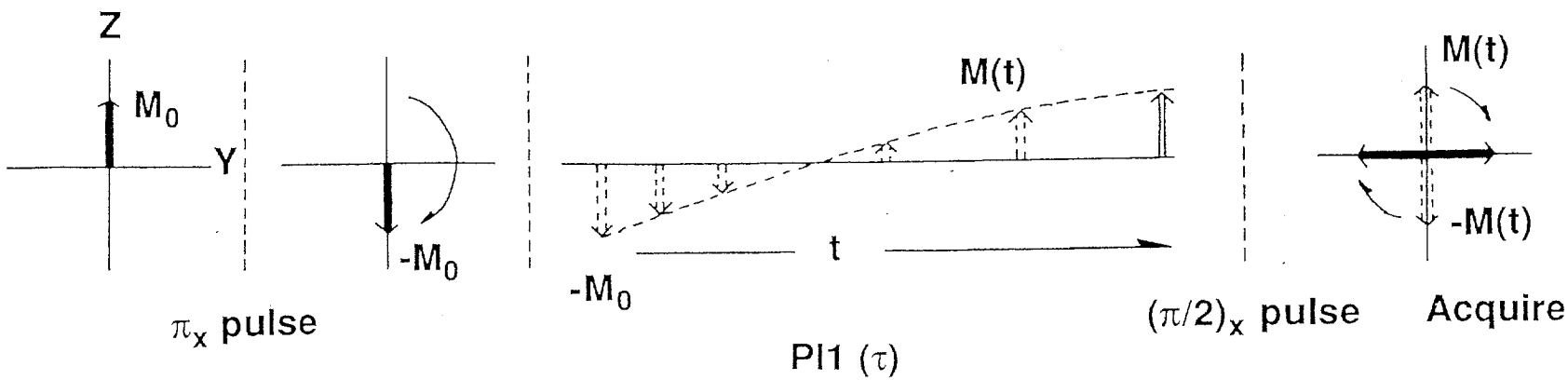

Fig.2-2 The Inversion-Recovery Method for Measuring T_1

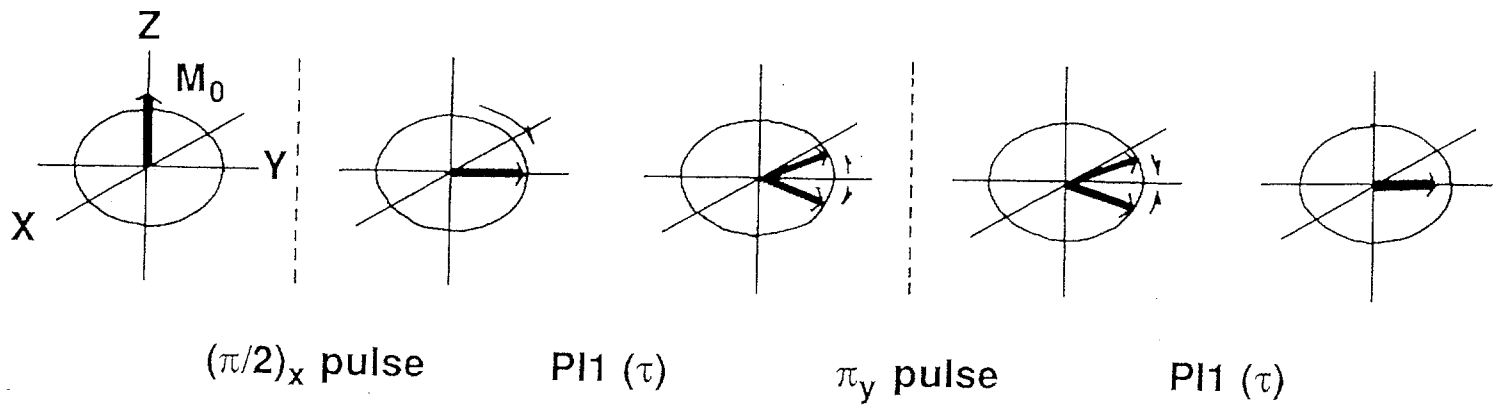

Fig.2-3 The CPMG Method for Mesuring T_2

purcell experiment) where we might try to measure the amplitude of the signal at the center of the 2τ intervals, or more practically perform the experiment repetitively with an increasing the last echo each time. As a good exercise in working with the rotating frame vector model compare the Carr-Purcell experiment with the Carr-Purcell-Meiboom-Gill (CPMG) variation which is $(\pi/2)_x$-τ-π_y-2τ-π_y-2τ-π_y-..... (Fig.2-3) and for the latter convince yourself that using π_y pulses instead of π_x still generates echoes (but along the +y axis only).

4 RESULTS AND DISCUSSION

4-1 Preparation of TiSbA

Titanium antimonates were prepared at different Sb/Ti molar ratios of 0.1~3.0 and at 60°C. All the samples of (A) and (B) prepared were hard white granules suitable for column operation. The formation of precipitation was very slow and the yield of TiSbA is low on the sample with Sb/Ti ratio of 0.1. The molar ratio of Sb/Ti in the product was nearly the same as the ratio of Sb/Ti in the initial mixed solution (Tables 2-2 and 2-3).

4-2-A X-ray diffraction pattern (A)

As can be seen from the X-ray diffraction patterns a~e in Fig.2-4, the TiSbA with Sb/Ti ratio of 0.11~1.1 showed weak rutile patterns. And as can be seen from patterns f and g in Fig.2-4, the TiSbA with Sb/Ti ratio of 1.4 showed nealy amorphous and that of 2.9 showed cubic antimonic acid (C-SbA),[13] respectively. In the samples with heating at 720°C, the X-ray diffraction patterns of the TiSbA with Sb/Ti ratios of 0.1~1.4 showed rutile pattern and increased their intensity of diffraction lines with decreasing Sb/Ti ratios (Fig.2-5 a-f). The TiSbA with Sb/Ti ratio of 2.9 with heating at 720°C showed a X-ray diffraction pattern indicating a mixture of Sb_6O_{13} and TiO_2 (rutile). Both amorphous antimonic acid (A-SbA) and C-SbA were decomposed to Sb_6O_{13} by heating at 700°C for 2 hours,[14] so this sample was found to be a mixture of hydrous titanium dioxide and A-SbA or C-SbA. On the other hand we could conclude that possibillity of a mixture with C-SbA or A-SbA is quite less in the TiSbA with Sb/Ti ratios of 0.11~1.4.

Considering these results, the formation region of the TiSbA with rutile structure is determined under 1.1 for Sb/Ti ratio (Fig.2-6).

4-2-B X-ray diffraction pattern (B) and lattice constant

The X-ray diffraction patterns for TiSbA with Sb/Ti ratios of 0.28~0.87 is shown in Fig.2-7. All the samples showed weak rutile petterns, and their intensities of the diffraction line ascribed to (110) plane increased with increasing of Sb/Ti ratio (Fig.2-8). patterns for TiSbA with Sb/Ti ratios of 0.28~0.87. As summarizing in Table 2-4, all the TiSbA with Sb/Ti ratios of 0.28~0.87 showed the similar lattice constants, a_0=

Table 2-2 Chemical Composition of Titanium Antimonates (A).

Sb/Ti in mixed solution	Sb/Ti in TiSbA	Chemical Composition	Theoretical Capacity
0.1	0.11	$TiO_2 \cdot 0.057Sb_2O_5 \cdot 0.60H_2O$	1.04 meq/g
0.3	0.34	$TiO_2 \cdot 0.17Sb_2O_5 \cdot 1.36H_2O$	2.14 meq/g
0.5	0.58	$TiO_2 \cdot 0.29Sb_2O_5 \cdot 1.34H_2O$	2.93 meq/g
0.7	0.77	$TiO_2 \cdot 0.38Sb_2O_5 \cdot 1.56H_2O$	3.30 meq/g
1.0	1.1	$TiO_2 \cdot 0.55Sb_2O_5 \cdot 2.60H_2O$	3.60 meq/g
1.5	1.4	$TiO_2 \cdot 0.71Sb_2O_5 \cdot 3.80H_2O$	3.75 meq/g
3.0	2.9	$TiO_2 \cdot 1.44Sb_2O_5 \cdot 7.93H_2O$	4.18 meq/g

Table 2-3 Chemical Composition of Titanium Antimonates (B).

Sb/Ti in mixed solution	Sb/Ti in TiSbA	Chemical Composition	Theoretical Capacity
0.30	0.28	$TiO_2 \cdot 0.14Sb_2O_5 \cdot 1.44H_2O$	1.86 meq/g
0.33	0.32	$TiO_2 \cdot 0.16Sb_2O_5 \cdot 1.32H_2O$	2.06 meq/g
0.49	0.48	$TiO_2 \cdot 0.24Sb_2O_5 \cdot 1.39H_2O$	2.62 meq/g
0.62	0.62	$TiO_2 \cdot 0.31Sb_2O_5 \cdot 1.58H_2O$	2.97 meq/g
0.74	0.69	$TiO_2 \cdot 0.34Sb_2O_5 \cdot 2.00H_2O$	3.02 meq/g
0.85	0.87	$TiO_2 \cdot 0.43Sb_2O_5 \cdot 1.80H_2O$	3.44 meq/g

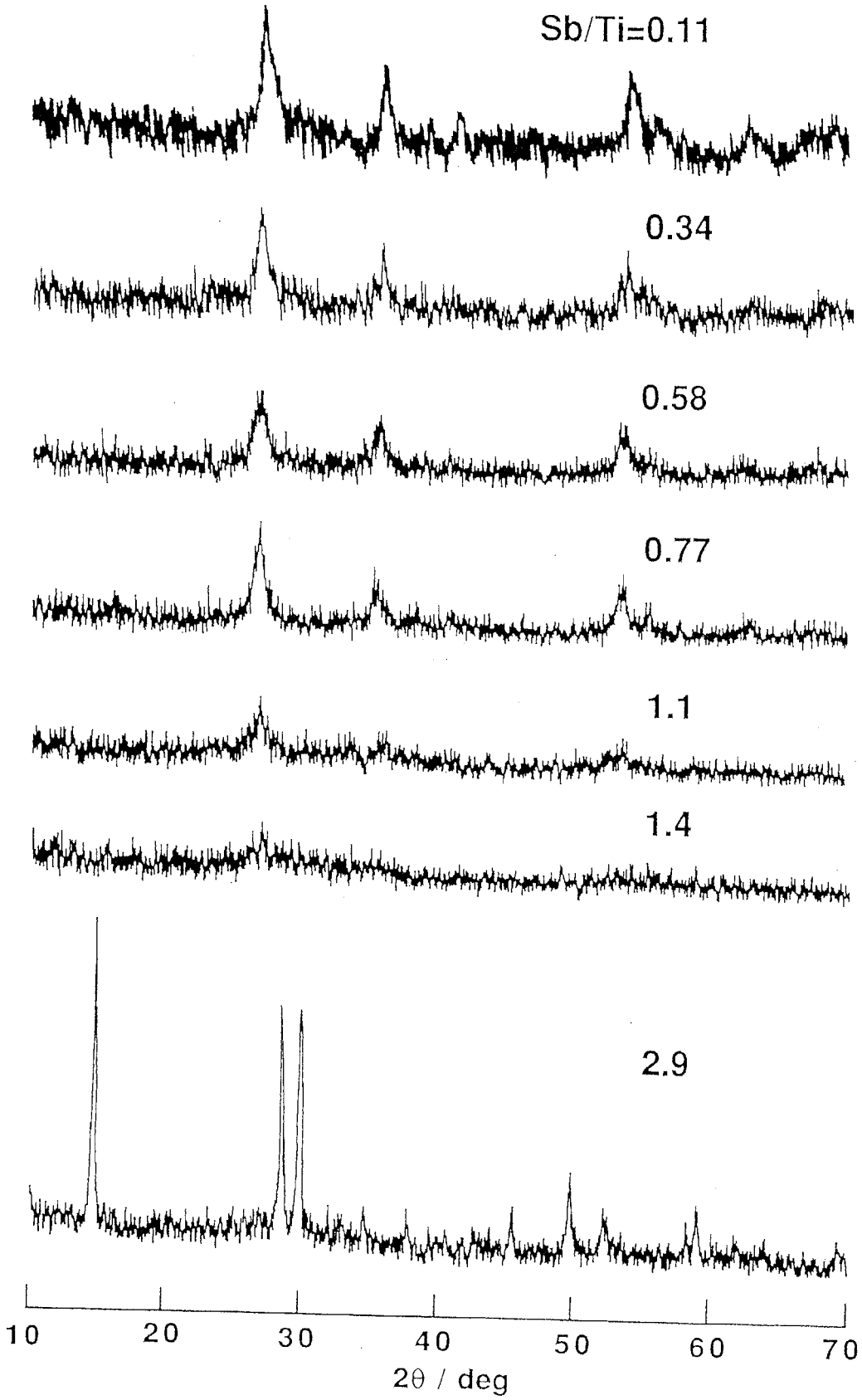

Fig.2-4 X-ray Diffraction Patterns for Various Samples of TiSbA (A) Dried at 60°C

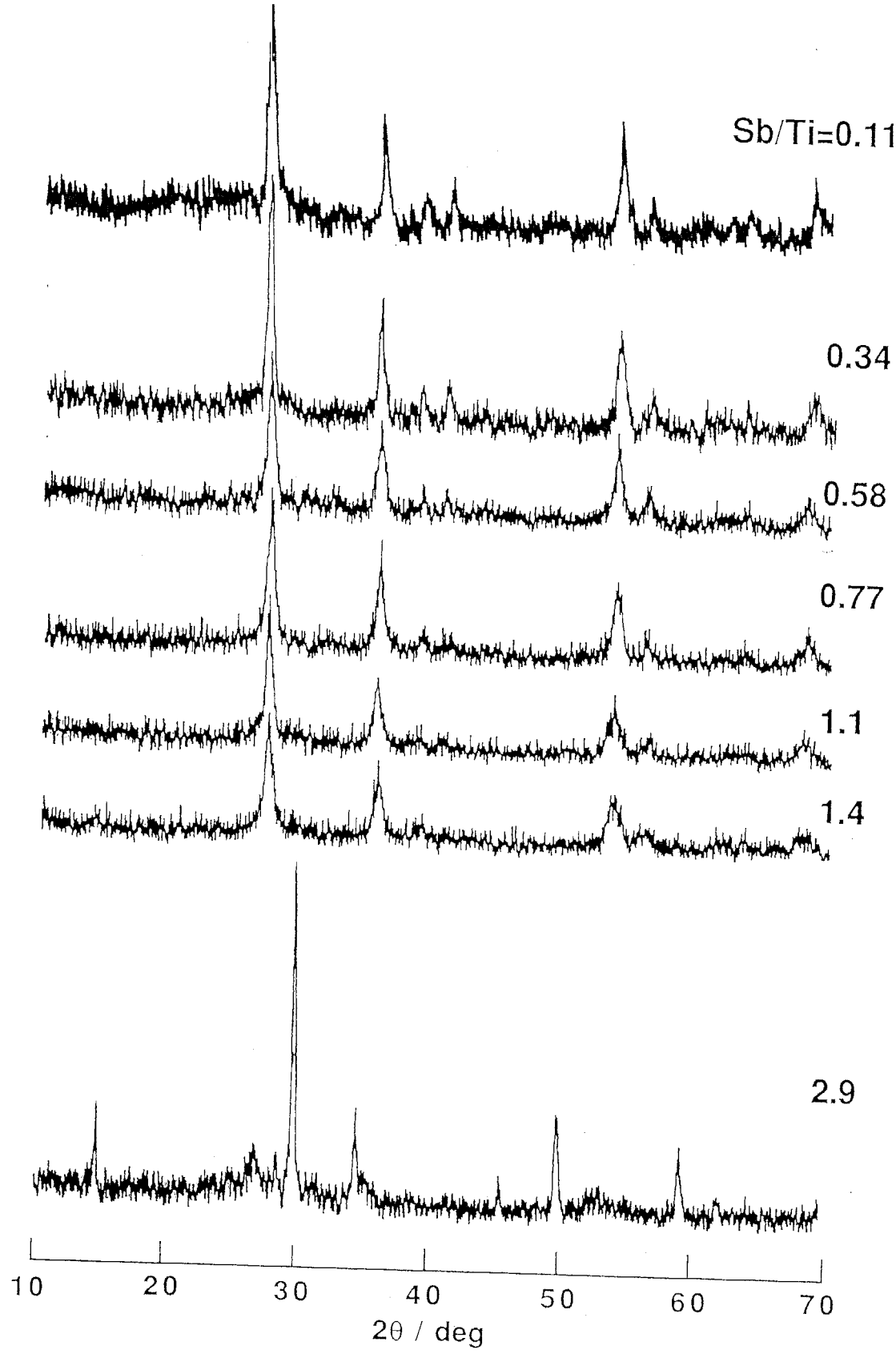

Fig.2-5 X-ray Diffraction Patterns for Various Samples of TiSbA (A) Heated at 720°C

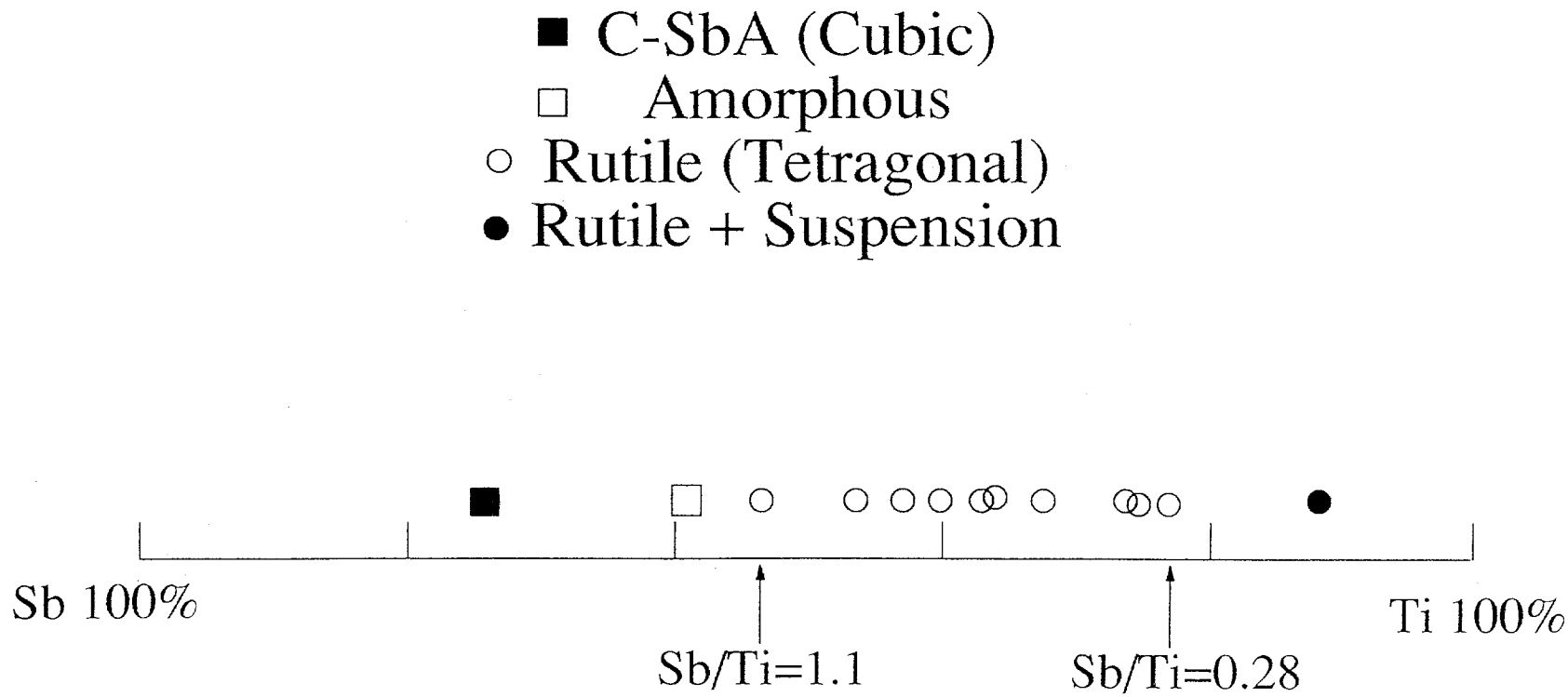

Fig.2-6 The Region of Formation of Rutile-type TiSbA at Differernt Mole Ratios of Mixed Solution

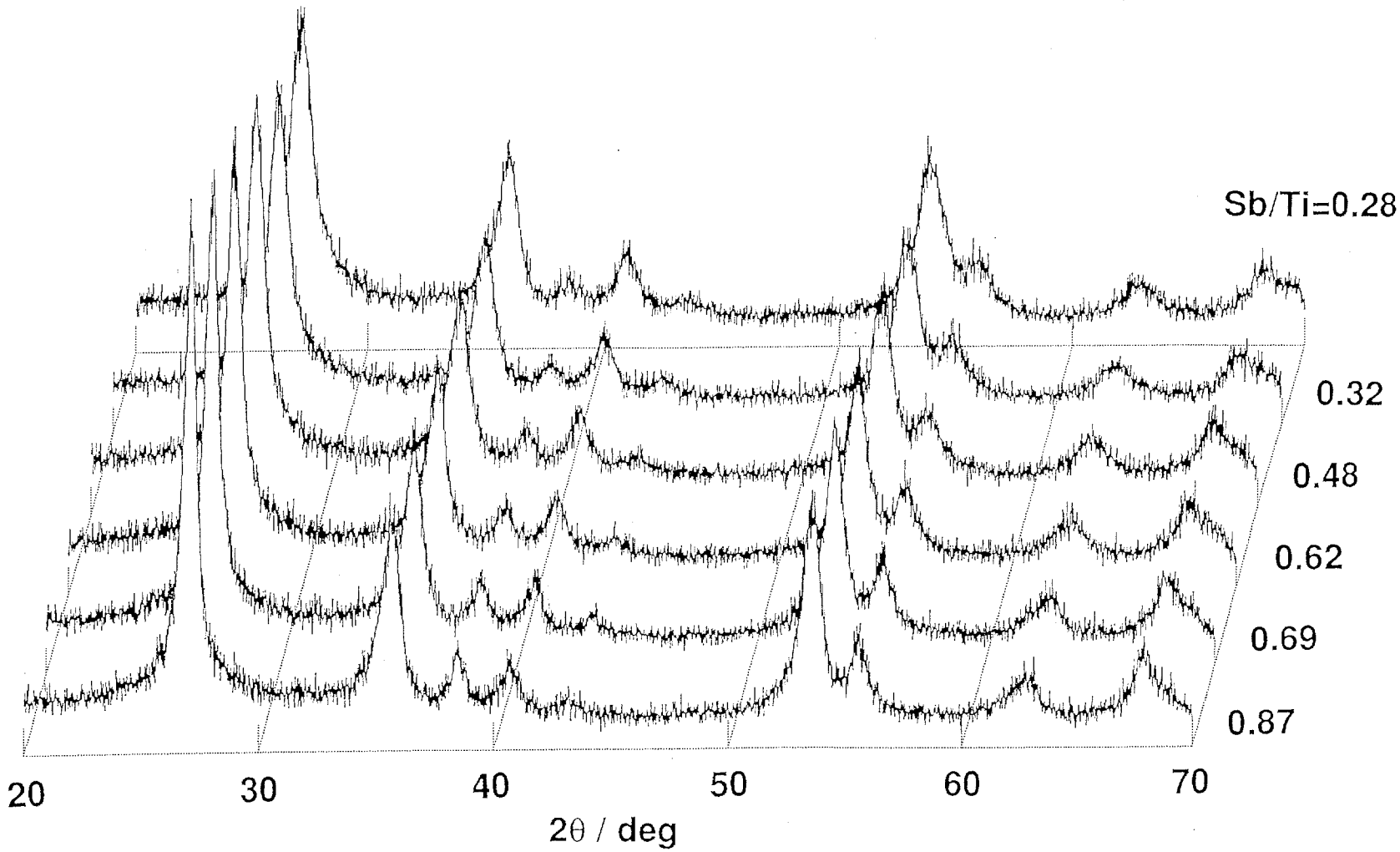

Fig.2-7 X-ray Diffraction Patterns for Various Samples of TiSbA (B)

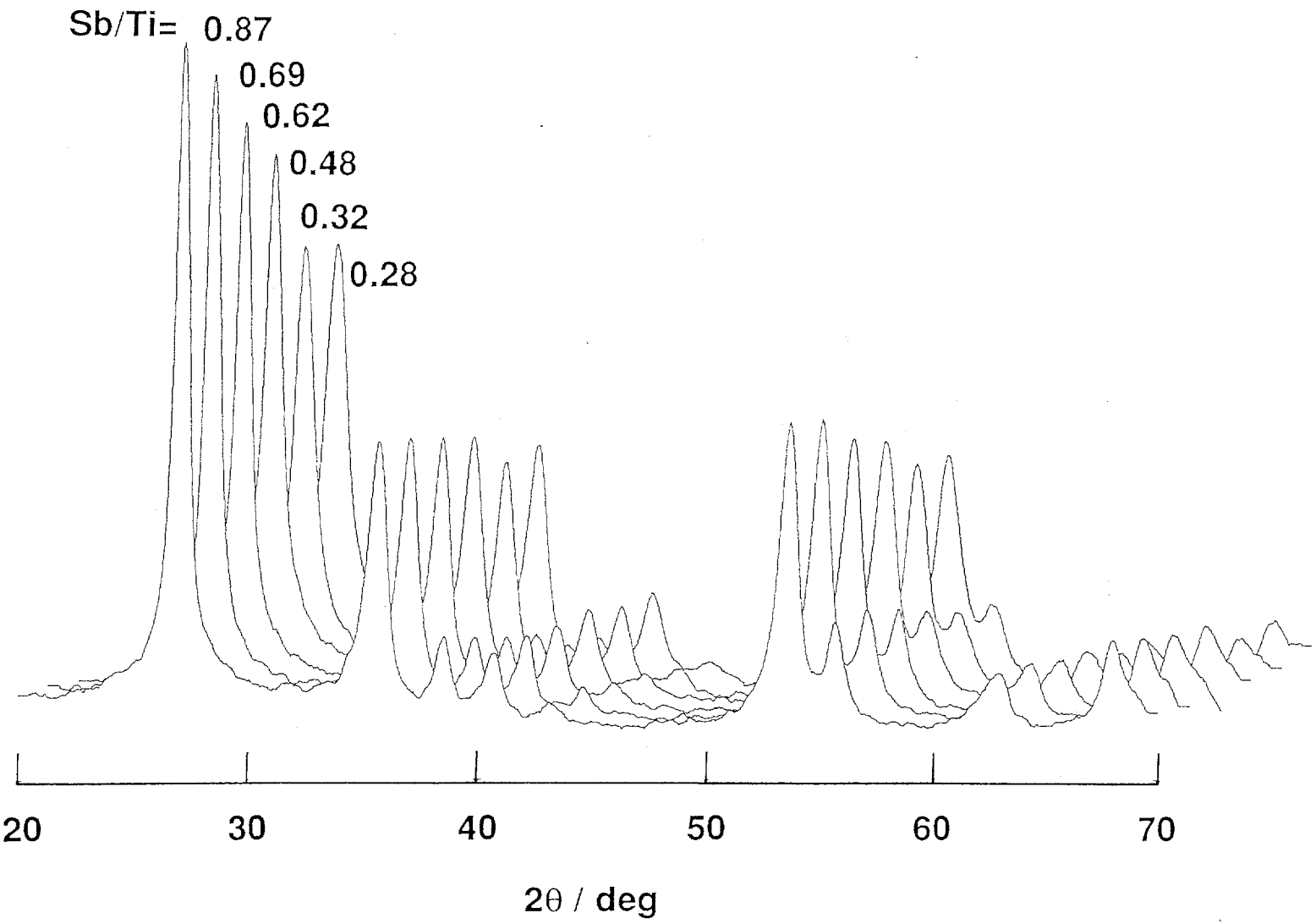

Fig.2-8 X-ray Diffraction Patterns after Smoothing for Various Samples of TiSbA

Table 2-4 Lattice Constants of Titanium Antimonates.

Sb/Ti in TiSbA	Lattice Constant a_0 /nm	c_0 /nm	Standard Deviation a_0 /nm	c_0 /nm
0.28	0.46720	0.29410	0.00151	0.00210
0.32	0.46709	0.29651	0.00083	0.00117
0.48	0.46672	0.29809	0.00090	0.00131
0.62	0.46575	0.29845	0.00022	0.00031
0.69	0.46741	0.29940	0.00049	0.00070
0.87	0.46745	0.29843	0.00023	0.00033
TiO_2 (Rutile) Wako Pure Chemical Co.	0.45929	0.29584	0.000004	0.000008
TiO_2 (Rutile) JCPDS 21-1276	0.45933	0.29592		

0.4657~0.4690 nm, c_0= 0.2952~0.2996 nm. It was found that a_0 value is larger than the a_0 value of the rutile type of titanium dioxide (a_0=0.45933 nm, c_0=0.29592 nm) and c_0 value is the nearly same as that. The diffraction lines ascribed to (101), (200), (110), (211) and (200) planes shifted to a little lower 2θ values with increasing of Sb/Ti ratios (Figs.2-9 and 2-10). The plot of a_0 and c_0 vs. Sb/Ti ratio shows in Fig.2-11. In view of the formula of tetragonal system

$$\frac{2\sin\theta}{d} = \frac{h^2 + k^2}{a_0^2} + \frac{l^2}{c_0^2}$$

the shifting of the diffraction lines ascribed to (200), (111), (211) and (220) planes can be due to the increase of a_0. The reason of shifting in the diffract line of (101) plane why the increasing of a_0 is larger than the decreasing of c_0 in Sb/Ti<0.6 and c_0 is increasing in Sb/Ti>0.6.

The tentative structure for TiSbA could be postulated as follows: the fixed charge from -OSbOH was distributed homogeneously onto the TiO_2 matrix by the dehydrated condensation as previously postulated for SnSbA.[15)]

4-3-A Thermal analysis (A)

Thermogravimetric (TG) and differential thermal analysis (DTA) curves of the TiSbA with different Sb/Ti ratios were shown in Fig.2-12. The endothermic peak at 100°C was assigned to the loss of the water for the TiSbA with Sb/Ti ratios of 0.11~0.77, at 105°C and 165°C for TiSbA (Sb/Ti=1.1), at 110°C and 175°C for TiSbA (Sb/Ti=1.4) and 115°C and 280°C TiSbA (Sb/Ti=2.9). The endothermic peak continued up to 580°C for TiSbA (Sb/Ti=0.11), 630°C for TiSbA (Sb/Ti=0.34), 670°C for TiSbA (Sb/Ti=0.58), 680°C for TiSbA (Sb/Ti=0.77). The weight loss continued up to the same temperatureas the end of endothermic peak for the TiSbA with Sb/Ti ratios of 0.11~0.77 due to the loss of water. The endothermic peak continued up to 600°C due to the loss of water and small exothermic peak was observed at 635°C due to the crystallization to TiO_2 (rutile) for TiSbA (Sb/Ti=1.1). For TiSbA (Sb/Ti=1.4) the feature of the loss of water is same as that for TiSbA (Sb/Ti=1.1), the large exothermic peak was observed at 655°C due to the same reason. The weight loss up to nearly 550°C due to the loss of water and up to 720°C because of deoxygenation with changed to Sb_6O_{13} for the TiSbA (Sb/Ti=2.9).

An experimental formula for the TiSbA prepared was estimated by assuming that the

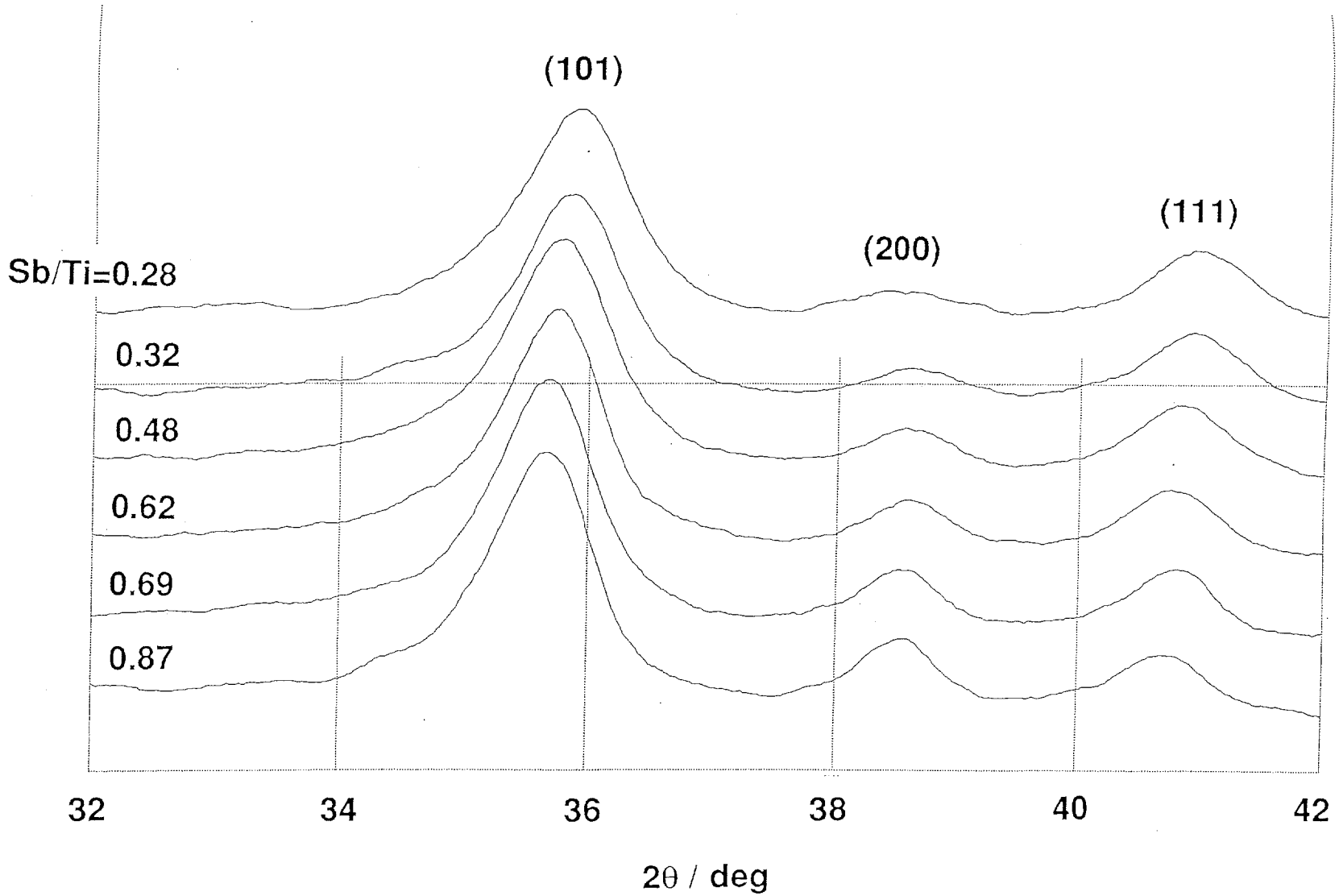

Fig.2-9 X-ray Diffraction Patterns of (101), (200) and (111) Planes for Various Samples of TiSbA

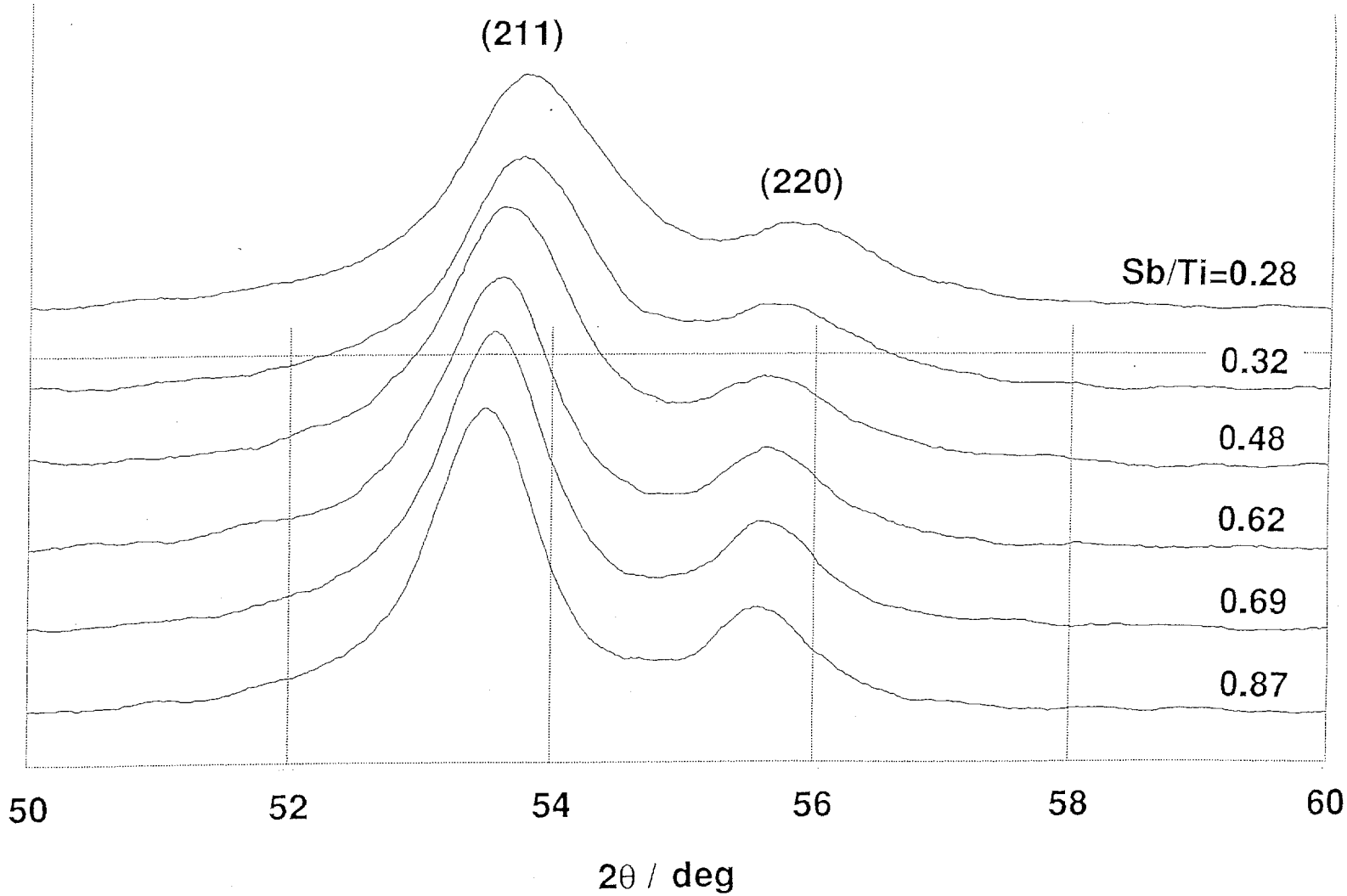

Fig.2-10 X-ray Diffraction Patterns of (211) and (220) Planes for Various Samples of TiSbA

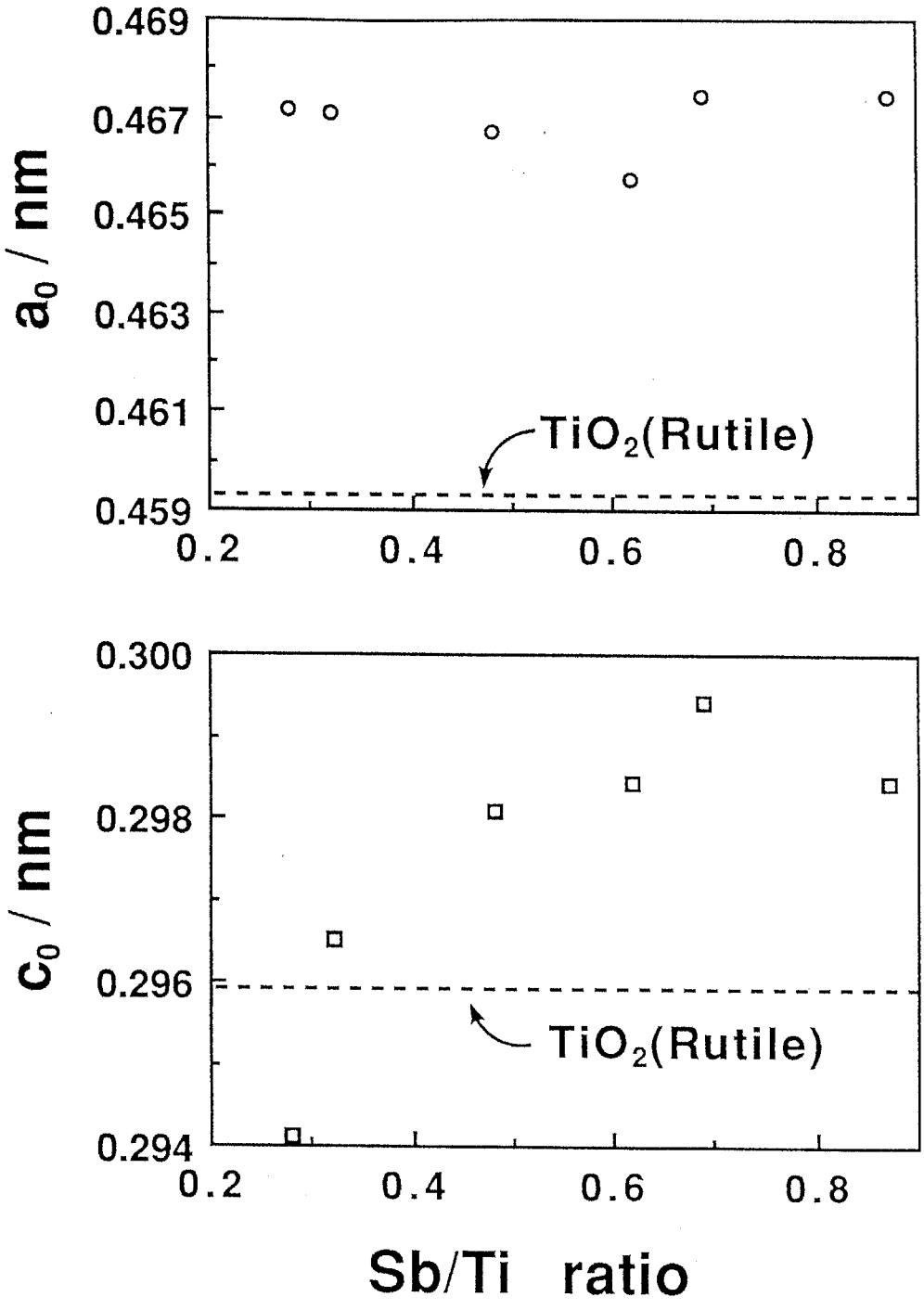

Fig.2-11 The Relationship between the Sb/Ti Ratio of TiSbA and Lattice Constants

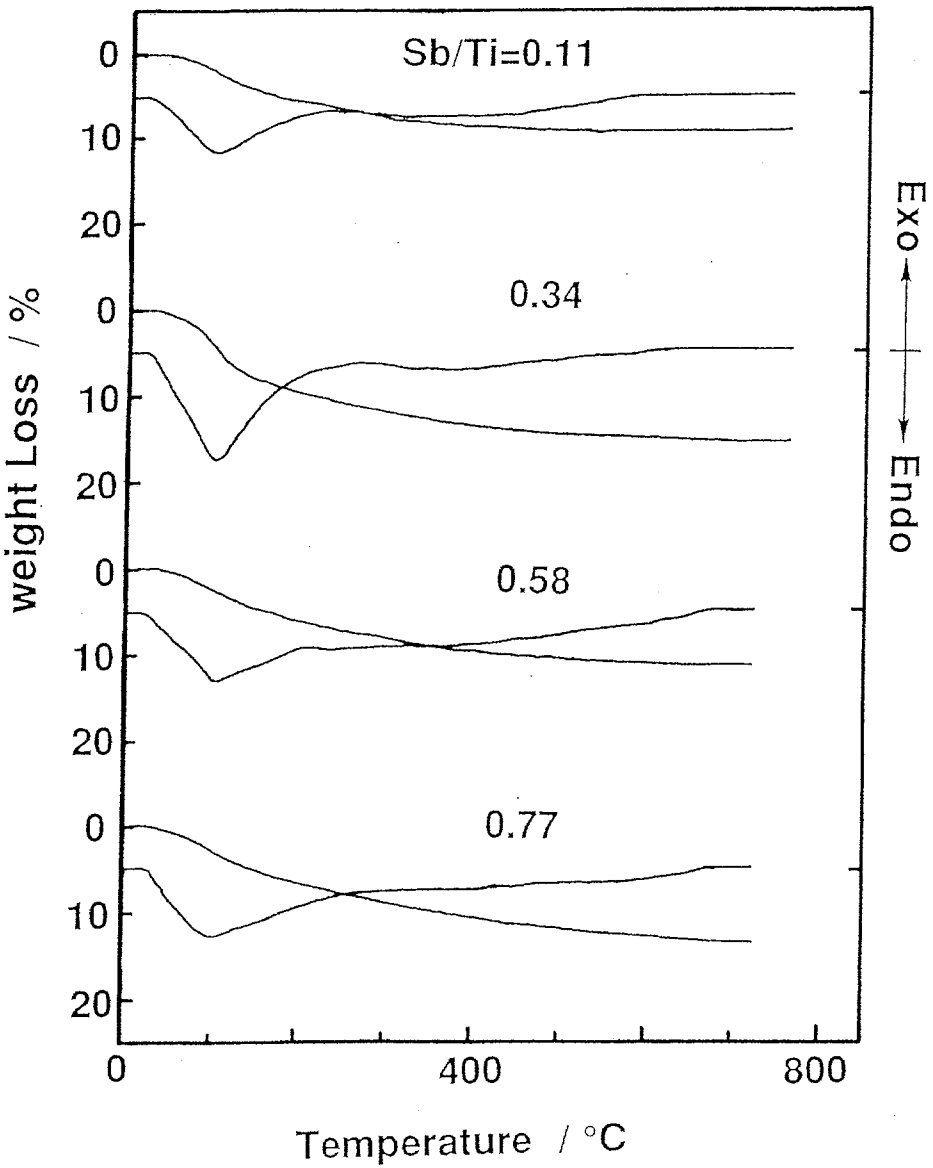

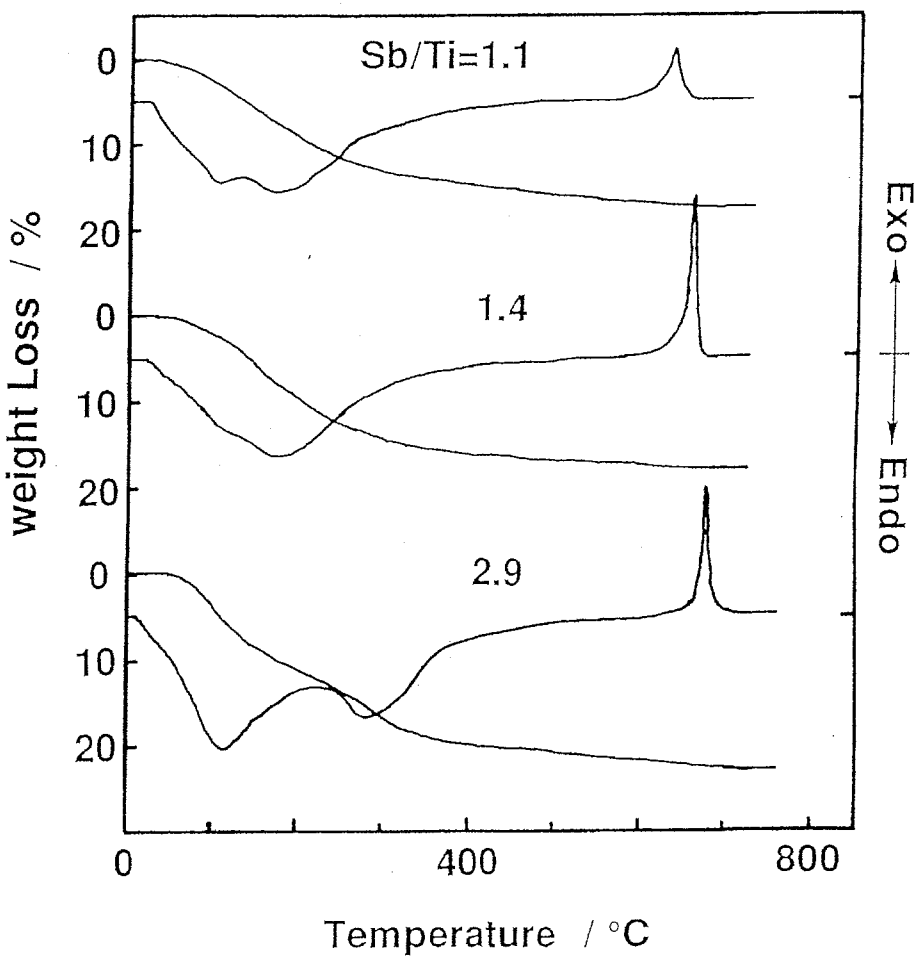

Fig.2-12 TG-DTA Curves for Various Samples of TiSbA (A)

Heating rate: 10°C / min.

heated sample at 700°C for the TiSbA with Sb/Ti ratios of 0.11~1.4 and at 550°C for the TiSbA (Sb/Ti=2.9), showed the ignition product to be composed of $TiO_2 \cdot mSb_2O_5$ (Table 2-2). The water content decreased with the decreasing Sb/Ti ratio in the TiSbA until Sb/Ti ratiio of 0.58. The water content of sample with Sb/Ti ratio of 0.34 is more than those of the samples with Sb/Ti ratio of 0.58 and 0.77.

4-3-B Thermal analysis (B)

TG-DTA curves for TiSbA with Sb/Ti ratios of 0.28~0.87 are shown in Fig.2-13. The main endothermic peak was observed at 100°C for all samples, and the small peak was containig up to 640°C for TiSbA (Sb/Ti=0.28 and 0.32), 660°C for TiSbA (Sb/Ti=0.48), 680°C for TiSbA (Sb/Ti=0.62 and 0.69), and 700°C for TiSbA (Sb/Ti=0.87). Their peaks could be due to the loss of the water. An experimental formula was estimated by the above method (Table 2-3).

4-4 Chemical Composition

The experimental formulas for the TiSbA prepared were represented by assuming that the heated samples (at 720°C for the TiSbA with Sb/Ti ratios of 0.28~1.4 and at 520°C for the TiSbA with Sb/Ti ratios of 2.9) are composed of $TiO_2 \cdot mSb_2O_5$.

The theoretical capacity was calculated from the experimental formula on the assumption that one antimony gives one hydrogen ion available for ion exchange. The experimental formula and theoretical capacity for TiSbA at different Sb/Ti ratios were summarized in Table 2-2 and 3.

4-5-A IR spectra (A)

Fig.2-14 shows the IR spectra of TiSbA with Sb/Ti ratios of 0.11~2.9. The absorption bands at 3800-2200 cm^{-1} and 1800-1500 cm^{-1} can be assingned to the stretching (ν_{OH}) and the deformation (δ_{OH}) vibrations of interstitial water with strong hydrogen bondings. The absorption bandsd observed between 1000-1200 cm^{-1} can be assigned to the SbOH deformation vibration (δ_{SbOH}), and a band around 600cm^{-1} is assigned to the stretching vibration of SbO and TiO (ν_{SbO},ν_{TiO}).[16] The absorption bands ascribed ν_{OH} and δ_{OH} of Sb-rich TiSbA (Sb/Ti=1.1~2.9) are wider absorption band than those of Sb-poor TiSbA (Sb/Ti=0.11~0.77). This could be due to increasing the strong hydrogen bond with increase in amount of Sb in TiSbA. The absorption band ascribed to δ_{SbOH} at 1200cm^{-1}

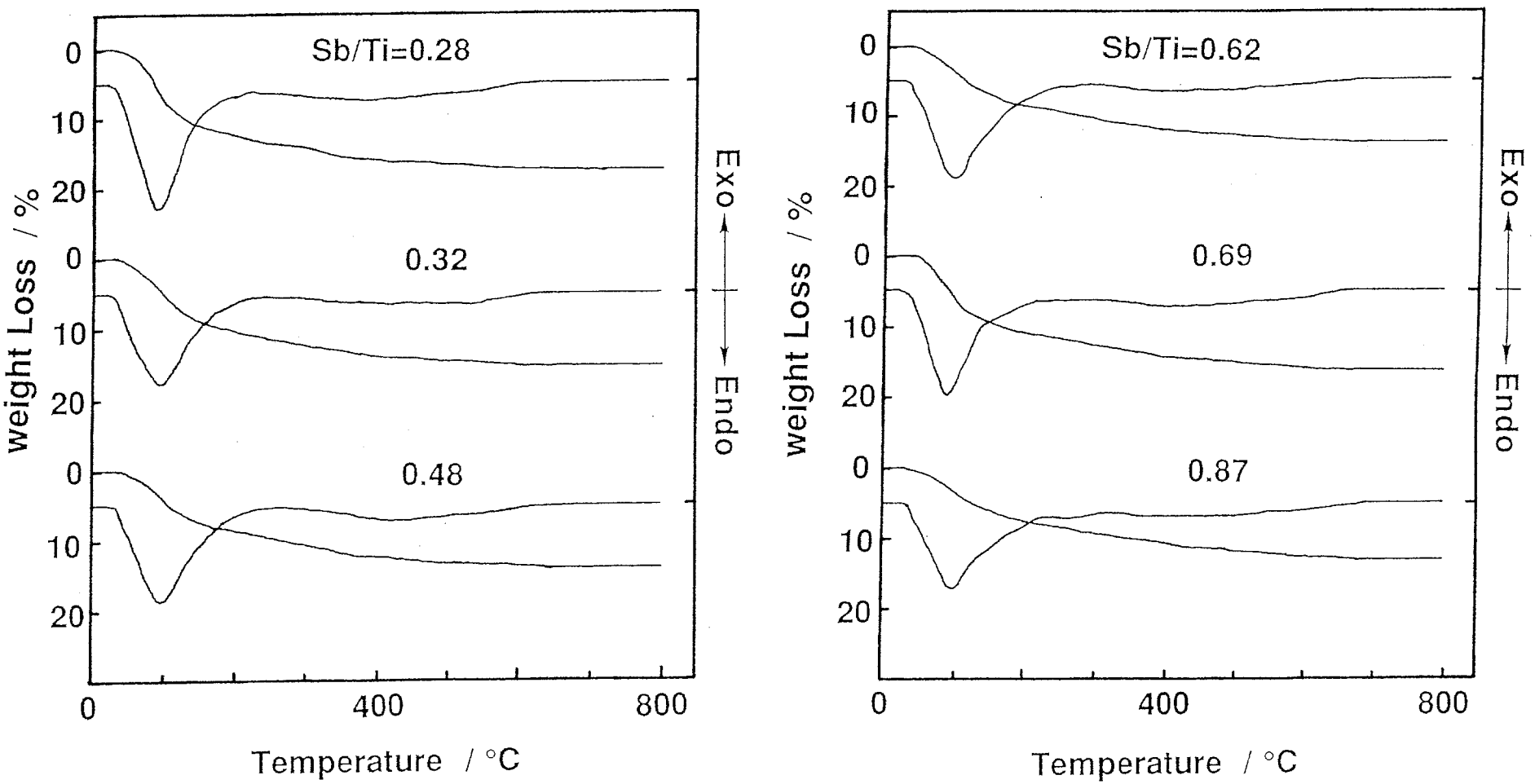

Fig.2-13 TG-DTA Curves for Various Samplesof TiSbA (B)

Heating rate: 10°C / min.

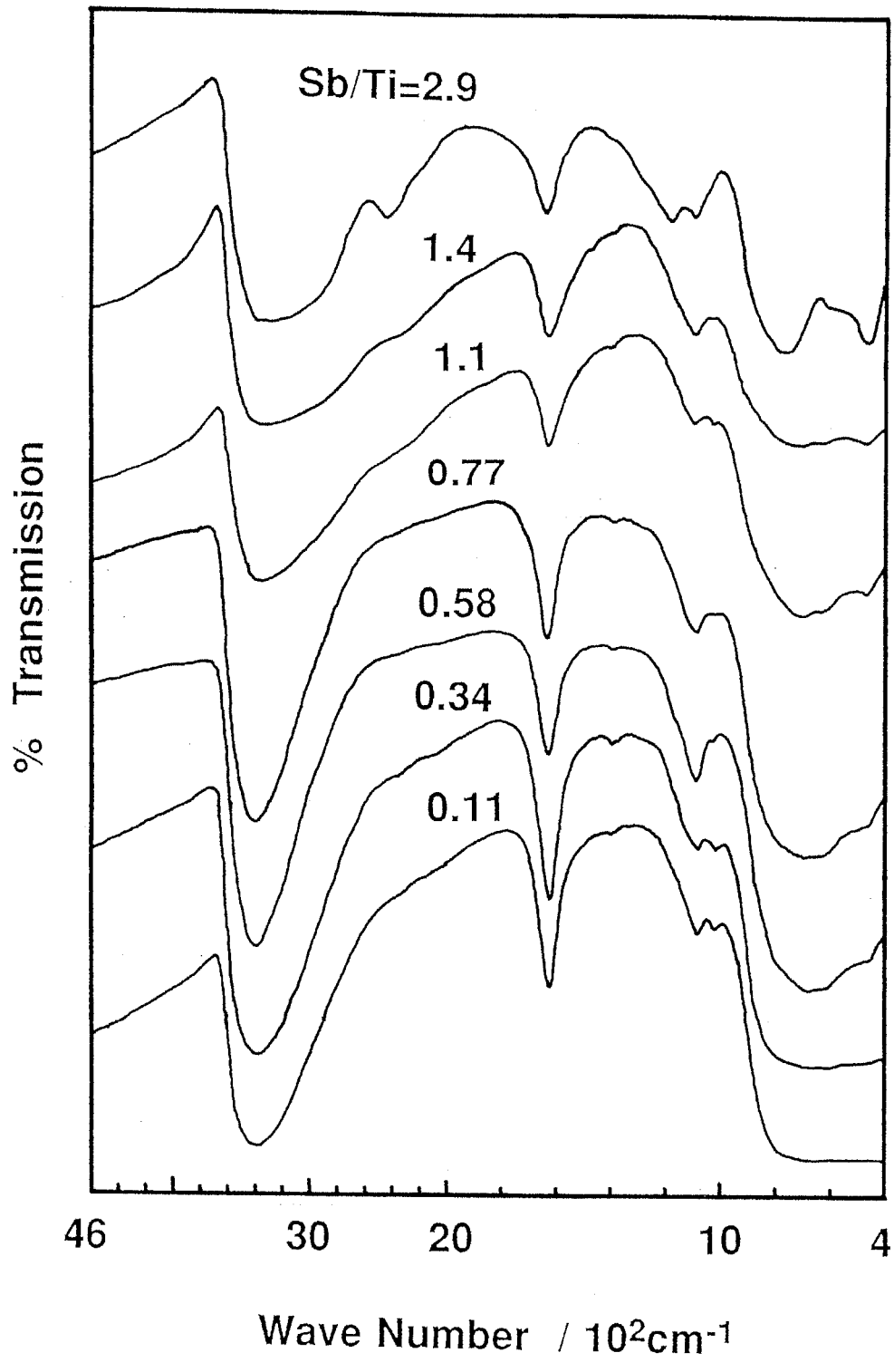

Fig.2-14 IR Spectra for Various Samples of TiSbA (A)

was increasing with the increase in Sb/Ti ratios, on the other hand the band at 1000cm^{-1} was decreasing with the increase in Sb/Ti ratios.

4-5-B IR spectra (B)

Fig.2-15 show the IR spectra of TiSbA with Sb/Ti ratios of 0.28~0.87. The absorption bands ascribed ν_{OH} at 3800~2600cm^{-1} and δ_{OH} at 1800~1500cm^{-1} were for similar all samples. The absorption band ascribed to δ_{SbOH} at 1000cm^{-1} was decreasing with the increase in Sb/Ti ratios. The absorption bands ascribed to ν_{SbO} and ν_{TiO} at 950~600cm^{-1} were similar and those at 600~400cm^{-1} were decreasing with the increase in Sb/Ti ratio.

4-6 EXAFS Study

Fig.2-16 and 17 show the raw data of Sb-K edge EXAFS and their Fourier transforms with the transformation region of k=2.2~13 Å for TiSbA with Sb/Ti ratios of 0.28~0.87. Fig.2-18 show the curve-fitting analysis data of above FT data for r=0.11~0.18 nm and summerized the results of their analyses in Table 2-5, using $LiSbO_3$ (N=6, r=0.1996nm) as reference materials, the results of data analyses for Sb_2O_3, C-SbA and monoclinic antimonic acid (M-SbA) are summerizing in Table 2-6 as comparision substances.

The bond distances Sb-O and coordination number of O atoms around Sb atom were found to be similar value of 0.1989~0.1996nm and 5.6~6.6, respectively, in TiSbA with Sb/Ti ratios of 0.28~0.87. It is known that C-SbA and M-SbA have octahedral coordinated Sb, so it could be found that TiSbA has octahedral coordinated Sb. The bond distance Sb-O is similar to that of Ti-O, so it is supposed that the fixed charge from -OSbOH was distributed homogeneously onto the TiO_2 matrix by the dehydrated condensation, considering the X-ray diffraction patterns show the same as TiO_2 (rutile).

Fig.2-19 show the raw data and the Fourier transforms of Sb-K edge EXAFS for heated sample up to 700°C of TiSbA with Sb/Ti ratios of 0.28~0.87. Fig.2-20 show the curve-fitting analysis data of above FT data for r=0.1-0.2 nm and summerized the results of their analyses in Table 2-6. The parameter were similar to those of the non-heated sample.

4-7 NMR Study

Fig.2-21 and 22 show the NMR spectra measured the relaxation time by inversion

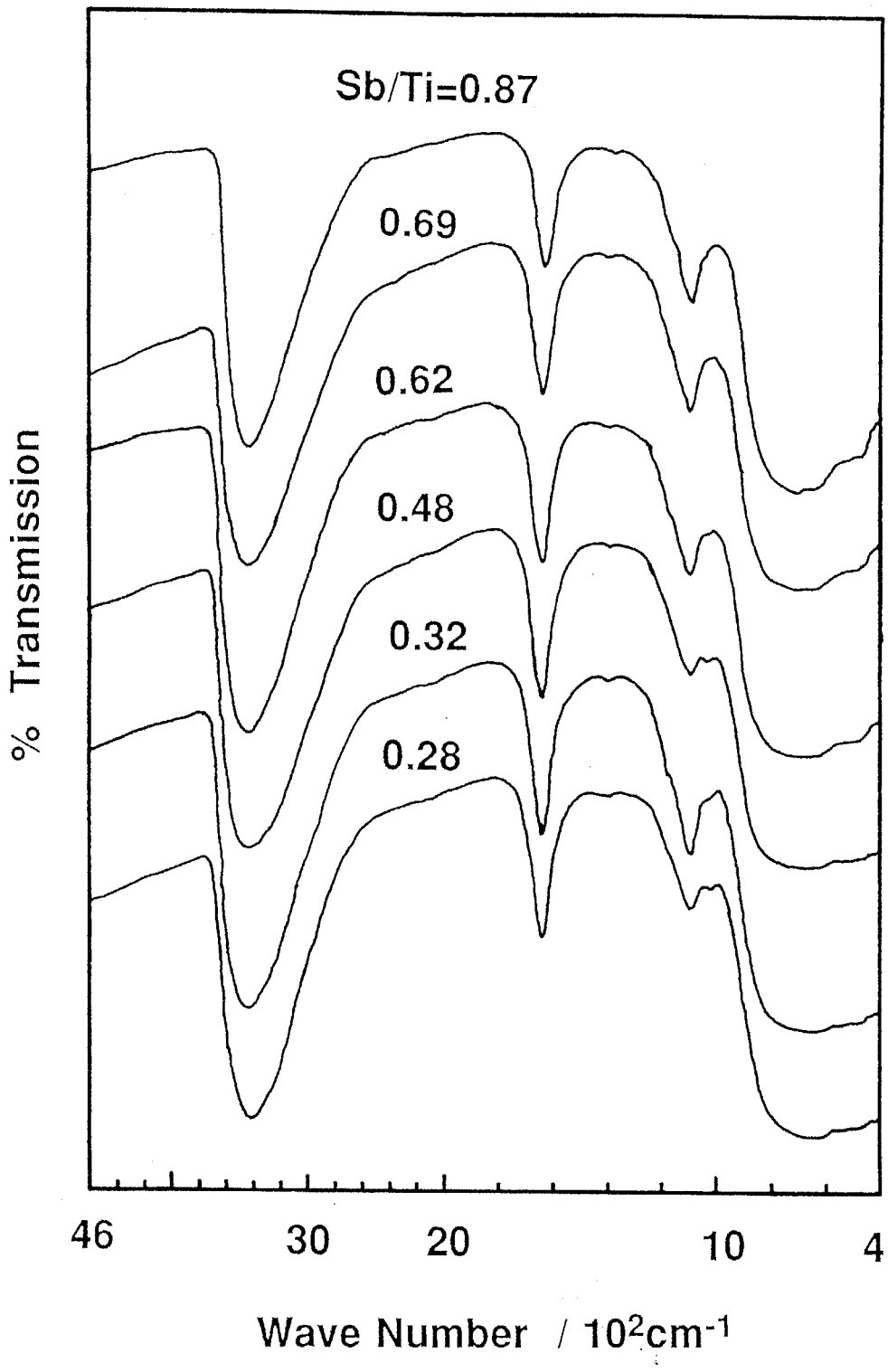

Fig.2-15 IR Spectra for Various Samples of TiSbA (B)

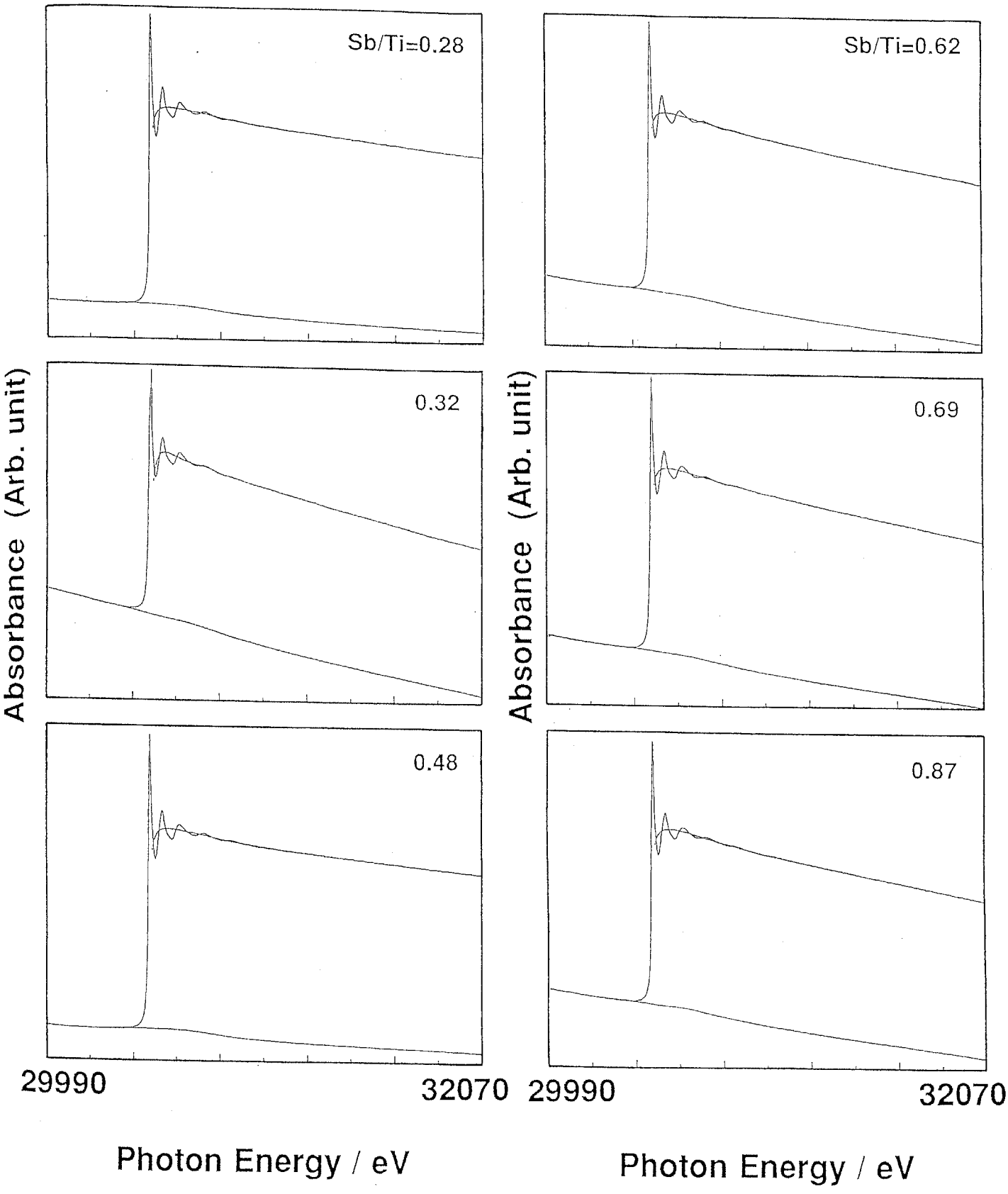

Fig.2-16 EXAFS Spectra for Various Samples of TiSbA

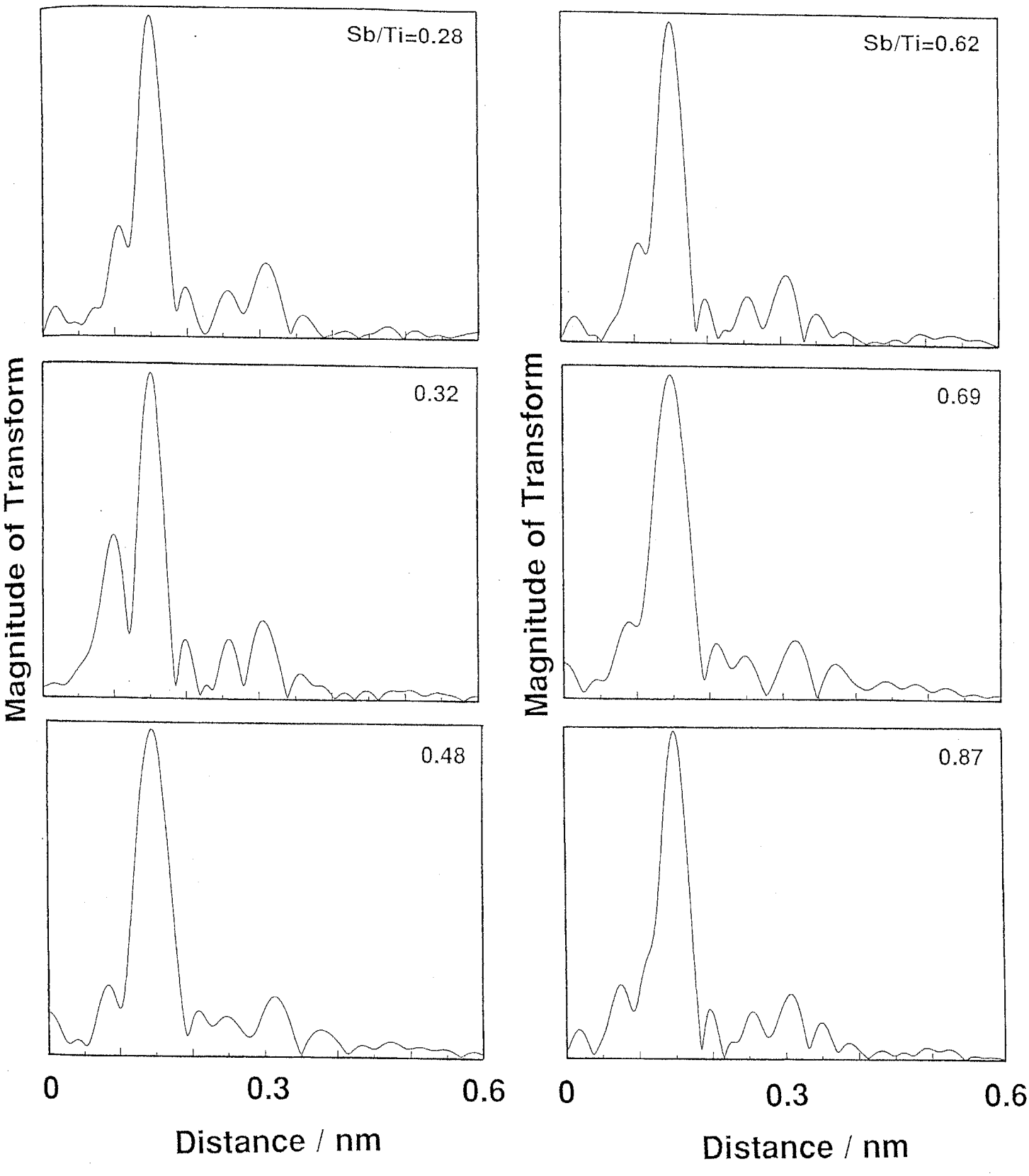

Fig.2-17 Fourier Transform of Sb K-edge EXAFS Data for Various Samples of TiSbA

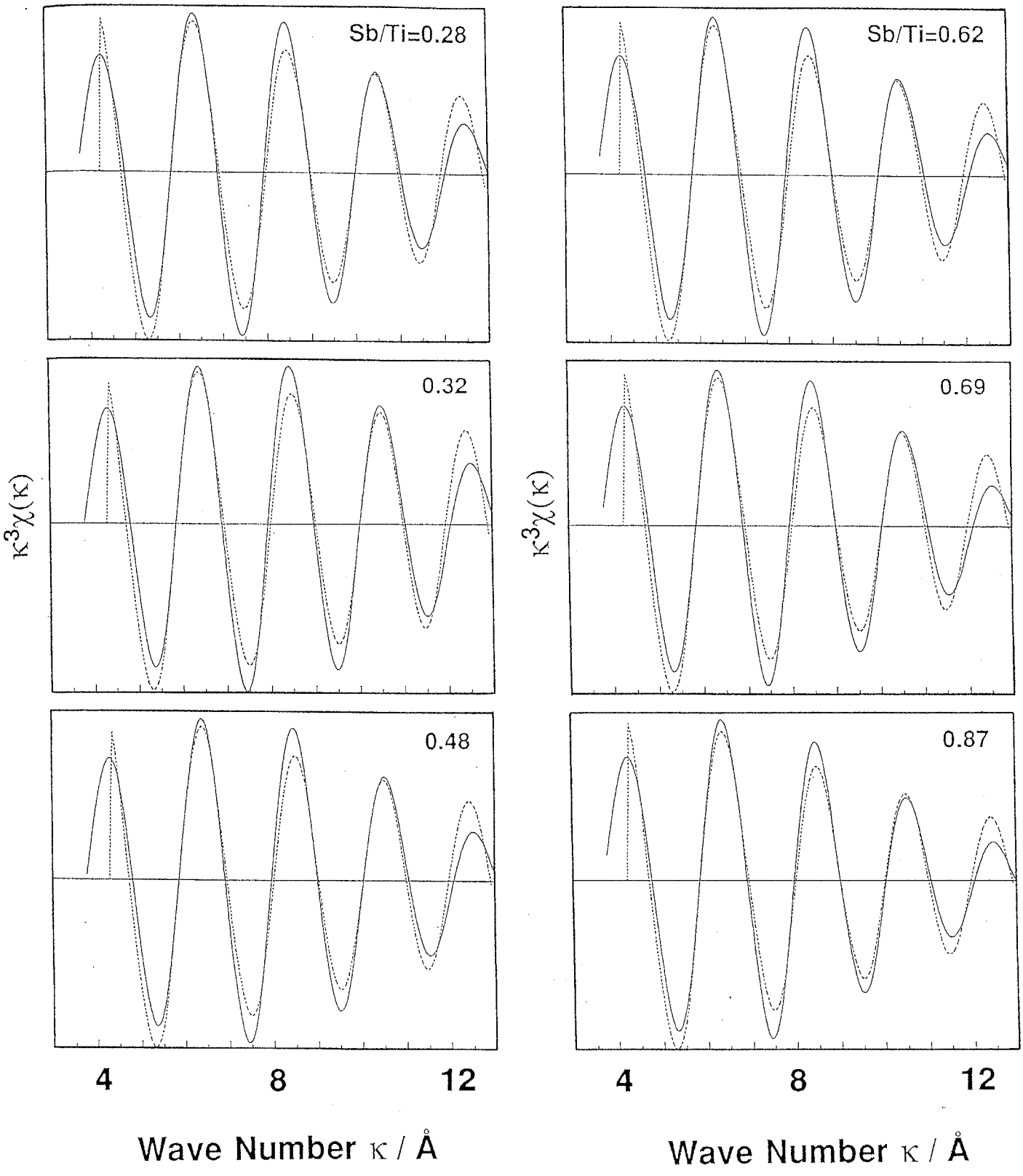

Fig.2-18 Curve Fitting Analyses for Various Samples of TiSbA
Obs.: ———— , Cal.: - - - -

Table 2-5 Curve Fitting Results of Sb K-Edge EXAFS for TiSbA.

Sb/Ti in TiSbA	C.N.	r / nm Sb-O	D.W. / nm	R-Factor
0.28	6.17	0.1996	0.00455	0.0600
0.32	5.55	0.1994	0.00364	0.0692
0.48	5.99	0.1992	0.00456	0.0626
0.62	5.97	0.1990	0.00480	0.0641
0.69	5.92	0.1989	0.00486	0.0634
0.87	6.64	0.1991	0.00578	0.0297

C.N.: Coordination Number, r: Interatomic Distance,

D.W.: Debye-Waller factor, R-factor: Reliability Factor

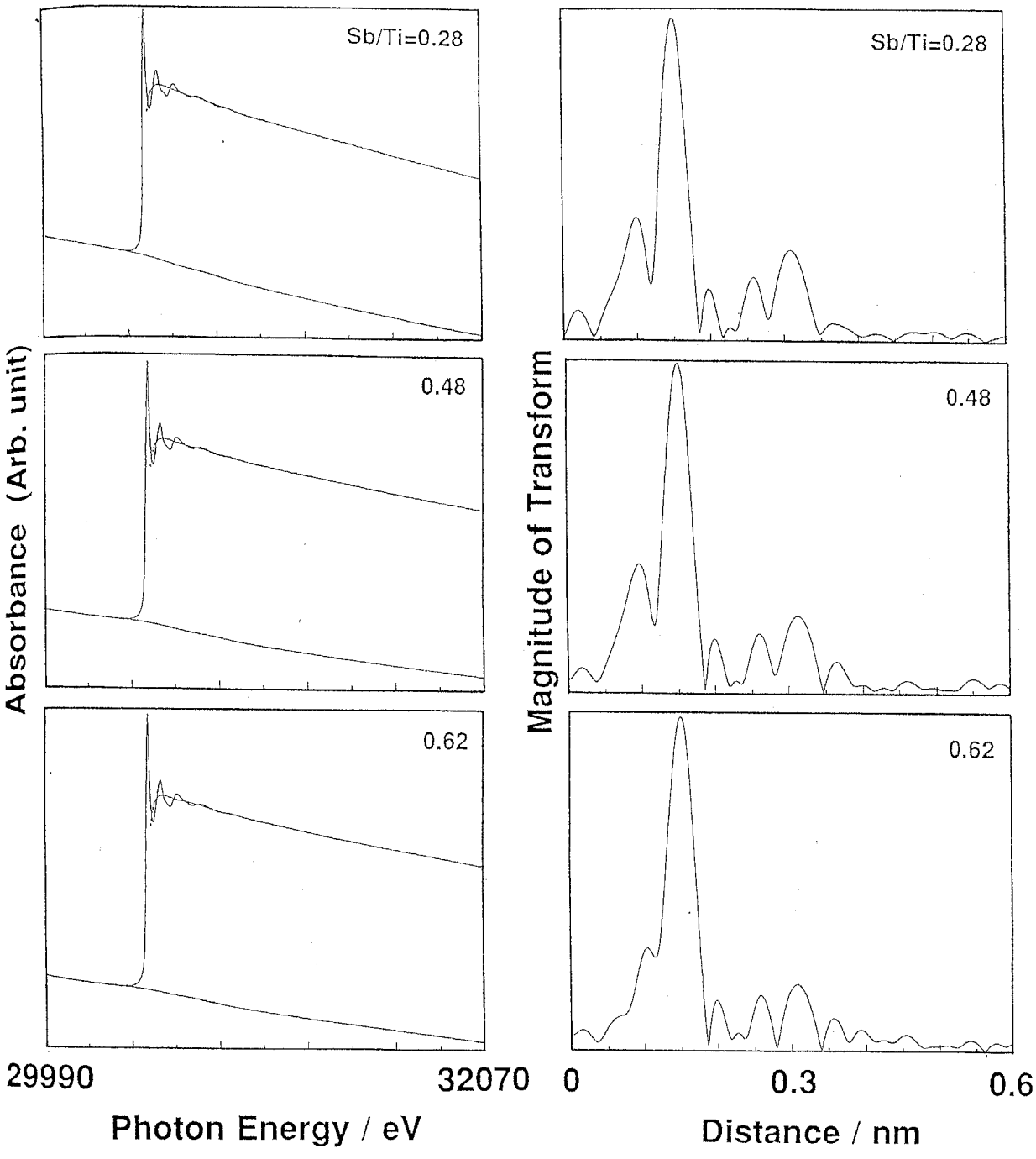

Fig.2-19 EXAFS Spectra and their Fourier Transforms for Various Samples of TiSbA Heated at 700°C

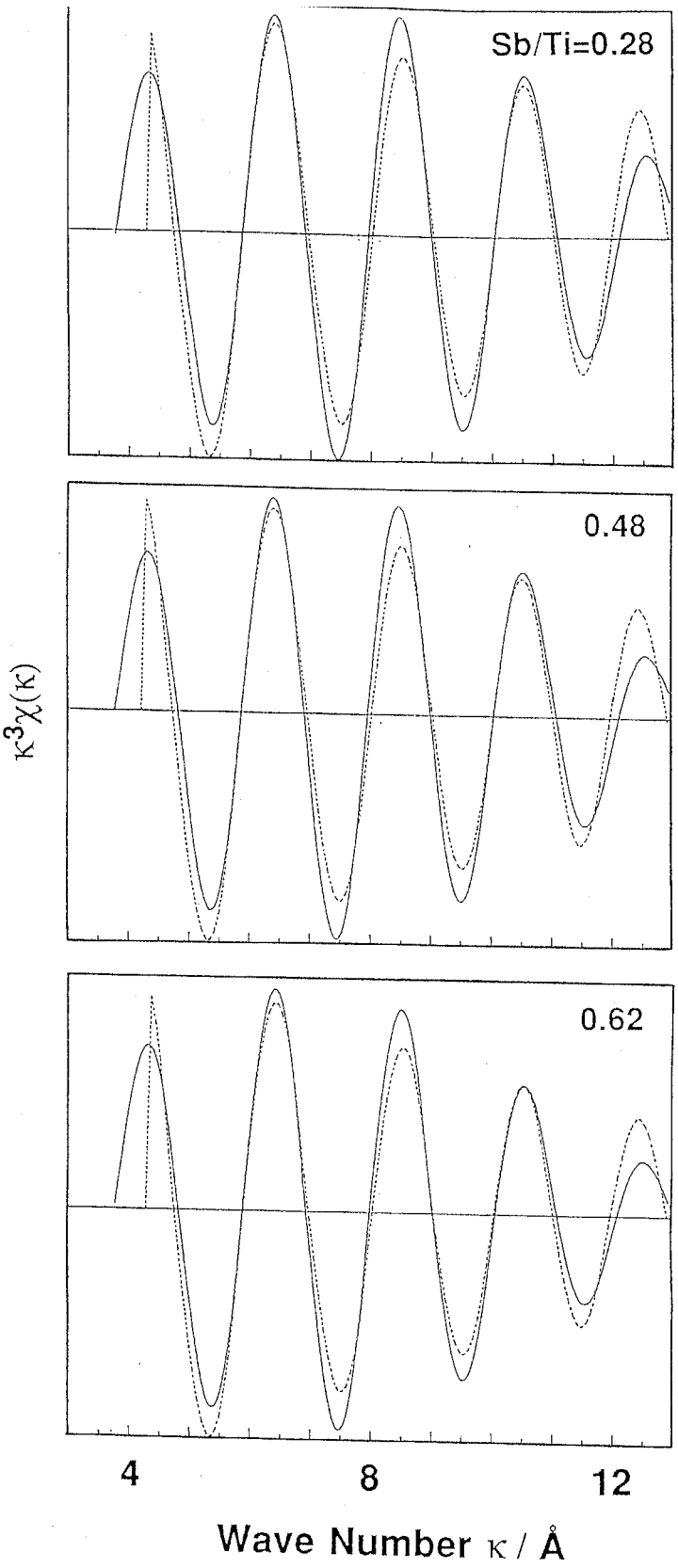

Fig.2-20 Curve Fitting Analyses for Various Samples of TiSbA Heated at 700°C
Obs.: ———— , Cal.: - - - -

Table 2-6 Curve Fitting Results of Sb K-Edge EXAFS for TiSbA Heated at 700°C and Sb Compounds.

Sb/Ti in TiSbA	C.N.	r / nm Sb-O	D.W. / nm	R-Factor
0.28	5.32	0.1990	0.00362	0.0687
0.48	5.44	0.1990	0.00374	0.0704
0.62	5.83	0.1991	0.00456	0.0661
$LiSbO_3$*	6	0.1996	0.00442	0.0627
$HSbO_3$	5.23	0.1972	0.00607	0.0510
C-SbA	5.83	0.1973	0.00513	0.0617
Sb_2O_3	3.39	0.1997	0.00453	0.0577

* Reference Material

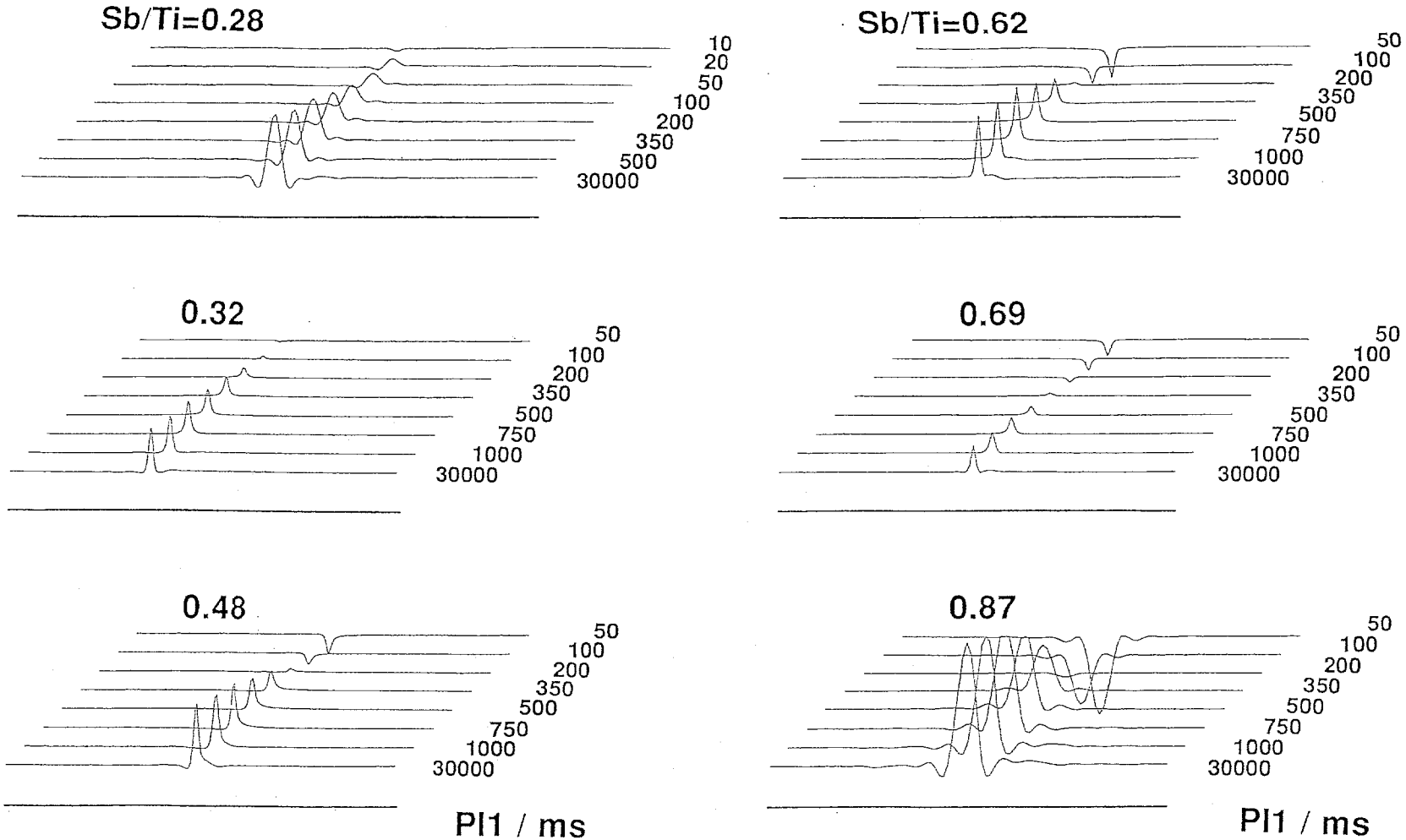

Fig.2-21 Real Spectra of ^{1}H in Various samples of TiSbA for T_1 mesurement

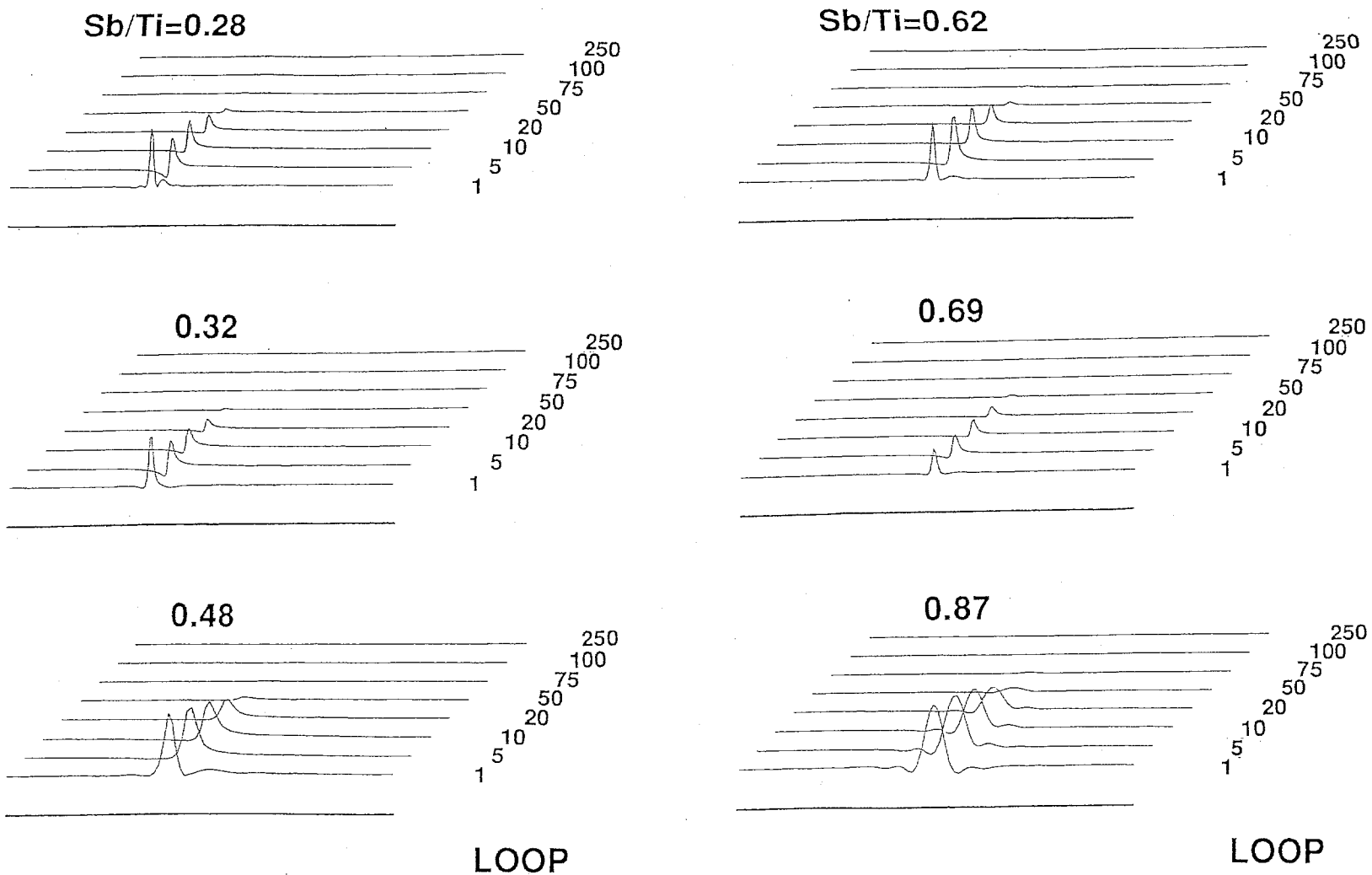

Fig.2-22 Real Spectra of ^{1}H in Various samples of TiSbA for T_2 mesurement

recovery method and CPMG method for T_1 and T_2, respectivery. Fig.2-23 shows the relaxation time T_1 and T_2 of ^1H for TiSbA with Sb/Ti = 0.28~0.87. T_1 and T_2 are increasing with increase in Sb/Ti ratio, so TiSbA with high Sb/Ti ratio has more motional free water like liquuid phase water in accordance with BPP theory.[17] Fig.2-24 shows the NMR spectra of ^1H in TiSbA for 500MHz, they could be concluded that TiSbA have 2 kinds of protons. The large peak is H of free water and small peak is H of OH for relation to ion exchange. This result is good agreement with two dehydration peak around 100°C and 200~600°C in TG-DTA curves. The low temperature and large peak could be due to the free water and the high temperature, long and small small peak could be due to exchangeable OH.

4-8 Structural model of TiSbA

It has been discussed that TiSbA has a tetragonal structure with a lattice parameter of a_0= 0.466nm and c_0= 0.295nm. TiSbA has a rutile type structure with partially substitution TiO_6 octahedron with SbO_6 octahedron. This structure is given in Fig.2-25. The framework of TiSbA is not variable with Sb/Ti ratio, so that the ion exchange selectivity of various TiSbA could be due to the H_2O or OH in TiSbA. To keep electric neutral Sb^{5+} substitute from Ti^{4+} and accompany with OH^-. The exchangeable H could be due to released from OH.

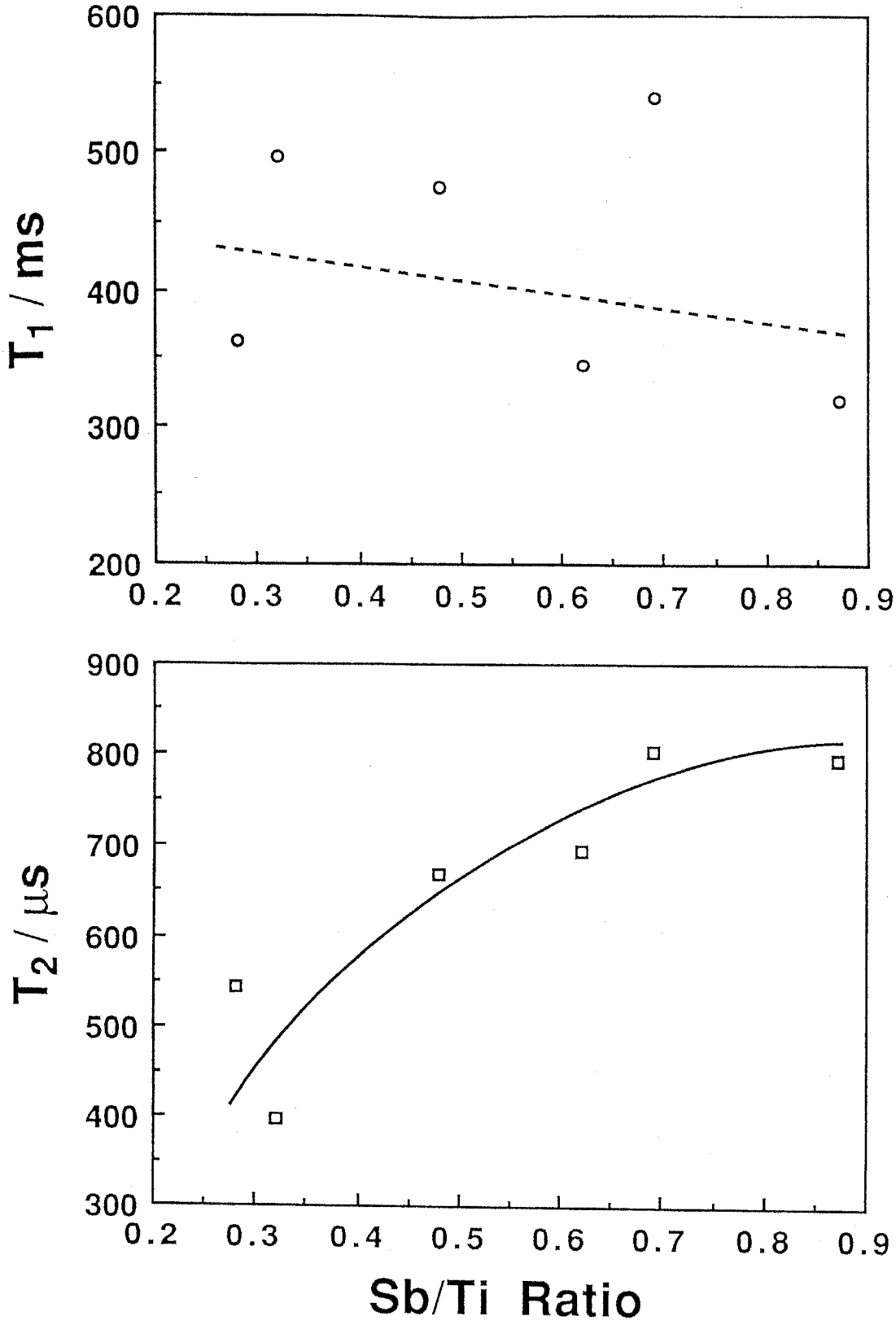

Fig.2-23 The Relaxation Time on TiSbA with Different Ratios of Sb/Ti

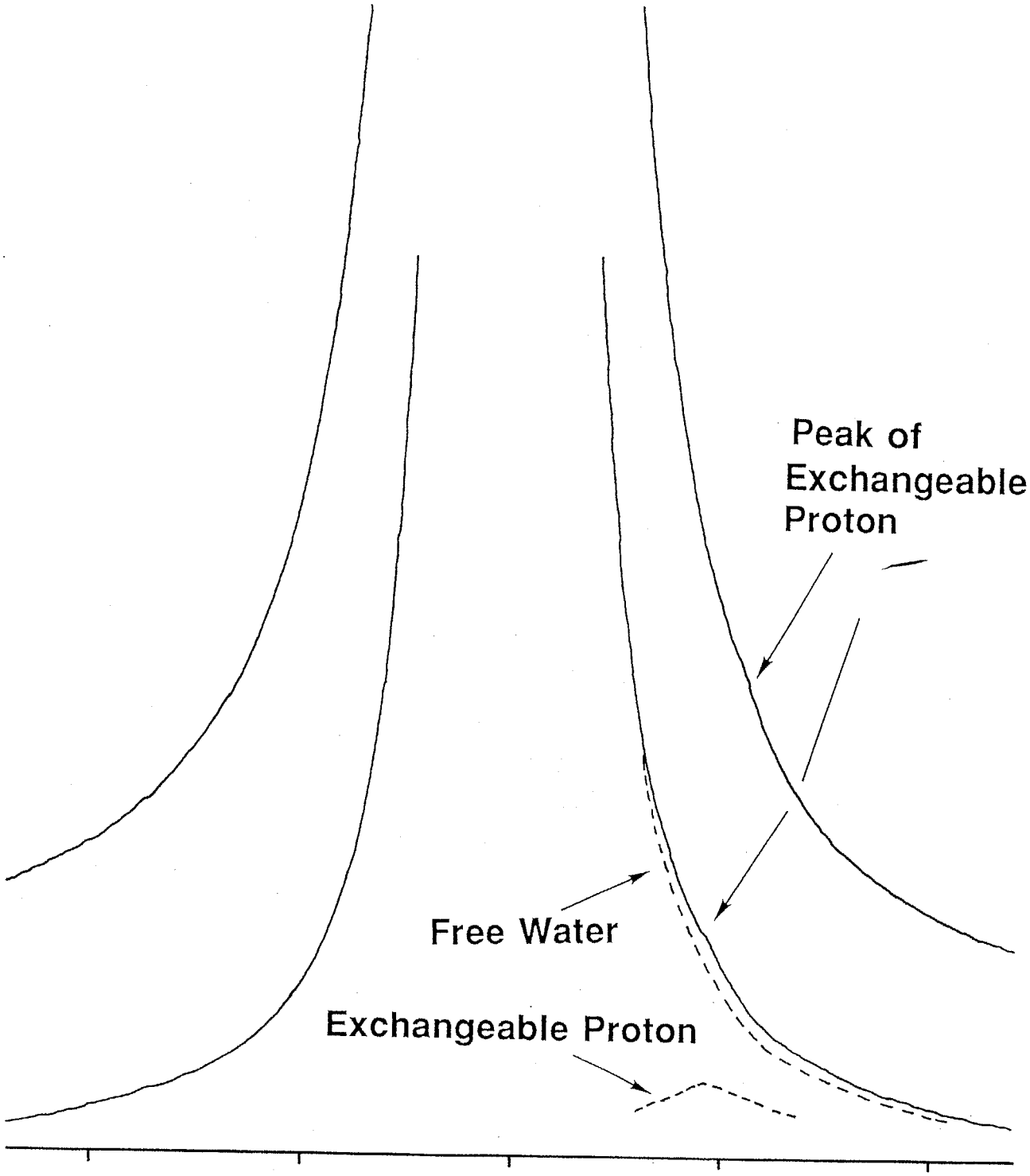

Fig.2-24 Foots of ^{1}H NMR Spectra of TiSbA (Sb/Ti=0.28 and 0.62) with their Simulation Curves
Observed: ———— , Simulated: - - - - -

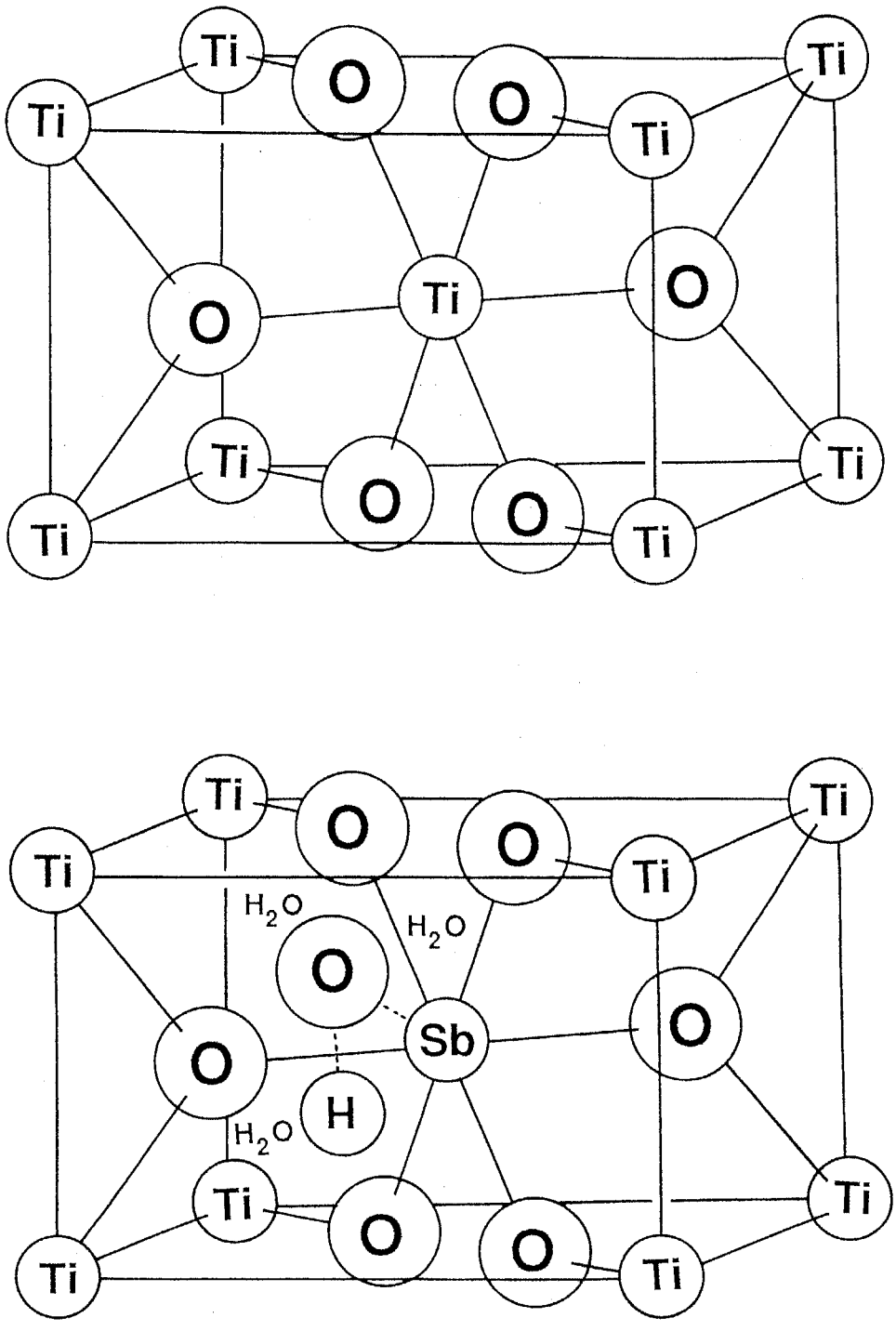

Fig.2-25 Schematic Representation of the Conceptual View for TiO_2 (Rutile) and TiSbA

5.REFERENCES

1. M. Abe, Bull. Chem. Soc. Jpn., *42,* 2683 (1969).
2. R. Chitrakar and M. Abe, Solvent Extr. Ion Exch., *7,* 721 (1989).
3. R. Chitrakar and M. Abe, Mat. Res. Bull., *23,* 1231 (1988).
4. T. Suzuki, M. Miyake, Y. Yoshikawa and T.yoshida, Nippon Kaisui Gakkaishi, *44,* 185 (1990).
5. J. S. Gill and S. N. Tandon, J. Radioanal. Chem., *20,* 5 (1974).
6. M. Qureshi and V. Kumar, J. Chem. Soc. A, 1488 (1970).
7. M. Abe, R. Chitrakar, M. Tsuji and K. Fukumoto, Solvent Extr. Ion Exch., *3,* 149 (1985).
8. P. A. Lee, P. H. Citrin, P. Eisenberger and B. M. Kincaid, Rev. Mod. Phys., *53,* 769 (1981).
9. B. K. Teo, EXAFS: Basic Principles and Data Analysis, Springer-Verlag, Berlin, 1986.
10. B. K. Teo and D. C. Joy (Eds.), EXAFS Spectroscopy, Plenum Press, New York, 1981.
11. J. Wong, F. W. Lytle, R. P. Messmer and D. H. Maylotte, Phys. Rev. B, *30,* 5596 (1984)
12. B. Hannoyer, J. Dürr, G. Calas, J. Petiau and M. Lenglet, Mat. Res. Bull., *17,* 435 (1982)
13. M. Abe and T. Ito, Nippon Kagaku Zasshi, *86,* 1259 (1965).
14. M. Abe and T. Ito, Bull. Chem. Soc. Jpn., *41,* 333 (1968).
15. M. Abe and N. Furuki, Solvent Extr. Ion Exch., *1,* 97 (1983).
16. M. Abe and T.Ito, Bull. Chem. Soc. Jpn., *41,* 2366 (1968).
17. N. Bloembergen, E. M. Purcell and R. V. Pound, Phys. Rev., *73,* 679 (1948).

CHAPTER 3
ION-EXCHANGE SELECTIVITIES OF TRIVALENT METAL IONS ON TITANIUM ANTIMONATE

1. INTRODUCTION

Abe et al.[1,2] have studied on the ion exchange properties of the titanium antimonate (TiSbA) for alkali metal ions, alkali earth metal ions and divalent transition metal and lead ions. The selectivity of microamounts is; $Na^+ < K^+ < Rb^+ < Li^+ < Cs^+$ for alkali metals,[3-5] $Mg^{2+} < Ca^{2+} < Sr^{2+} < Ba^{2+}$ for alkaline earth metals[3] and $Mn^{2+} < Ni^{2+} < Cd^{2+} < Zn^{2+} < Co^{2+} < Cu^{2+} < Fe^{2+} < Pb^{2+}$ for divalent metal ions on TiSbA.[6] Qureshi and Kumar have studied on the ion exchange property of titanium antimonate prepared by the hydrolysis of $TiCl_4$ and $SbCl_5$ with NH_3 solution.[7] The selectivity at pH 2 is $Al^{3+} < Ga^{3+} < Pr^{3+} < Y^{3+} < In^{3+} < Sm^{3+} < Sc^{3+} = Ce^{3+} < La^{3+}$ for the sample of Sb/Ti=1, $Al^{3+} < Sc^{3+} < Y^{3+} < Ga^{3+} < Sm^{3+} < Pr^{3+} < In^{3+} < La^{3+} < Ce^{3+}$ for the sample of Sb/Ti=0.43, $Al^{3+} < Y^{3+} < Pr^{3+} < Sc^{3+} < Sm^{3+} < La^{3+} < Ce^{3+} < Ga^{3+} < In^{3+}$ for the sample of Sb/Ti=0.28. But the systematic study on the ion exchange property of trivalent metal ions on titanium antimonate free from NH_3 has not been reported. It is expected that a titanium antimonate prepared without using NH_3 solutionwill show the different selectivity for trivalent metal ions.

The separation of gallium from alminium is important in analytical chemistry and removal of gallium from the waste solution with Bayer process. The chromatographic separation of Ga^{3+} and In^{3+} from Al^{3+} is difficult on organic cation exchangers because of low separation factor for this pair.

The present study was carried out to describe the ion exchange property for microamout of some trivalent metal ions (Al^{3+}, Ga^{3+}, In^{3+}, Cr^{3+} and Fe^{3+}) on TiSbA prepared with different antimony and titanium ratios (Sb/Ti) without using NH_3 solution, and the chromatographic separations were carried out for group 13 (3B) elements (Al^{3+}, Ga^{3+} and In^{3+}). And the ion exchange property for microamout of some rare earth metal ions (Y^{3+}, La^{3+}, Pr^{3+}, Nd^{3+}, Eu^{3+}, Gd^{3+} and Yb^{3+}) was studied on TiSbA prepared with different antimony and titanium ratios (Sb/Ti).

2. THEORY

2-1 Ion-exchange ideality

When an exchanger (solid phase) is equilibrated with an electrolyte solution, the ion exchange reaction of trivalent metal ions / H^+ exchange system on an exchanger in H^+-form can be represented by the following expression,

$$3\,\overline{H^+} + M^{n+} \rightleftarrows \overline{M^{n+}} + 3H^+ \quad \text{------(1)}$$

where bar refers to exchanger phase and M^{3+} is the trivalent metal ions.

The thermodynamic equilibrium constant K of the above reaction can be defined as,

$$K = \frac{[H^+]^3\ \overline{X}_M\ \gamma_H^3\ f_M}{[M^{3+}]\ \overline{X}_H^3\ \gamma_M\ f_H^3} \quad \text{------(2)}$$

where $[H^+]$ and $[M^{3+}]$ are the molalities of HNO_3 and metal nitrate in solution, and γ_H and γ_M are the ionic activity coefficients of H^+ and M^{3+} in solution. $\overline{X}_H$ and $\overline{X}_M$ are the equivalent fractions of the exchanging H^+ and M^{3+} in the exchanger phase respectively. Whereas f_H and f_M are the activity coefficients of H^+ and M^{3+}, respectively, in the exchanger phase. The standard states chosen are such that f_H and f_M are unity when the exchanger is in its pure H^+ and pure M^{3+} forms, respectively, and γ_H and γ_M are unity when the $[H^+]$ and $[M^{3+}]$ approach zero.

In the following treatment molalities $[H^+]$ and $[M^{3+}]$ are replaced by the equivalent ion fractions:

$$X_M = \frac{3[M^{3+}]}{3[M^{3+}] + [H+]}\ ,\ X_H = \frac{[H+]}{3[M^{3+}] + [H^+]} \quad \text{-----(3)}$$

$$\overline{X}_M = \frac{3[\overline{M}^{3+}]}{3[\overline{M}^{3+}] + [\overline{H}^+]}\ ,\ \overline{X}_H = \frac{[\overline{H}^+]}{3[\overline{M}^{3+}] + [\overline{H}^+]} \quad \text{-----(4)}$$

$$X_M + X_H = 1\ ,\ \overline{X}_M + \overline{X}_H = 1 \quad \text{-----(5)}$$

The total normality (TN) and the theoretical or total capacity (TC) are kept constant throughout the ion-exchange process:

$$3[M^{3+}] + [H^+] = TN,\quad 3[\overline{M}^{3+}] + [\overline{H}^+] = TC \quad \text{-----(6)}$$

By using these definitions, Eq.(2) becomes

$$K = K_H^M \frac{f_M}{f_H^3} \quad \text{-----(7)}$$

where K_H^M is the corrected selectivity coefficient an refers to

$$K_H^M = \frac{\bar{X}_M X_H^3 \gamma_H^3}{\bar{X}_H^3 X_M \gamma_M} 3 (TN)^{3-1} \quad \text{-----(8)}$$

The distribution coefficient Kd, of M^{3+} is defined by,

$$Kd = \frac{[\overline{M^{3+}}]}{[M^{3+}]} = \frac{TC \bar{X}_M}{TN X_M} \quad \text{-----(9)}$$

The K_H^M value at the infinitesimal exchange is important for basically interpreting and predicting the ion-exchange behavior. It can be expressed using Kd as follows.[8,9] Eqs. (5) and (8) are combined to give the corrected selectivity coefficient:

$$K_H^M = \frac{\bar{X}_M (1-X_M)^3}{(1-\bar{X}_M)^3 X_M} \Gamma\eta \quad \text{-----(10)}$$

where $\eta = 3(TN)^{3-1}$, $\Gamma = \gamma_H^3/\gamma_M$

Therefore:

$$(K_H^M)_{X_M, \bar{X}_M \to 0} = (\frac{\bar{X}_M}{X_M})_{X_M, \bar{X}_M \to 0} (\Gamma\eta)_{X_M, \bar{X}_M \to 0} \quad \text{-----(11)}$$

On inserting Eq.(9) in Eq.(11),

$$(K_H^M)_{X_M, \bar{X}_M \to 0} = (\frac{TC}{TN} Kd)_{X_M, \bar{X}_M \to 0} (\Gamma\eta)_{X_M, \bar{X}_M \to 0} \quad \text{-----(12)}$$

Thus, the corrected selectivity coefficient at infinitesimal exchange can be determined by measuring Kd at infinitesimal exchange. In this chapter, discussions will be given using Kd value which parallels the corrected selectivity coefficient in infinitesimal exchange. Taking the logarithm of Eq.(12) and using Eq.(6),

$$\log(Kd)_{X_M,\ \bar{X}_M \to 0} = \log\frac{TC}{3} + \log(\frac{1}{\Gamma}K_H^M)_{X_M,\ \bar{X}_M \to 0} - 3\ \log[HNO_3] \quad \text{-----(13)}$$

The former two terms on the right hand can be approximated as a constant, and therefore Kd determination at the very small $\bar{X}_M$ in the ion-exchange process will show that the slope of plot of log $(Kd)_{X_M,\bar{X}_M \to 0}$ vs. log $[HNO_3]$ is -3.

As the best approximation, the distribution coefficients of various metal ions are compared at a constant initial concentrations of 1×10^{-4} mol dm^{-3}.

2-2 Ion-exchange chromatography

Chemical separations commonly occur as a result of the distribution of the chemical components between two phases of matter. Chromatography is also a method of continuous chemical separation. Types of different chromatographies[10] are characterized by the nature of the stationary and mobile phases. In ion-exchange chromatography, a small amount of sample is introduced as a thin band at the top of ion-exchange column. The adsorbed ions are then eluted down the column by a suitable eluent in a series of sorption-desorption steps. Each ion then travels down the column at different rates depending on the selectivity coefficient and separation factor of the respective ion and emerge as distinct band. If the selectivity coefficients of the sample ions differs sufficiently the elution bands are more clear (i.e. with no overlaping). From the plate theory, the following correlation holds between the Kd values and the peak elution volume V_{max},

$$V_{max} = I + M\ Kd \quad \text{---------(14)}$$

where I and M are interstitial volume and weight of the exchanger in the column, respectively. In an extension of the plate theory of Martin and Synge[11] and Beukenkamp et al,[12] the Vmax in equation 14 can also be represented in terms of the distribution ratio (C) in a solution as follows,

$$V_{max} = I\ (1 + C) \quad \text{----------(15)}$$

If the elution curves show gaussian distribution, the total number of theoretical plates p in the column are evaluated[13] by the equation,

$$p = \frac{2C}{1 + C} \times \frac{V_{max}}{V_a - V_{max}} \quad \text{-----(16)}$$

where V_a is the volume eluted when the concentration of solute in the eluate times e (base of the natural system of logarithms) is equal to the value of the maximum concentration of the solute in eluate (i.e. concentration of solute × e = max. concentration). The importance of the sorption isotherms in chromatography lies in their shapes and in magnitudes of slopes of lines drawn through points corresponding to the amounts of solute introduced into the system. The shape of elution curve depends on the ion-exchange isotherm.[14] In linear isotherm (Fig.3-1a) the isotherm is a straight line with a constant slope of unity. Under this condition the concentration of the solute in the stationary phase is directly proportional to the concentration of the solute in the mobile phase. Chromatographic elution band will therefore be nearly symmetrical and the retention time will be independent of the concentration as shown by the dotted lines.

In the Langmuir type isotherm,[15] (Fig.3-1b) the band will show nearly sharp front and rear tailing. In such a case the Kd of metal ion is inversely dependent on the initial metal ion concentration. Moreover depending on the amount injected, the band maximum will vary. For example the slope of line 1 (Fig.3-1b) is greater than that of line 2 and so on. The retention time of the solute peak maximum in the former case will be longer than the latter. That is, the retention time of the peak maximum decreases as the amount injected is increased. Solutes giving to anti-Langmuir[15] type isotherm (Fig.3-1c) will show tailing front and sharp rear and the retention time will increase as the amount injected is increased. In this case, the Kd value is directly proportional (dependent) to initial metal ion concentration.

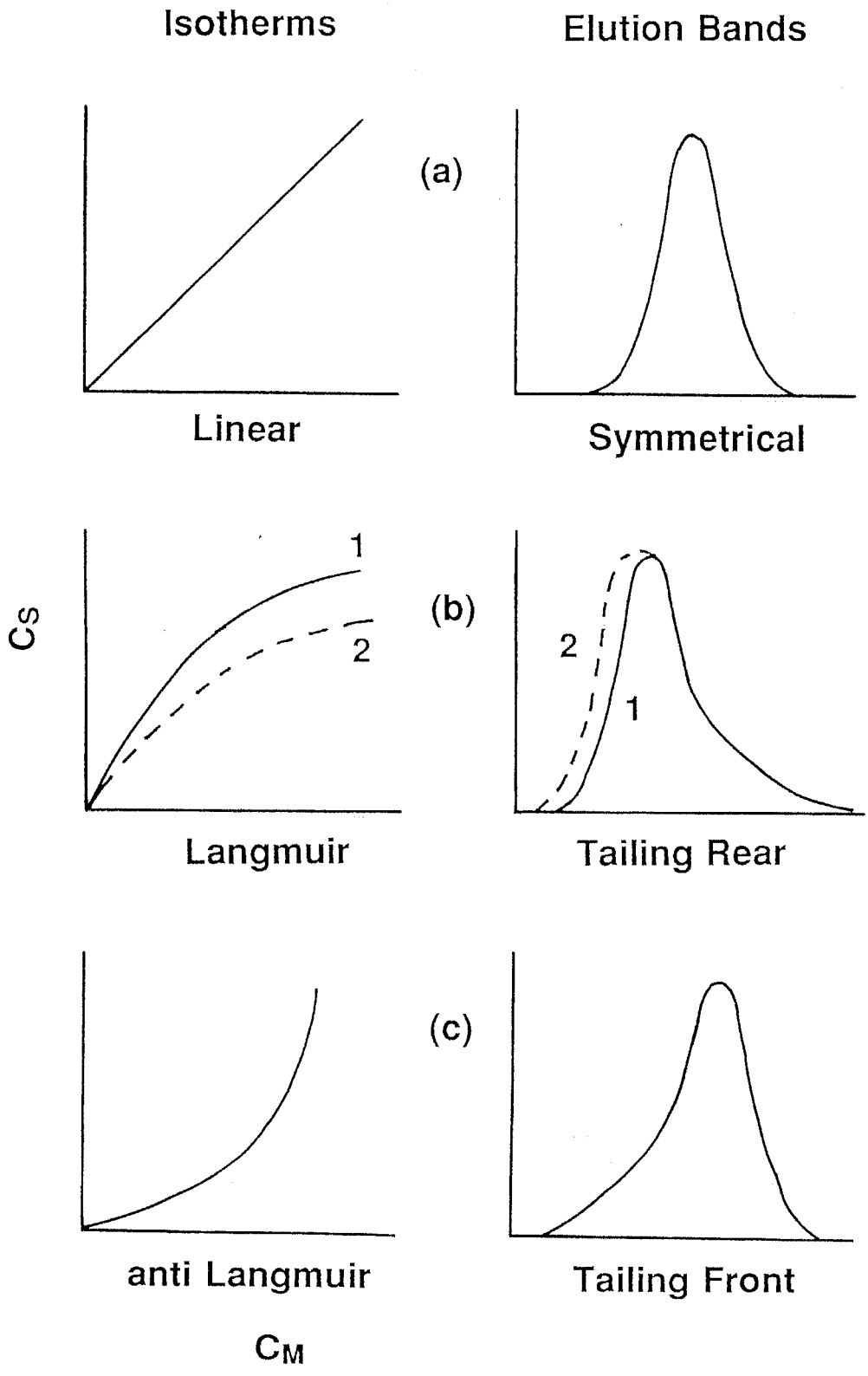

Fig.3-1 Three Possible Ion-exchange Isotherms and Shapes of Respective Elution Bands
C_S: $[M^+]$ in stationary, C_M: $[M^+]$ in mobile phase

3. EXPERIMENTAL

3-1 Reagents

The reagents used were all of analytical grade reagents supplied by Wako Chemical Co. Ltd. (Japan).

3-2 Sample solutions

Standard solutions containing 0.1M (1M = 1mol dm^{-3}) metal ion in 0.1M nitric acid media solution were prepared by dissolving weighed amount of each high purity (>99.9%) metal, aluminium, gallium and indium in about 2M HNO_3 solution, and iron(III) nitrate nona-hydrate and chromium(III) nitrate hexa-hydrate in 0.1M HNO_3 solution.

Standard solutions containing 0.1M metal ion in 0.1M nitric acid media solution were prepared by dissolving weighed amount of each high purity metal oxide, La_2O_3, Nd_2O_3, Eu_2O_3 and Yb_2O_3 in about 1M HNO_3 solution, and $Y(NO_3)_3 \cdot 6H_2O$, $Pr(NO_3)_3 \cdot 6H_2O$ and $Gd(NO_3)_3 \cdot 6H_2O$ in 0.1M HNO_3 solution.

3-3 Distribution coefficients (Kd)

The values of distribution coefficient (Kd) of trivalent metal ions were determined as follows; 0.10g of TiSbA in the hydrogen ion form was equlibrated with 10.0cm^3 of the solution containing 1×10^{-4}M metal ions in nitric acid solutions of different concentrations at 30±1°C with intermittent shaking. The concentration of the metal ions in the solid and liquid phases were deduced from the concentration relative to the initial concentration in the solution. The Kd values were calculated after attainment of the equilibrium from the following equation (that is same as Eq.(9)):

$$Kd = \frac{amount\ of\ metal\ ions\ in\ exchanger}{amount\ of\ metal\ ions\ in\ solution} \times \frac{cm^3\ of\ solution}{g\ of\ exchanger}$$

The concentration of Fe^{3+} and In^{3+} were determined by Varian Techtron 1100 atomic absorption spectrometer, and that of Al^{3+}, Ga^{3+}, Cr^{3+} and all rare earth metal ions were determined by ICP-AES.

3-4 Ion exchange separation

Mutual separations of Al^{3+}, Ga^{3+} and In^{3+} were carried out on a relatively small

column (3cm × 0.5cm i.d.) of TiSbA (Sb/Ti=0.77) and TiSbA (Sb/Ti=0.34). A mixed solution containing 20μmol of Al^{3+} and 2μmol of Ga^{3+} and In^{3+} was loaded on the top of the column and the eluted with HNO_3 solution at different concentrations.

The effluents were collected to determined the metal concentrations by using a drop-counting type fraction collector (Ohtake Works, Model UM-160). The effluents were charged continuously by a high pressure pump (Nihon Seimitsu Kagaku, Model NSP-800-50DX).

4. RESULTS AND DISCUSSION

4-1 Time dependence for adsorption

The time dependence of adsorption of the trivalent metal ions on TiSbA in the nitric acid media was measured qualitatively in order to determine the equilibrium distribution coefficients. The ion exchange reaction of trivalent metal ions were relatively slow, therefore the time required to attain equilibrium for Al^{3+} and Cr^{3+} was 20 days, and that for Ga^{3+}, In^{3+} and Fe^{3+}, approximately 1 month (Fig.3-2). For lithium, cesium and divalent transition metal ions studied on TiSbA,[3,6] slow rates of adsorption were also reported. The ion exchange reaction of rare earth metal ions were relatively slow too, therefore the time required to attain equilibrium for Y^{3+}, La^{3+}, Eu^{3+} and Yb^{3+} was 20 days (Fig.3-3).

4-2 Ion-exchange selectivity

The Kd values of Al^{3+}, Ga^{3+} and In^{3+} obtained in a nitric acid media (0.2M HNO_3) were plotted against the Sb/Ti ratio of TiSbA (Fig.3-4). The maximum Kd values were observed for both Al^{3+}, Ga^{3+} and In^{3+} at Sb/Ti ratio of 0.77, and the Kd values increased with an increase in the Sb/Ti ratio from 0.34 to 0.77 and a decrease in the Sb/Ti ratio from 1.4 to 0.77. For alkali metal ions except for Na^+ studied on TiSbA, the maximum Kd values at Sb/Ti ratio of 0.64 were also reported.[3] A small Kd value of Al^{3+} was obtained at Sb/Ti=0.34. The Al^{3+}-Ga^{3+} separation factor was estimated to be 4.8×10^3 on TiSbA at Sb/Ti=0.34. The Al^{3+}-In^{3+} and Al^{3+}-Ga^{3+} separation factors (α) were plotted against the Sb/Ti ratio of TiSbA in Fig.3-5 (a) and (b).

Figures 3-6 and 3-7 show the plots of log Kd vs. log [HNO_3] at Sb/Ti=0.77 and 0.34, respectively. As can be seen from both Figs.3-6 and 3-7, a linear relationship with a tangent of about -3 was obtained for all trivalent metal ions on the TiSbA at different ratios of Sb/Ti (0.77 and 0.34). The tangent value of -3 indicates that the TiSbA samples give an ideal 3:1 ion exchange reaction at Sb/Ti=0.77 and 0.34. Also Figs.3-6 and 3-7 show that the selectivity sequence is $Al^{3+} < Cr^{3+} < Ga^{3+} < In^{3+} < Fe^{3+}$ at 10^{-4}mol dm^{-3}. In the region of high concentration of HNO_3 on In^{3+} and Fe^{3+}, the ion exchange reaction deviated from the ideal line. Diamond and Whitney [16] have pointed out that as a result of decreased water activity at high concentration of inorganic acid, the hydrated cations lose a part of the water molecules from their hydration shell, forming a direct bond with cation exchange site and yielding high Kd value.

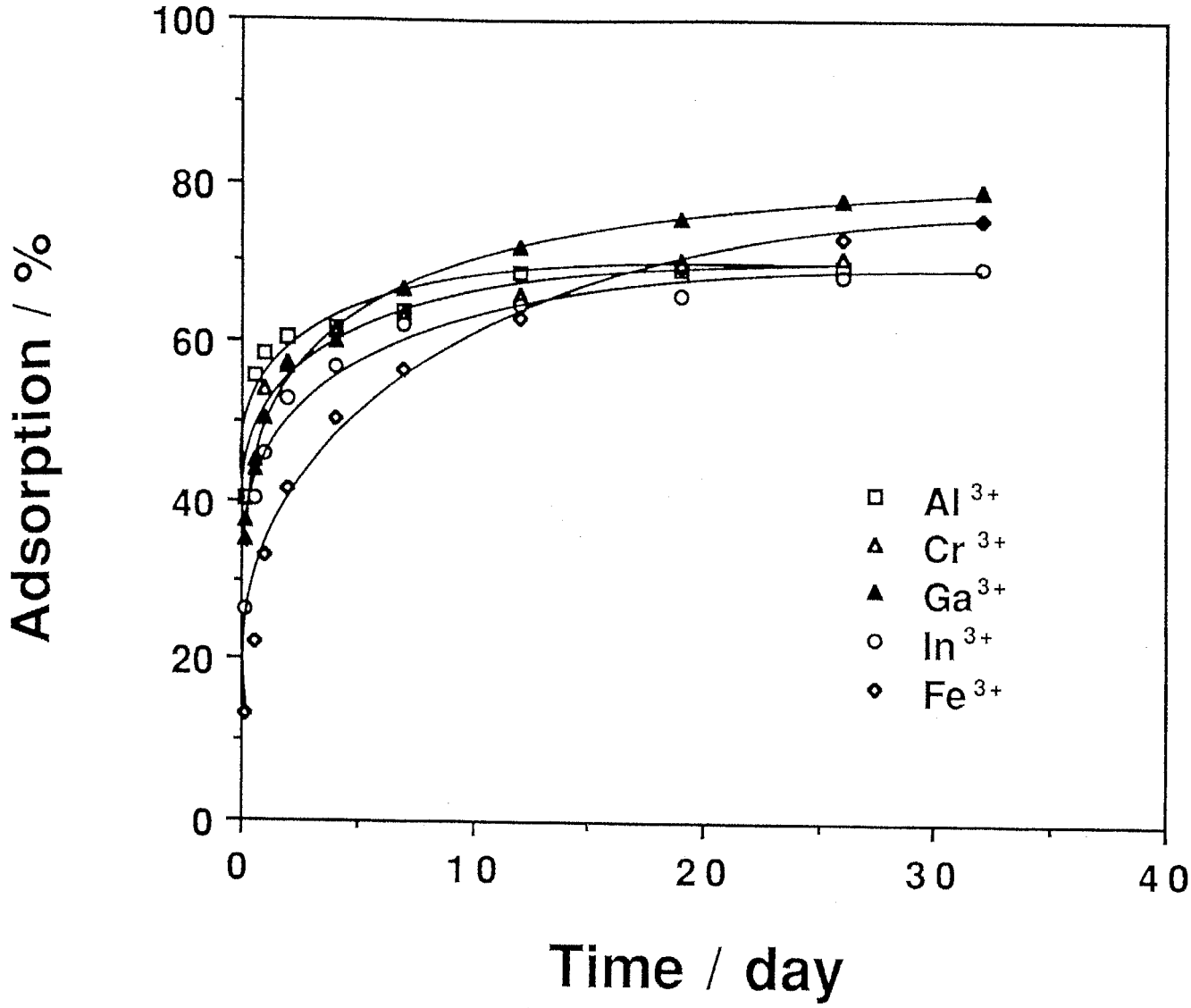

Fig.3-2 Time Dependence for Adsorption of Trivalent Metal Ions on TiSbA

Initial Concn. of Metal Ions, 10^{-4} M; TiSbA (Sb/Ti=0.77), 0.25 g; Total Vol., 25 cm^3; Temp., 30±1 °C; Concn. of HNO_3, 0.1 M for Al^{3+}, 0.15 M for Cr^{3+}, 0.2 M for Ga^{3+}, 0.6 M for In^{3+}, 1 M for Fe^{3+}

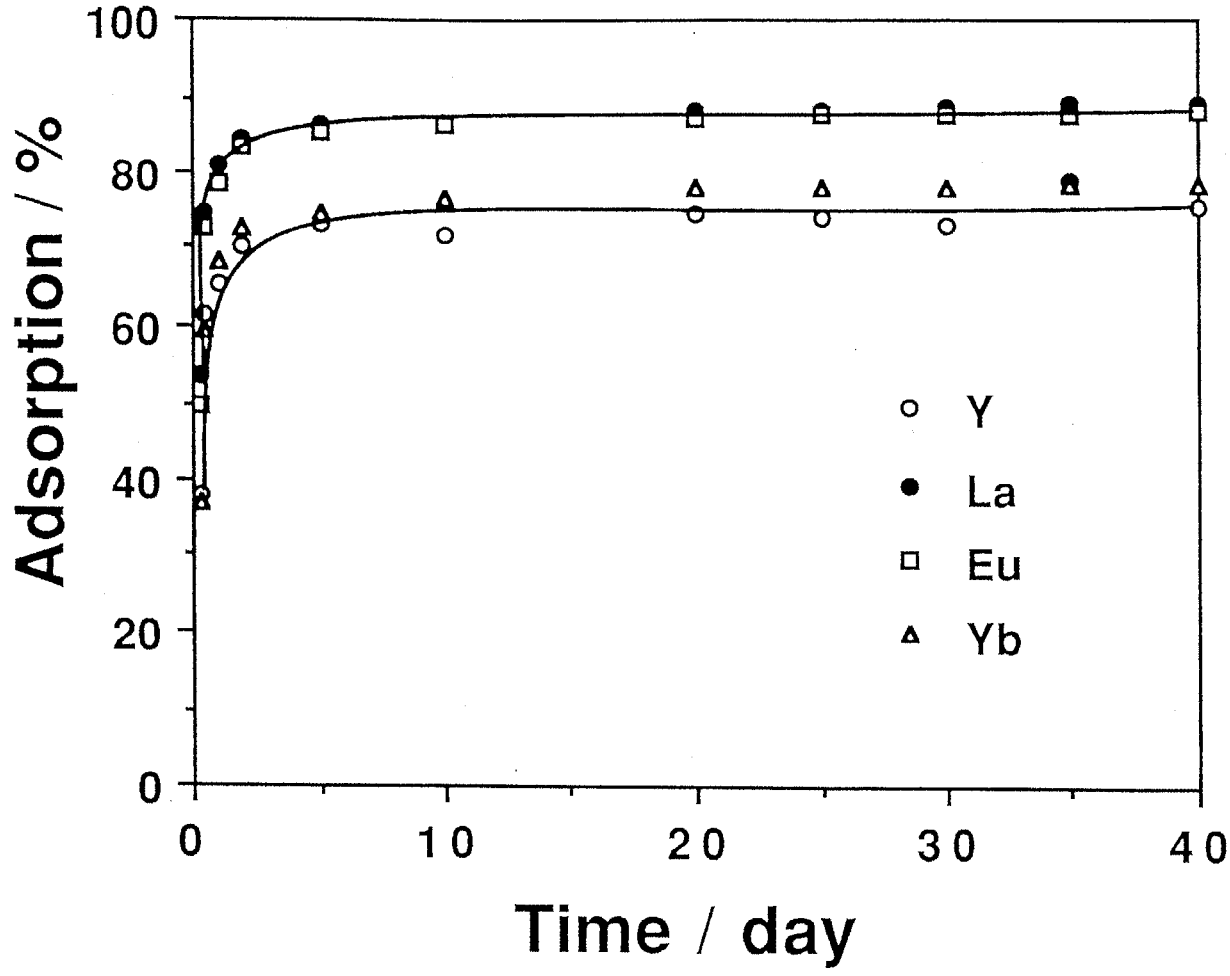

Fig.3-3 Time Dependence for Adsorption of Rare Earth Metal Ions on TiSbA

Initial Concn. of Metal Ions, 10^{-4} M; TiSbA (Sb/Ti=0.62), 0.50 g; Total Vol., 50 cm^3; Temp., 30±1 °C; Concn. of HNO_3, 0.1 M

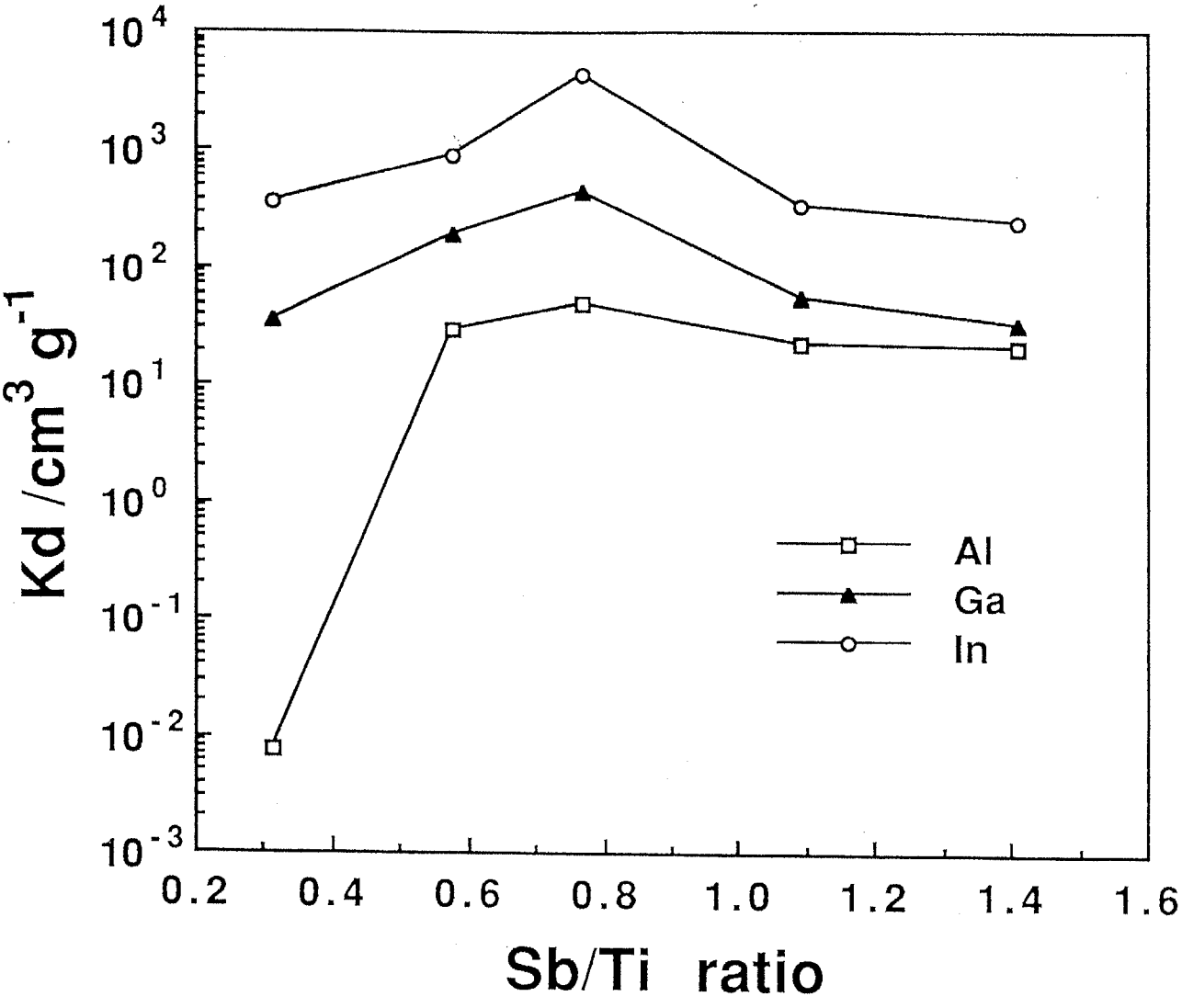

Fig.3-4 Kd Values of Al^{3+}, Ga^{3+} and In^{3+} as a Function of Different Mole Ratios of Sb/Ti

Initial Concn. of Metal Ions, 10^{-4} M; TiSbA, 0.10 g; Total Vol., 10 cm^3; Temp., 30±1 °C; Concn. of HNO_3, 0.2 M

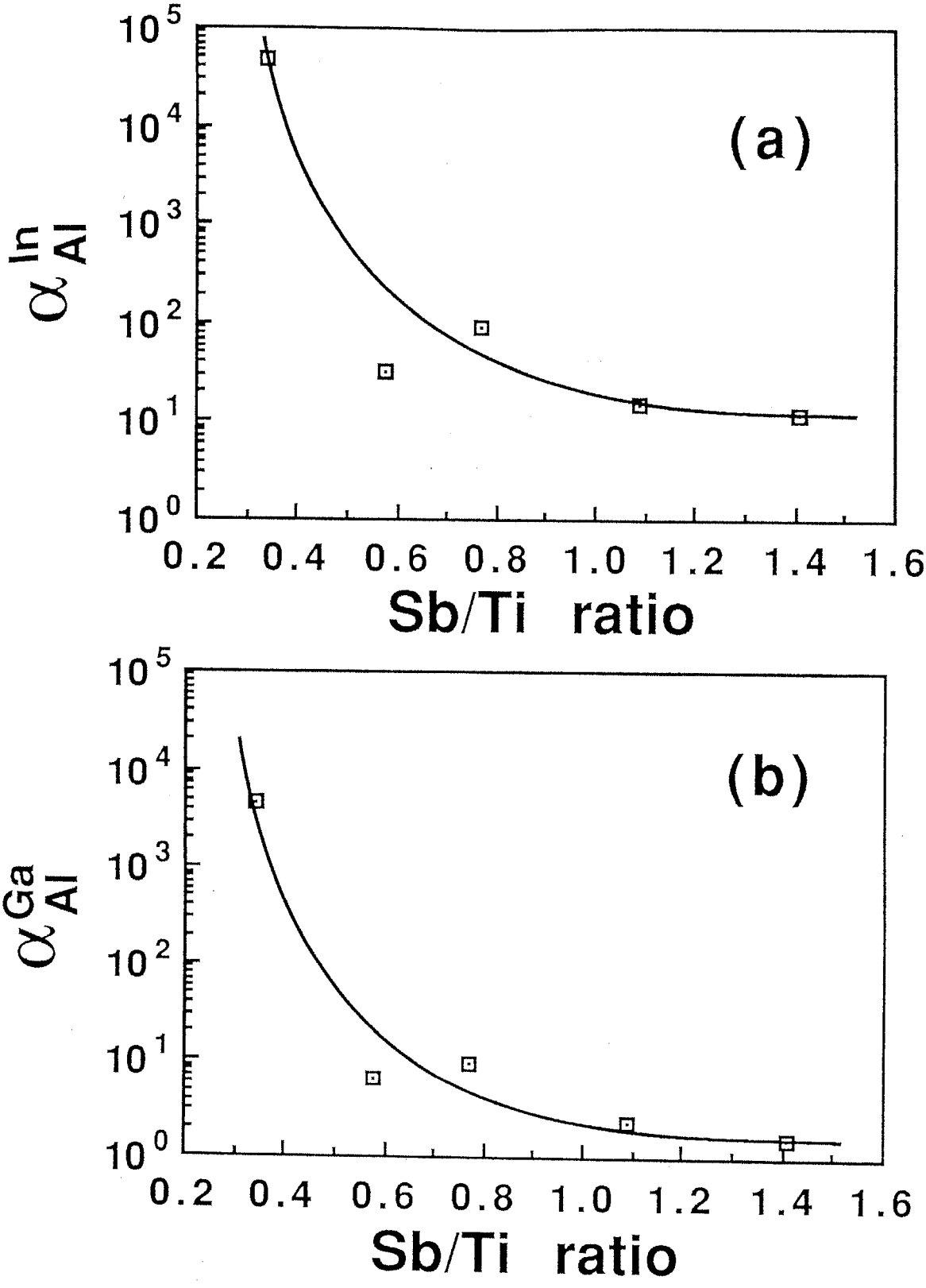

Fig.3-5 Separation Factor of Al^{3+}-In^{3+} (a) and Al^{3+}-Ga^{3+} (b) on TiSbA with Different Mole Ratios of Sb/Ti

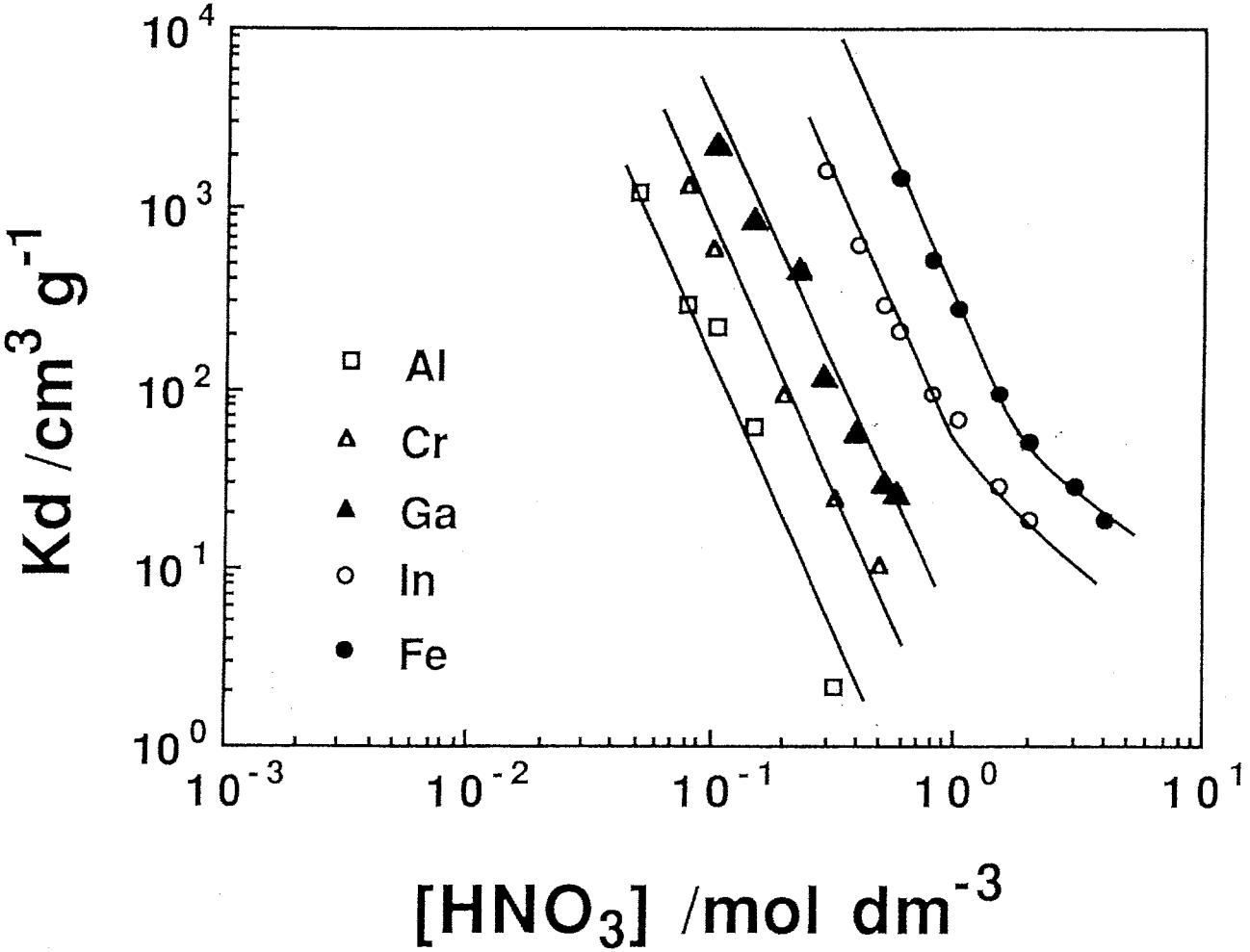

Fig.3-6 Log-Log Plot of $[HNO_3]$ vs. Kd Values of Metal Ions on TiSbA (Sb/Ti=0.77)

Initial Concn. of Metal Ions, 10^{-4} M; TiSbA, 0.10g;
Total Vol., $10cm^3$; Temp., 30±1 °C

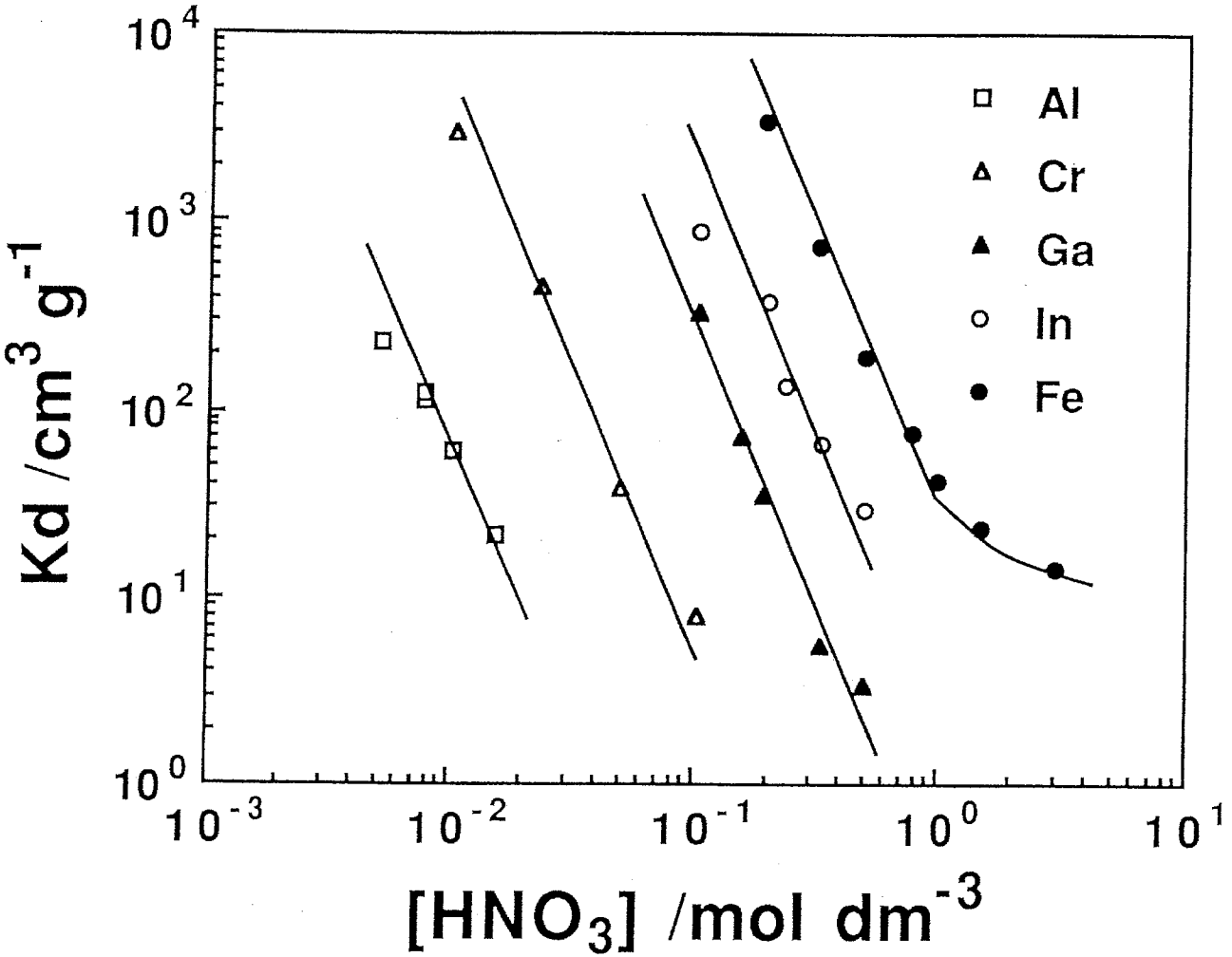

Fig.3-7 Log-Log Plot of [HNO_3] vs. Kd Values of Metal Ions on TiSbA (Sb/Ti=0.34)
Initial Concn. of Metal Ions, 10^{-4} M; TiSbA, 0.10g;
Total Vol., 10cm^3; Temp., 30±1 °C

The Kd values and separation factors (α) for trivalent metal ions, which were evaluated from Figs.3-6 and 3-7 are summarized in Table 3-1 (Some were estimated by extrapolation to 0.5M HNO_3). The Kd values and separation factors (α) on commercially strong-acid type cation exchange resin, BIO-RAD AG50W-X8,[17] are also included in Table 3-1 for comparison. As can be seen here, the selectivity sequence of $Al^{3+} < Cr^{3+} < Ga^{3+} < In^{3+}$ for TiSbA is the same as reported for BIO-RAD AG50W-X8. The Kd value of Fe^{3+} for TiSbA is extremely high, compared BIO-RAD AG50W-X8. The separation factors between neighbouring pairs of metal ions on TiSbA are larger than those observed on BIO-RAD AG50W-X8 having similar Kd values. The Al^{3+}-Ga^{3+} and Al^{3+}-In^{3+} separation factors on TiSbA with Sb/Ti ratios of 0.34 were larger than those on BIO-RAD AG50W-X8. Improved separation factors were observed between Al^{3+}-Ga^{3+} and Al^{3+}-In^{3+} on BIO-RAD AG50W-X4 by complex formation with HCl or HBr,[18] which makes the method less suitable for the separation of small amounts of Ga^{3+} and In^{3+} from large amounts of Al^{3+}, because its selectivity sequence is $Al^{3+} >> Ga^{3+} >> In^{3+}$. The selectivity sequence on TiSbA (Sb/Ti=0.34) is $Al^{3+} << Ga^{3+} < In^{3+}$, so that the TiSbA is suitable for separation of small amounts Ga^{3+} and In^{3+} from large amounts of Al^{3+}.

The log Kd of Eu^{3+} obtained on TiSbA with differet Sb/Ti ratio were plotted against log [HNO_3] (Fig.3-8). The Kd values increased with an increase in the Sb/Ti ratio from 0.28 to 0.87. For divalent transition metal ions on TiSbA, the increasing Kd values with an increase Sb/Ti ratio were also reported.[6] Fig.3-9 shows the plot of log Kd vs. log [HNO_3] for the rare earth metal ions on TiSbA at Sb/Ti=0.69. In this ion-exchange reaction, a linear relationship with tangent of about -3 was obtained for all rare earth metal ions on TiSbA. And Fig.3-9 shows that the selectivity sequence $Y^{3+} < Yb^{3+} < Gd^{3+} < Eu^{3+} < Nd^{3+} = Pr^{3+} < La^{3+}$ at 10^{-4}mol dm^{-3}. The Kd values and separation factors for the rare earth metal ions are summarized in Table 3-2. In the similar to other trivalent metal ions, the Kd values and separation factors on BIO-RAD AG 50W-X8 are also included in Table 3-2 for comparison. The selectivity sequence is the same as reported for BIO-RAD AG 50W-X8. The separation factors between neighbouring pairs of metal ions on TiSbA are larger than those observed on BIO-RAD AG50W-X8. Also, Fig.3-9 shows the plot of log Kd vs. log [HNO_3] for the group 13 element ions on TiSbA at Sb/Ti=0.69, the selectivity sequence of trivalent metal ions $Al^{3+} < Y^{3+} < Yb^{3+} < Ga^{3+} = Gd^{3+} < Eu^{3+} < Nd^{3+} = Pr^{3+} < La^{3+} < In^{3+}$.

Table 3-1 Kd Values and Separation Factors (α) for Trivalent Metal Ions on TiSbA.

Exchanger	Media		Metal				
			Al^{3+}	Cr^{3+}	Ga^{3+}	In^{3+}	Fe^{3+}
TiSbA (Sb/Ti=0.77)	HNO_3 0.5M	Kd	2.5_3	9.5_0	$2.9_0 \times 10$	$2.8_9 \times 10^2$	$1.8_2 \times 10^3$
		α	3.8	3.1	10	6.3	
TiSbA (Sb/Ti=0.34)	HNO_3 0.5M	Kd	$4.9_0 \times 10^{-4}$	$4.0_5 \times 10^{-2}$	2.3_6	$1.4_7 \times 10$	$2.5_5 \times 10^2$
		α	83	58	6.2	17	
			Fe^{3+}	Al^{3+}	Cr^{3+}	Ga^{3+}	In^{3+}
BIO-RAD 50W-X8*)	HNO_3 0.5M	Kd	362	392	418	445	680
		α	1.1	1.1	1.1	1.5	

α is defined by Kd^A / Kd^B

*) F. W. E. Strelow et al., Anal. Chem., **37**, 106 (1965)

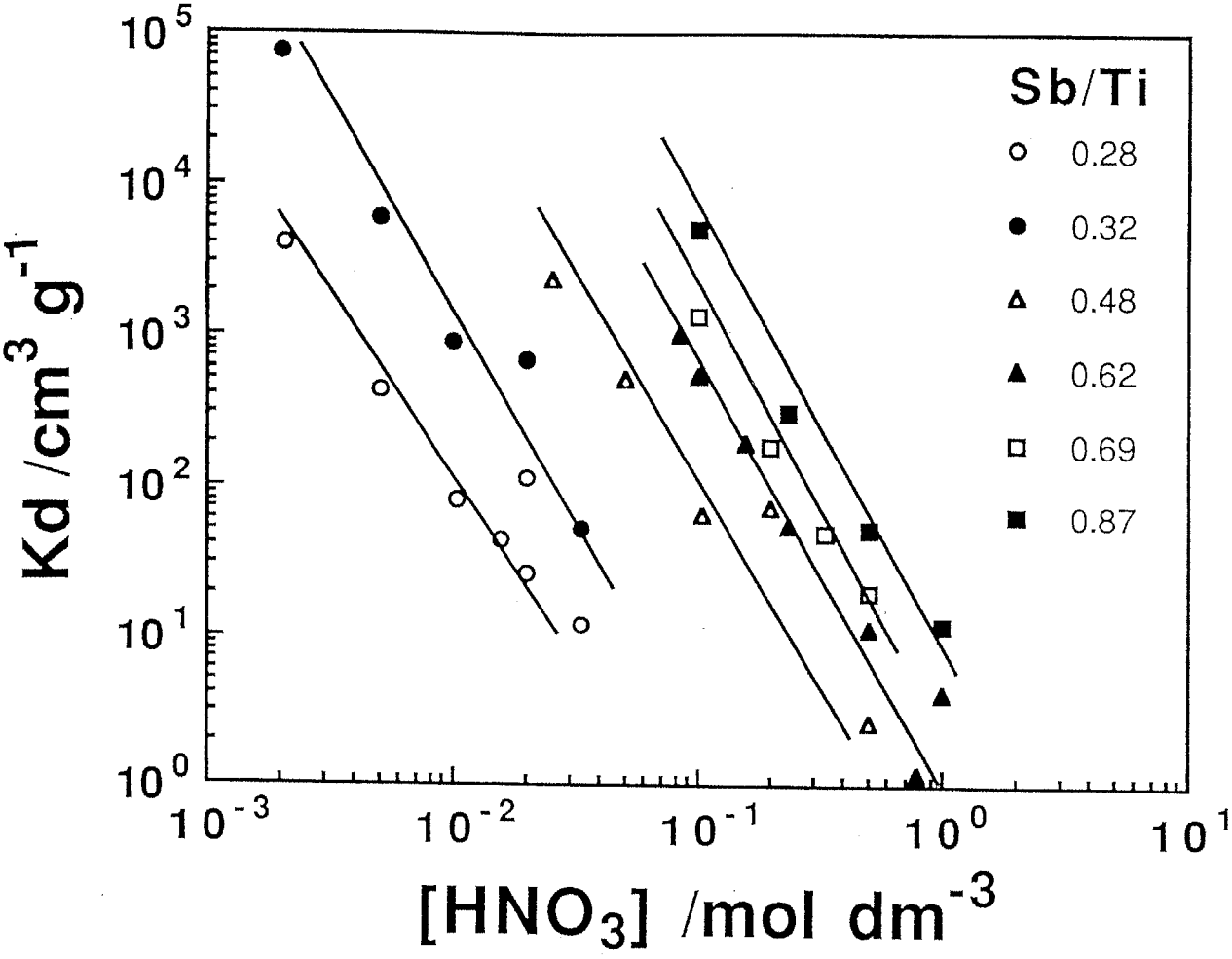

Fig.3-8 Log-Log Plot of $[HNO_3]$ vs. Kd Values of Eu^{3+} on TiSbA with Different Sb/Ti ratio
Initial Concn. of Metal Ions, 10^{-4} M; TiSbA, 0.10g;
Total Vol., $10cm^3$; Temp., 30±1 °C

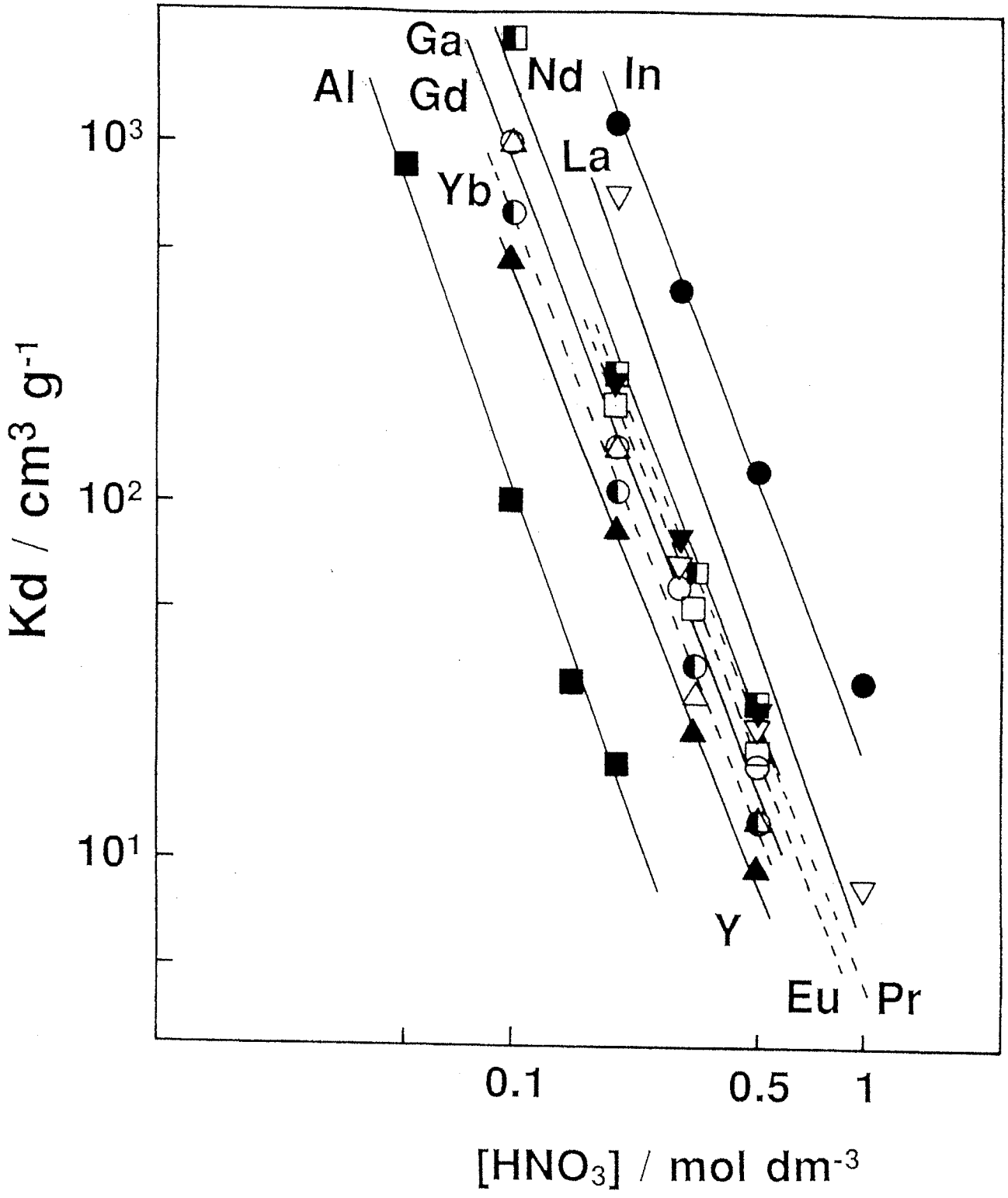

Fig.3-9 Log-Log Plots of [HNO_3] vs. Kd Values of Metal Ions on TiSbA (Sb/Ti=0.69)

Initial Concn. of Metal Ions, 10^{-4} mol dm^{-3};
TiSbA, 0.10 g; Total Vol., 10 cm^3; Temp., 30±1°C

Table 3-2 Kd Values and Separation Factors (α) for Rare Earth Metal Ions on TiSbA.

Exchanger	Media		Metal						
			Y^{3+}	Yb^{3+}	Gd^{3+}	Eu^{3+}	Pr^{3+}	Nd^{3+}	La^{3+}
TiSbA	HNO_3	Kd	$8.4_2 \times 10^1$	$1.0_7 \times 10^2$	$1.4_5 \times 10^2$	$1.8_2 \times 10^2$	$2.1_7 \times 10^2$	$2.2_7 \times 10^2$	$1.0_5 \times 10^3$
(Sb/Ti=0.69)	0.2M	α	1.3	1.4	1.3	1.2	1.0	4.6	
			Gd^{3+}	Y^{3+}	Yb^{3+}	La^{3+}			
BIO-RAD	HNO_3	Kd	1000	1020	1150	1870			
50W-X8*)	0.5M	α	1.0	1.1	1.6				

α is defined by Kd^A / Kd^B

*) F. W. E. Strelow et al., Anal. Chem., **37**, 106 (1965)

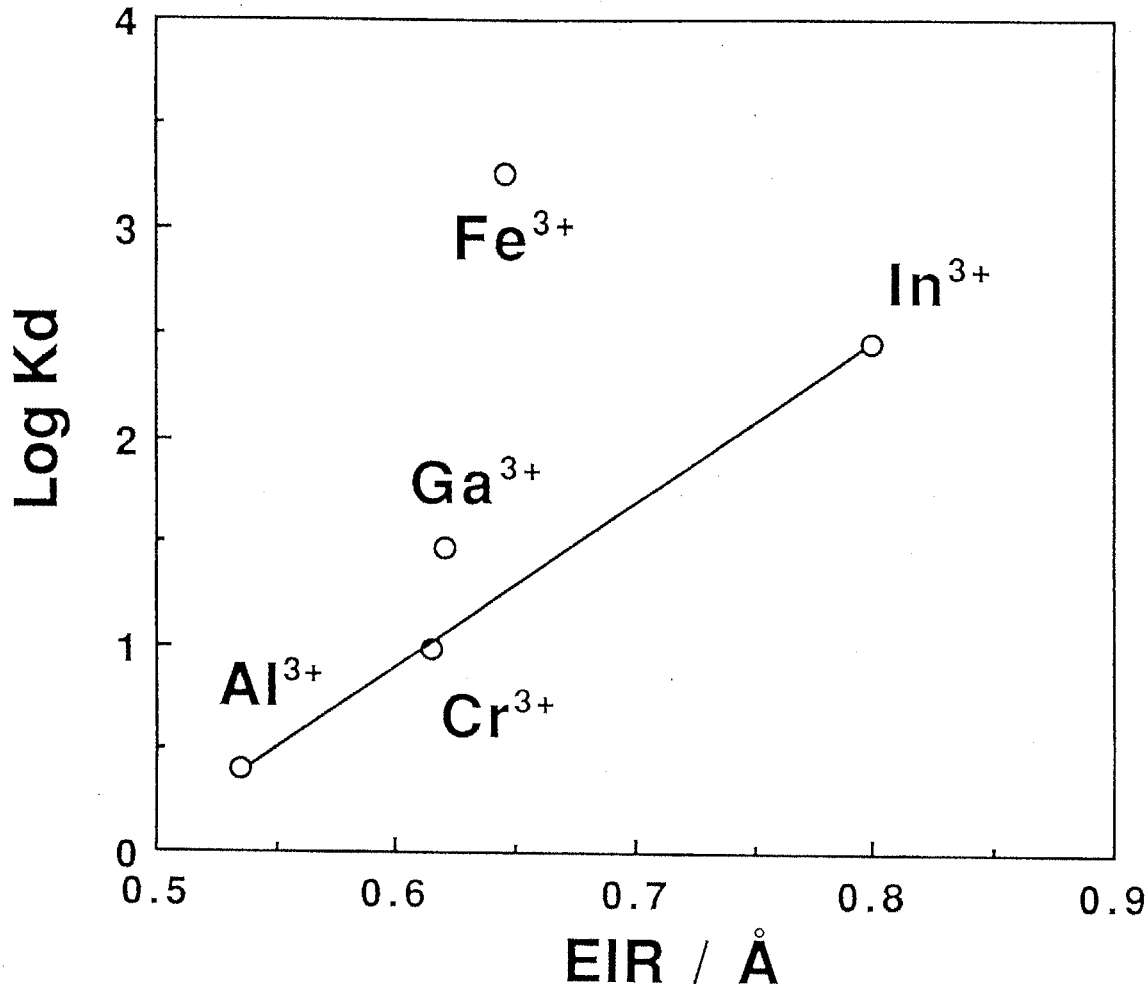

Fig.3-10 The Kd of Various Trivalent Metal Ions on TiSbA (Sb/Ti=0.77) as a Function of Effective Ionic Radii of Metal Ions

Some inorganic exchangers such as C-SbA[19] or MnO_2[20] show size preference selectivity for ions having effective ionic radii (EIR). The log Kd values of trivalent metal ions on TiSbA at Sb/Ti=0.77 were plotted against the EIR of metal ions (Fig.3-10). The result shows that there is a good correlation except for Fe^{3+}. The EIR values used were those reported by Shannon.[21] This selectivity order of trivalent metal ions might be explained as follows; for the trivalent metal ions, the observed order of selectivity was the same as that of their increasing EIR, i. e., their decreasing hydrated ionic radii. This suggests that the energy required for the dehydration of metal ions so that they can occupy a site in the exchanger plays an important role in determining the selectivity series. However, these considerations would not be adapted to the Fe^{3+}. The log Kd values of the group 13 and rare earth metal ions on TiSbA at Sb/Ti=0.69 were plotted against the EIR of metal ions in Fig.3-11. Two different selectivity series were found the group 13 metal ions and the rare earth metal ions. The difference in the electron cofiguration of the ion-exchange cations may be responsible for the result; the latter takes $s^2p^6f^n$ configuration and the former takes a different configuration.

4-3 Ion-exchange isotherm

The ion-exchange behaviors of Al^{3+}, Ga^{3+} and In^{3+} can be well understood based on the ion exchange isotherm (Fig.3-12). The theoretical capacity (TC) in Table 2-2 was used for the isotherm. The diagonal line corresponds to the corrected selectivity coefficient $K_H^M = \eta\Gamma$. When X_M is very small, $\overline{X}_M$ of Ga^{3+} or In^{3+} is much larger than that of Al^{3+}. Ga^{3+} and In^{3+} are selectively retained in the ion exchanger at the low concentration of the metal ions in the solution, while Al^{3+} is less selective. Thus, the Ga^{3+} and In^{3+} will be slowly eluted with long tailings, which is characteristic of the Langmuir type isotherm. These features are to be studied in more detail on a basis of the Kielland plot, i.e., plot of log K_H^M vs. $\overline{X}_M$. The Kielland plot is conjugate expression of ion-exchange isotherm.[9] The Kielland plots of trivalent metal ions are discussed in the chapter 4.

4-4 Chromatographic separation

It is evident from the studies on Kd values that some interesting separations may be possible for a pair of trivalent metal ions on a TiSbA column without the use of a complexing agent. Especially separation of small amount of Ga^{3+} and In^{3+} from large

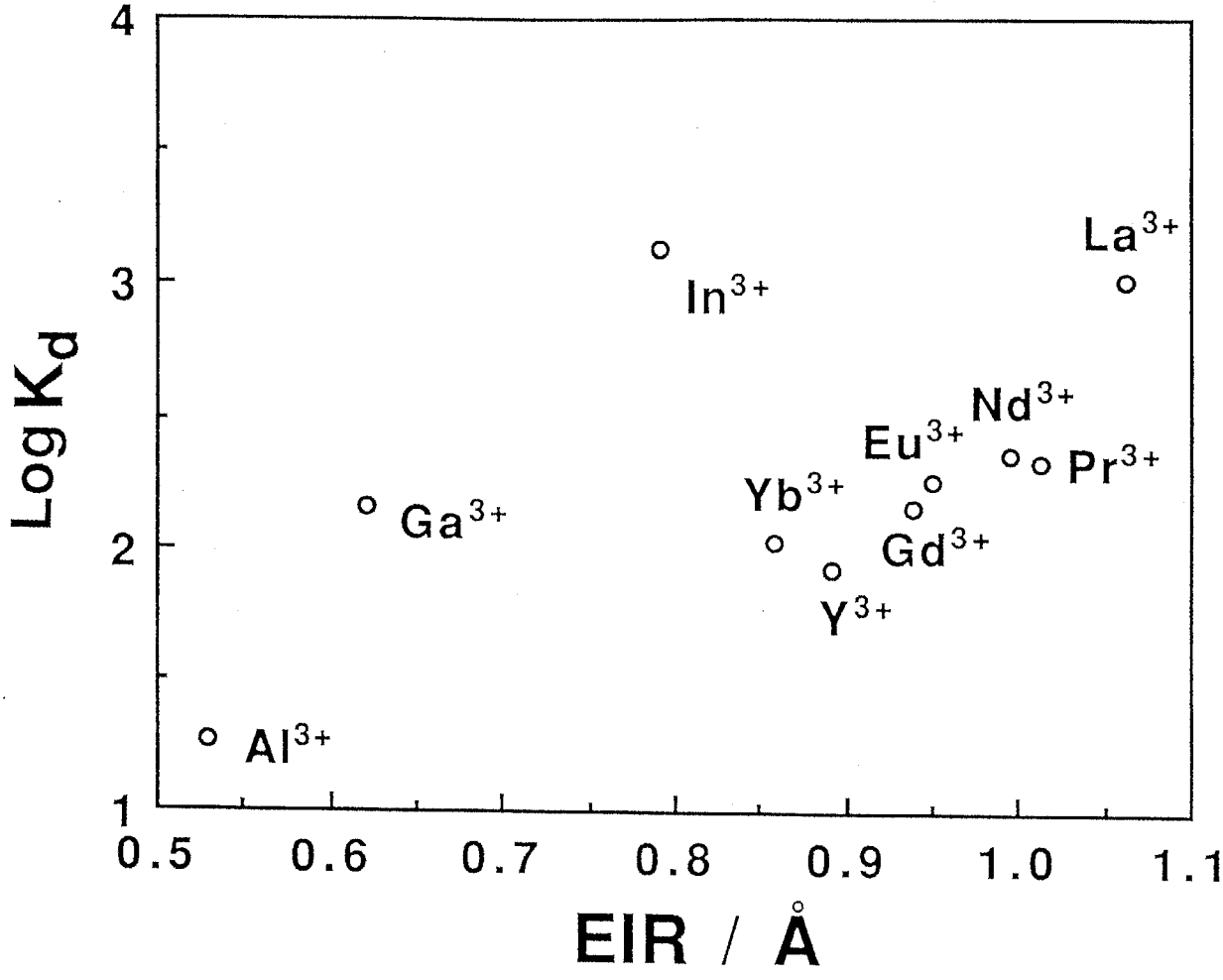

Fig.3-11 The Kd of Various Trivalent Metal Ions on TiSbA (Sb/Ti=0.69) as a Function of Effective Ionic Radii of Metal Ions

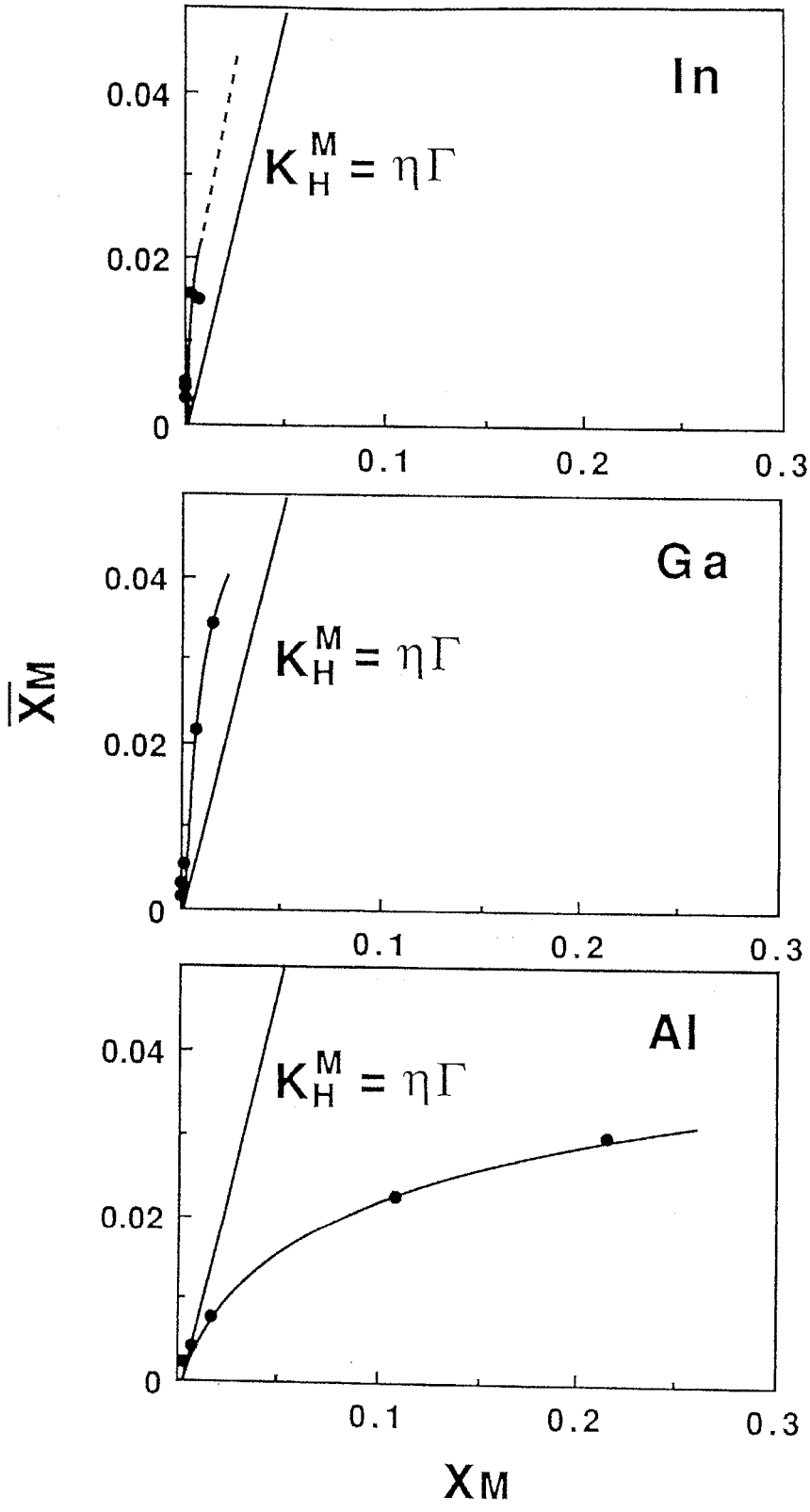

Fig.3-12 Ion Exchange Isotherms of Al^{3+}, Ga^{3+} and In^{3+} on TiSbA (Sb/Ti=0.34)

TiSbA, 0.10 g; Total Vol., 10 cm^3; TN, 0.008 N for Al^{3+}, 0.15 N for Ga^{3+}, 0.4 N for In^{3+}; Temp., 30±1 °C

amount of Al^{3+} is one of the important and difficult problem for field of analytical and separation chemistry. Some attempts including complex formation and solvent extraction have been carried out for the separation of this combination.[22,23] Chromatographic separation is very useful for the separation of low selectivity for large amount of undesirable element and high selectivity for desirable element.

Relatively small columns (3cm × 0.5cm i.d.) containing 0.4g and 0.35g of TiSbA with Sb/Ti ratio of 0.77 and 0.34, respectively, were used throughout. In order to prevent strong adsorption of Al^{3+}, the column was initially felt with a 0.15M HNO_3 and 0.025M HNO_3 for TiSbA with Sb/Ti= 0.77 and 0.34, respectively. Then, a solution containing 20μmol of Al^{3+}, 2μmol of Ga^{3+}, and 2μmol of In^{3+} was added to the top of the column and the elution was carried out using nitric acid with different concentrations. The order of elution of metal ions coincided with the equilibrium distribution coefficients; the successful separation of Al^{3+}-Ga^{3+}-In^{3+} was performed with 0.15M HNO_3 for Al^{3+}, 0.3M HNO_3 for Ga^{3+} and 2.0M HNO_3 for In^{3+} on the column of TiSbA with Sb/Ti ratio of 0.77 (Fig.3-13). And the successful separation of Al^{3+}-Ga^{3+}-In^{3+} was performed with 0.025M HNO_3 for Al^{3+}, 0.15M HNO_3 for Ga^{3+} and 2.0M HNO_3 for In^{3+} on the column of TiSbA with Sb/Ti ratio of 0.34 (Fig.3-14). The elution peak of Al^{3+} was sharp, however, long tails were observed for Ga^{3+} and In^{3+}. The recoveries of Al^{3+}, Ga^{3+} and In^{3+} were 100%, 75% and 93%, respectively, as the effluent up to 330cm^3 on the column of TiSbA with Sb/Ti ratio of 0.34. Although Ga^{3+} and In^{3+} were separated from Al^{3+}, tailing during elution and elution yields were encountered.

The reason of the long tails of Ga^{3+} and In^{3+} was discussed in the section 4-3 of this chapter. The low yields are considered to be due to the strong retention of cations to the exchanger particle during the time between feeding and elution periods. After the separation, TiSbA in the column was dissolved in sulfuric acid, and the concentration of Ga^{3+} and In^{3+} were determined. It was found that Ga^{3+} and In^{3+} were remained in the exchanger.

The quantitative separation of Al^{3+}-Ga^{3+} was achieved with 0.025M HNO_3 for Al^{3+} and 1.0M HNO_3 for Ga^{3+} in the similar conditions (Fig.3-15). The elution peak of Ga^{3+} eluted by 1.0M HNO_3 was more sharp and recovery of Ga^{3+} was improved to 89%.

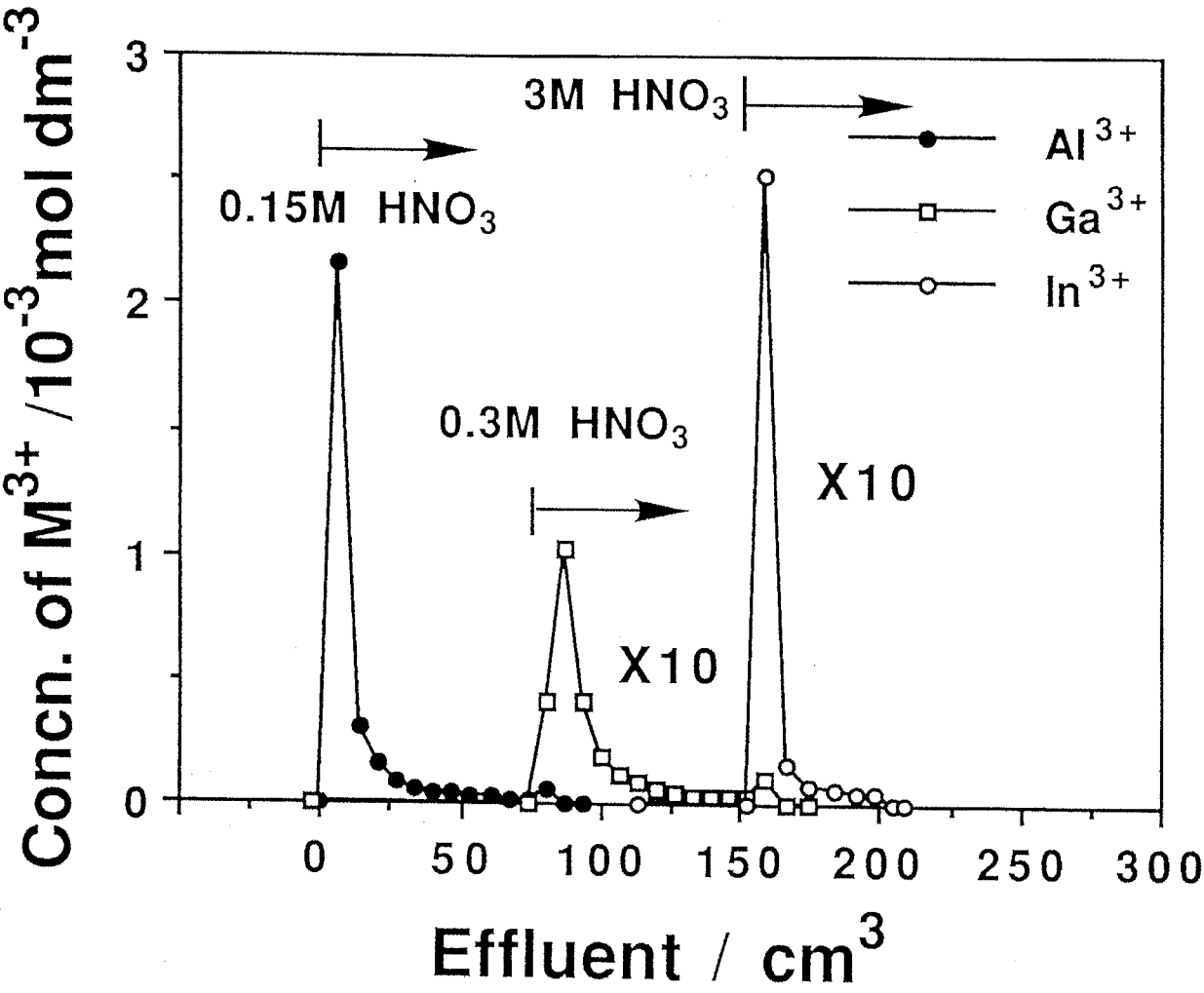

Fig.3-13 Chromatographic Separation of Trivalent Metal Ions with TiSbA (Sb/Ti=0.77) Column

Column, 3 cm x 0.5 cm i.d.; Loadings, 20 μmol for Al^{3+}, 2 μmol for Ga^{3+} and In^{3+}; Flow Rate, 0.08 cm^3/min.

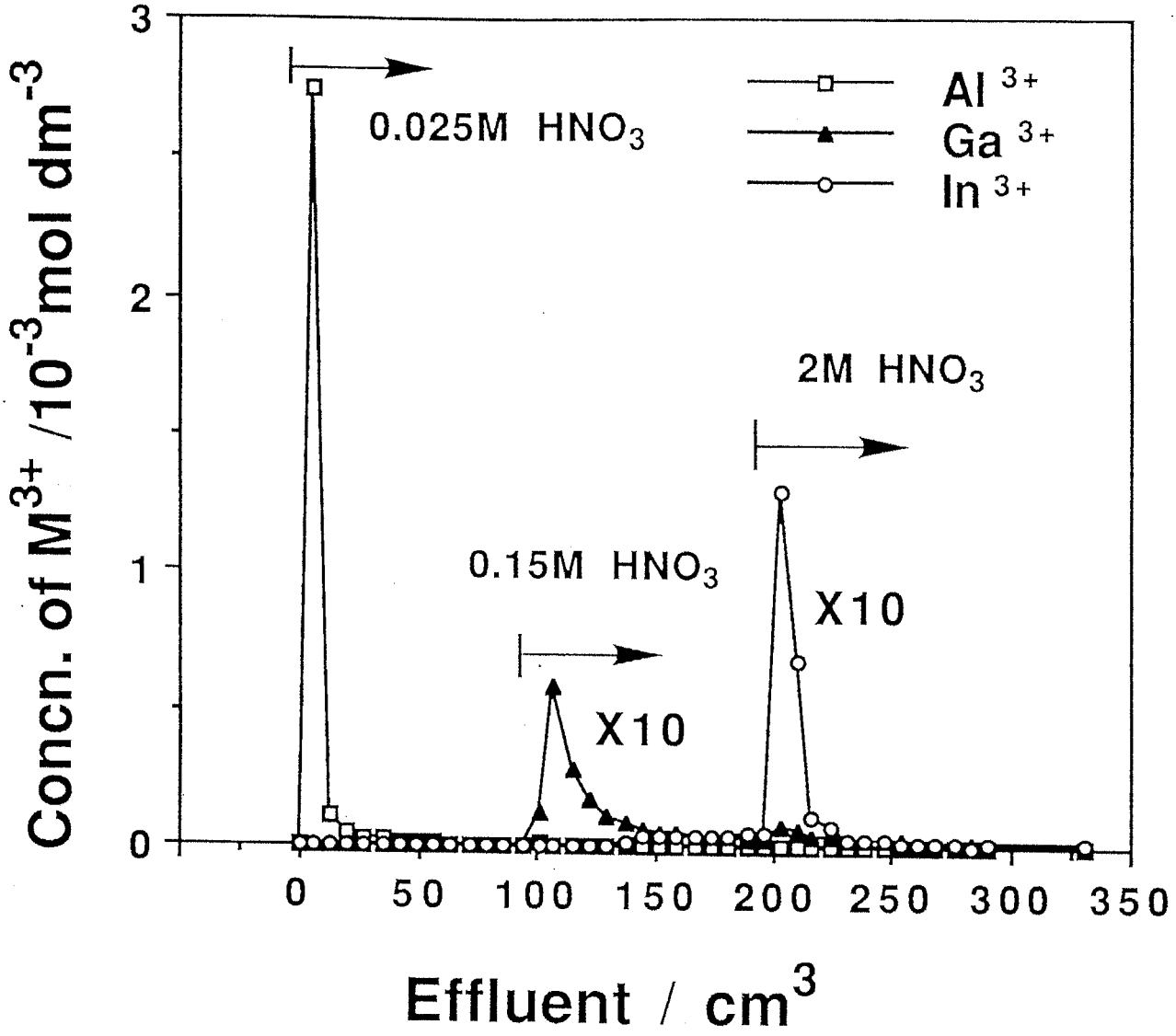

Fig.3-14 Chromatographic Separation of Trivalent Metal Ions with TiSbA (Sb/Ti=0.34) Column
Column, 3 cm x 0.5 cm i.d.; Loadings, 20 μmol for Al^{3+}, 2 μmol for Ga^{3+} and In^{3+}; Flow Rate, 0.08 cm^3/min.

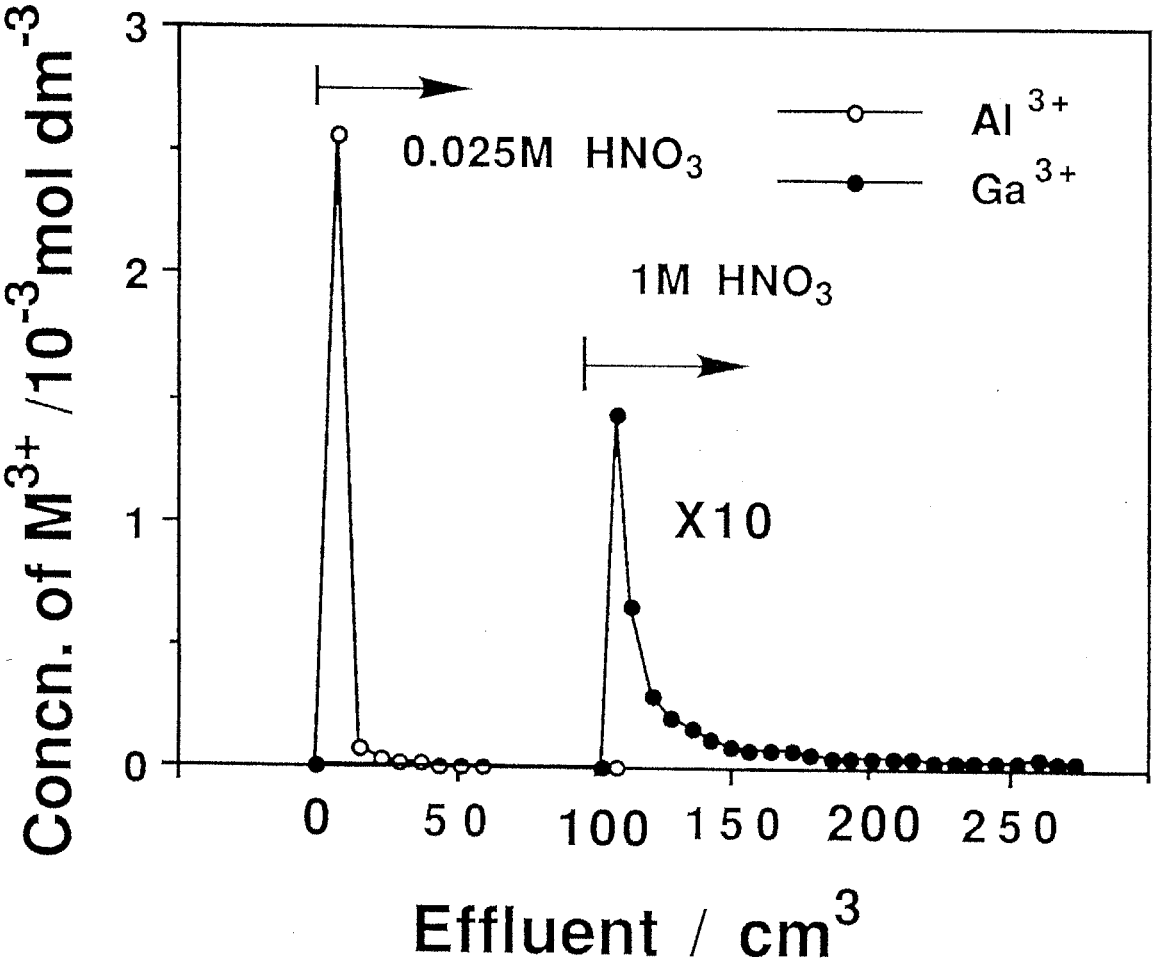

Fig.3-15 Chromatographic Separation of Trivalent Metal Ions with TiSbA (Sb/Ti=0.34) Column.
Column, 3 cm x 0.5 cm i.d.; Loadings, 20 μmol for Al^{3+}, 2 μmol for Ga^{3+} ; Flow Rate, 0.08 cm^3/min.

5. REFERENCES

1. M. Abe and M. Tsuji, Chem. Lett., 1561 (1983).
2. M. Tsuji and M. Abe, Rep. Asahi Grass Found. Ind. Technol., *42,* 287 (1983).
3. M. Abe, R. Chitrakar, M. Tsuji and K. Fukumoto, Solvent Extr. Ion Exch., *3,* 149 (1985).
4. M. Abe and R. Chitrakar, Hydrometallugy, *19,* 117 (1987).
5. R. Chitrakar and M. Abe, Bull. Chem. Soc. Jpn., *60,* 2272 (1986).
6. R. Chitrakar and M. Abe, Analyst, *111,* 339 (1986).
7. M. Qureshi and V. Kumer, J. Chromatogr., *62,* 431 (1971).
8. M. Tsuji and S. Komarneni, Sep. Sci. Technol., *26,* 647 (1991).
9. M. Tsuji and S. Komarneni, Sep. Sci. Technol., *27,* 813 (1992).
10. J. C. McDonald, Inorganic Chromatographic Analysis, John Wiley and Sons, New York, 1985 ; J. Michal, ibid., Van Nostrand Reinhold Co., London, 1970.
11. A. J. P. Martin and R. L. M. Synge, Biochem. J., *35,* 1385 (1941).
12. J. Benkenkamb, W. Rieman III and S. Lindenbaum, Anal. Chem., *26,* 505 (1954).
13. M. Abe, Sep. Sci. Technol., *15,* 23 (1980).
14. J. A. Dean, Chemical Separation Methods, Van Nostrand Reinhold Co. New York, 1969, p.66.
15. K. Dorfner, Ion Exchangers Properties and Applications, Ann Arbor Sci. Pub. Inc. Michigan, 1972, p.198,205.
16. J. A. Marinsky, Ion Exchange, Marcel Dekker, New York, 1966, p.355.
17. F. W. E. Strelow, R. Rethemyer and C. J. C. Bothma, Anal. Chem., *37,* 106 (1965).
18. F. W. E. Strelow and T. N. van der Walt, Talanta, *34,* 895 (1987).
19. A. Clearfield (Ed.), Inorganic Ion Exchange Materials, CRC Press, Boca Raton, FL, 1982.
20. M. Tsuji and M. Abe, Solvent Extr. Ion Exch., *2,* 253 (1984).
21. R. D. Shannon, Acta Crystallogr., Sect. A, *32,* 751 (1976).
22. F. Culkin and J. P. Riley, Analyst, *83,* 208 (1958).
23. K. Ohta and M. Suzuki, Anal. Chim. Acta, *85,* 83 (1976).

CHAPTER 4
HYPOTHETICAL THERMODYNAMIC ANALYSIS ON TITANIUM ANTIMONATE

1. INTRODUCTION

The unusual selectivity on TiSbA was observed for alkali metals, alkali earth metals,[1] divalent transition metals[2] and trivalent metals.[3,4] It has been known that the selectivity on inorganic ion exchangers depends much on the equivalent fraction of metal ions in the exchangers. If the window of ion-exchange site is small compared with the dimension of entering cation, an ion-sieve effect occurs. Typical examples are given by high selectivities toward Cs^+ on Al^{3+}-substituted tobermorite,[5,6] K^+ on a cryptomelane-type hydrous manganese dioxide,[7-9] and Li^+ on λ-type manganese dioxide[10] and rancieite type manganic acid.[11]

The ion-exchange isotherm has the importance for the thermodynamic interpretation of the ion-exchange phenomena and designs of the chromatographic separation. In the former, the isotherm is rewritten to the so-called Kielland plot (plot of the corrected selectivity coefficient K_H^M vs. fractional exchange $\overline{X}_M$) which plays a central part. In the latter, the distribution coefficients (Kd) are used for the conventional location of the elution peak. Recently, Tsuji et al. has combined these two ways of expressions for the ion exchange selectivity to develop an analytical calculation method of the distribution coefficient (Kd) using the Kielland plot as a continuous function of the initial concentration of the exchanging ion and temperature.[12,13] The procedure allows a unified treatment of the ion exchange through the Kielland plot. An ion exchange study over various exchange composition may be needed for understanding of their selectivities. However, it is very difficult to study full range of the ion exchange composition because of incomplete exchange for the steric effect.

The present work has been concerned with the interpretation of the selectivity of M^{3+} / H^+ exchange system over various exchange composition on TiSbA. And the hypothetical thermodynamic parameters for the ideal exchange with no steric effect were evaluated from the selectivity coefficient at infinitesimal exchange. Also, the objectives are (1) to derive the Langmuir equation often used in the adsorption and/or ion exchange fields, and (2) to better understand the ion exchange behavior for trivalent metal ions on the titanium antimonate cation exchanger through the Langmuir equation and the Kielland

plot.

2. THEORETICAL

2-1 Thermodynamic expressions for "ideal exchange"

The equilibrium ion-exchange reaction on a particular exchanger can be characterized by the exchange isotherm. The ion-exchange isotherm indicates the ionic composition and the types of exchange sites on the exchanger as a function of experimental conditions. The isotherm is a graphical representation of ion-exchange behavior of an exchanger based on the experimental observations which covers all possible experimental conditions at a given temperature. Such a graphical representation is shown in Fig.4-1. The ordinate of these plots i.e. $\overline{X}_M$ is the equivalent fraction of the M^{n+} ion in the exchanger phase and can be defined as,

$$\overline{X}_M = \frac{meq\ of\ M^{n+}\ /\ g\ of\ exchager}{meq\ of\ (M^{n+}+H^+)\ /\ g\ of\ exchanger}$$

and the abscissa X_M is the equivalent fraction of M^{n+} in the solution phase and is defined as,

$$X_M = \frac{meq\ of\ M^{n+}\ /\ g\ of\ solution}{total\ meq\ of\ (M^{n+}+H^+)\ in\ solution}$$

Based on the experimental conditions and types of exchangers the exchange isotherm can be of five different types[14] i.e. curves in Fig.4-1 a~e. Each curve can be defined as follows,

a) Higher selectivity for the entering cation over the entire range of exchanger composition.
b) Entering cations show a selectivity reversal with increasing equivalent fraction in the exchanger.
c) Selectivity for the leaving cations over the entire range of exchanger composition.
d) Exchange of ions does not go to completion although entering cation is initially preferred and the degree of exchange gives a value lower than unity.
e) Hysterisis effects may result from the formation of two exchange phases.

The cation-exchange reactions between H^+ and M^{n+} are represented by

$$n\ \overline{H^+} + M^{n+} \rightleftarrows \overline{M^{n+}} + nH^+ \qquad (1)$$

The thermodynamic equilibrium constant, K, is defined in the reversible system by

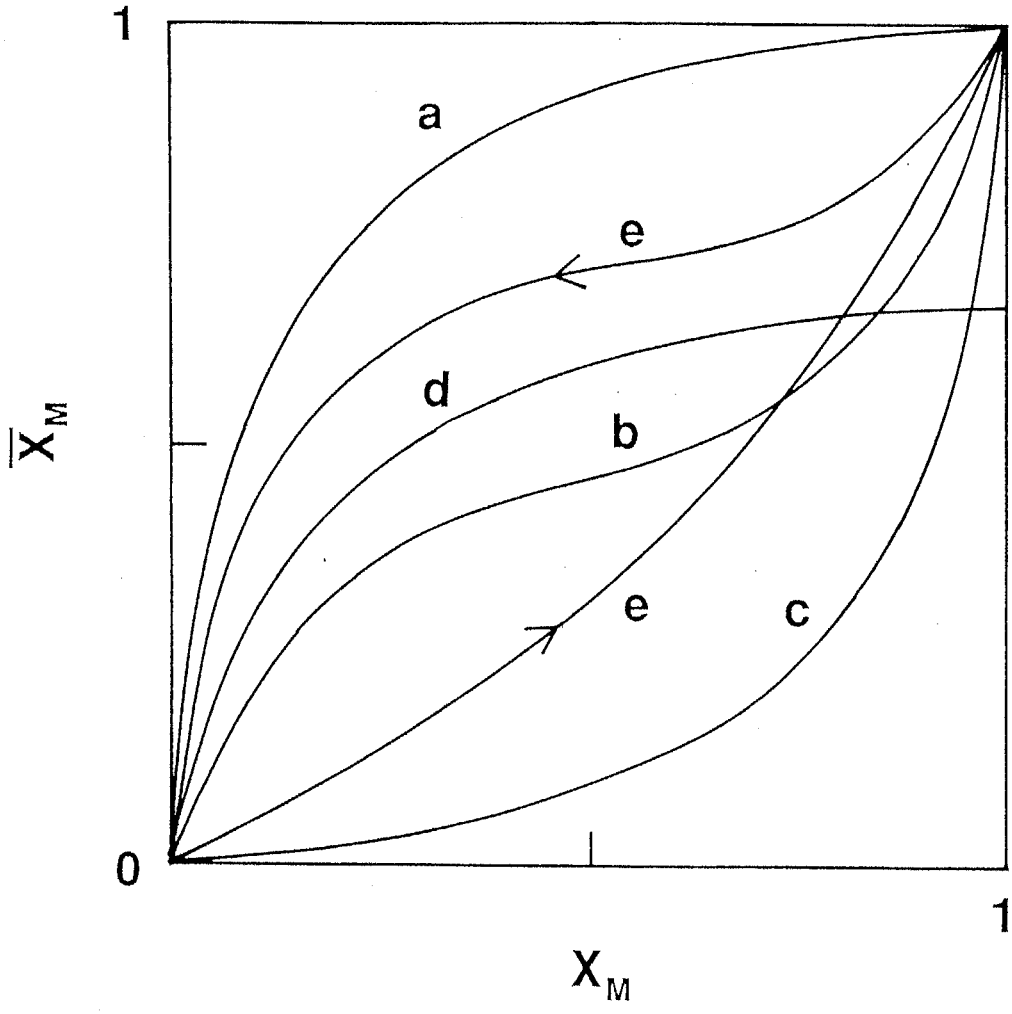

Fig.4-1 Different Types of Ion-Exchange Isotherms

$$K = \frac{[H^+]^n \, \overline{X}_M \, \gamma_H^n \, f_M}{[M^{n+}] \, \overline{X}_H^n \, \gamma_M \, f_H^n} \qquad (2)$$

In these equations, the overbar on the character denotes the exchanger phase, $\overline{X}_H$ and $\overline{X}_M$ are the equivalent ion fractions in the exchanger, and f_H and f_M are the activity coefficients for the ions in the exchanger. $[H^+]$ and $[M^{n+}]$ are the molalities of the above two exchanging ions in solution, where they have activity coefficients γ_H and γ_M. The standard states chosen are such that f_H and f_M are unity when the exchanger is in its pure H^+ and pure M^{n+} forms, respectively, and γ_H and γ_M are unity when the $[H^+]$ and $[M^{n+}]$ approach zero.

In the following treatment, molalities $[H^+]$ and $[M^{n+}]$ are replaced by the equivalent ion fractions:

$$X_M = \frac{n[M^{n+}]}{n[M^{n+}] + [H^+]} \quad , \quad X_H = \frac{[H^+]}{n[M^{n+}] + [H^+]} \qquad (3)$$

$$\overline{X}_M = \frac{n[\overline{M}^{n+}]}{n[\overline{M}^{n+}] + [\overline{H}^+]} \quad , \quad \overline{X}_H = \frac{[\overline{H}^+]}{n[\overline{M}^{n+}] + [\overline{H}^+]} \qquad (4)$$

and

$$X_M + X_H = 1 \quad , \quad \overline{X}_M + \overline{X}_H = 1 \qquad (5)$$

By using the total normality (TN) and the theoretical or total capacity (TC), which are kept constant in the ion-exchange process:

$$n[M^{n+}] + [H^+] = TN \quad , \quad n[\overline{M}^{n+}] + [\overline{H}^+] = TC \qquad (6)$$

Equation (2) becomes

$$K = K_H^M \frac{f_M}{f_H^n} \qquad (7)$$

where K_H^M refers to the selectivity coefficient:

$$K_H^M = \frac{\overline{X}_M \, X_H^n}{\overline{X}_H^n \, X_M} \, \eta\Gamma \qquad (8)$$

η and Γ are given by

$$\eta = n(TN)^{n-1} \qquad and \qquad \Gamma = \frac{\gamma_H^n}{\gamma_M} \tag{9}$$

The application of Gibbs-Duhem equation to the ion-exchange system gives for K:[15]

$$\ln K = (1 - n) + \int_0^1 \ln K_H^M \, d\,\bar{X}_M + \Delta \tag{10}$$

The third term on the right of Eq.(10), Δ, is negligible when compared with the experimental accuracy in measuring the equilibrium.[16] A plot of log K_H^M vs. $\bar{X}_M$ (Kielland plot) is generally represented by the polynomial function:[17]

$$\log K_H^M = \log(K_H^M)_{X_M,\, \bar{X}_M \to 0} + \sum_{m=1}^{n} (m+1)\, C_m \bar{X}_M^m \tag{11}$$

where C_m may be called the generalized Kielland coefficient.

Equations (10) and (11) are combined to give the thermodynamic constant K:

$$\ln K = (1-n) + 2.303 \sum_m C_m + \ln(K_H^M)_{X_M,\, \bar{X}_M \to 0} \tag{12}$$

That is, the thermodynamic equilibrium constant is determined by the valence of the exchanging cation (n), the generalized Kielland coefficients (C_m), and the intercept of the Kielland plot, $(K_H^M)_{X_M, \bar{X}_M \to 0}$. The Gibbs standard free energy change is given by:

$$\Delta G^o = -RT \left((1-n) + 2.303 \sum_m C_m + \ln(K_H^M)_{X_M,\, \bar{X}_M \to 0} \right) \tag{13}$$

This equation is combined with the van't Hoff equation to determine the standard enthalpy change ΔH^o.

$$\frac{\partial (\Delta G^o)}{\partial (1/T)} = -\Delta H^o \tag{14}$$

Finally the standard entropy change is given by the relation:

$$\Delta G^o = \Delta H^o - T\Delta S^o \tag{15}$$

On the other hand, the selectivity coefficient at infinitesimal exchange $(K_H^M)_{X_M, \bar{X}_M \to 0}$ can be evaluated by measuring the distribution coefficient Kd at the tracer experiment,

as has been derived by Tsuji and Komarneni[13)]

$$(K_H^M)_{X_M,\ \bar{X}_M \to 0} = \frac{n\ (TN)^n}{TC}\ \frac{\gamma_H^n}{\gamma_M}\ (Kd)_{X_M,\ \bar{X}_M \to 0} \qquad (16)$$

The ratio of the activity coefficient γ_H^n/γ_M can be calculated by using the $\gamma_{\pm HY}$ and $\gamma_{\pm MY_n}$ where Y denotes the common anion, according to the Glueckauf's relation.[18)]

The selectivity coefficient of when the C_m values are zero may be used as an index of the ion-exchange selectivity for the "ideal" exchange (C_m=0) with no steric hindrance.

$$\ln K_{ideal} = (1-n) + \ln(K_H^M)_{X_M,\ \bar{X}_M \to 0} \qquad (17)$$

Using Eq.(16), we get:

$$\ln K_{ideal} = (1-n) + \ln\frac{n\ (TN)^n}{TC}\ \frac{\gamma_H^n}{\gamma_M}\ (Kd)_{X_M,\ \bar{X}_M \to 0} \qquad (18)$$

and

$$\Delta G^o_{ideal} = -RT \ln K_{ideal} \qquad (19)$$

The formality of the above relations, Eqs.(14) and (15), is also valid for the "ideal exchange".

The Kd value at infinitesimal exchange (very small $\bar{X}_M$) is very important for interpreting the chromatographic behavior of metal ions. It will be often constant at the tracer concentration also in the inorganic ion exchanger, which in turn means that the selectivity coefficient is constant or that the generalized coefficient C_m is null. The Kd value at any $\bar{X}_M$ ($0<\bar{X}_M<1$) can be calculated according to the method reported previously.[13)] The evaluation process is briefly described as follows. It is defined by

$$Kd = \frac{[\bar{M}^{n+}]}{[M^{n+}]}$$

Using Eqs. (3), (4) and (6), we can get

$$Kd = \frac{TC\ \bar{X}_M}{TN\ X_M} \qquad (20)$$

Equation (8) provides an X_M for a specified $\bar{X}_M$ once the Kielland plot was empirically

given. The Kd value can be calculated as a function of the concentration of the exchanging ion $(TN)X_M$ in one total normality TN_1. The same set of $(X_M, \overline{X}_M)$ can be used to calculate the Kd value in other total normality TN_2 as a function of the $(TN_2)X_M$. Thus, the Kd value can be calculated in various total normalities as long as the ion exchange is involved in. Moreover, if the van't Hoff plot is given, we can evaluate the Kd values at other temperatures by reasonable extrapolation or interpolation of the Kielland plot.

2-2 Derivation of the Langmuir equation

The Langmuir equation has been extensively used for expression of adsorption phenomena of molecules and ions. It is given in the familiar form of

$$Q_M = \frac{K\,Q_{max}C_M}{1 + KC_M} \quad or \quad \frac{1}{Q_M} = \frac{1}{K\,Q_{max}C_M} + \frac{1}{Q_{max}} \tag{21}$$

where Q_M and C_M is the equilibrium concentrations of adsorbate M in solid and in solution, respectively, Q_{max} is the maximum value of Q_M, and K is called the Langmuir constant which is a fitting parameter. The chemical meaning of K is ambiguous in the ion-exchange process of inorganic ion exchangers, because the process can occur not only on the surface but in the crystal lattice. This expression of adsorption can be derived in the ion-exchange process as follows.

(1) case of n=1

Equation (8) is reduced to:

$$K_H^M = \frac{\overline{X}_M\,X_H}{\overline{X}_H\,X_M}\,\Gamma \quad or \quad \frac{K_H^M}{\Gamma} = \frac{\overline{X}_M\,X_H}{\overline{X}_H\,X_M} \tag{22}$$

By using Eq.(5) and rearranging, we can get:

$$\frac{1}{\overline{X}_M} = \frac{\Gamma}{K_H^M}\frac{1}{X_M} + \frac{K_H^M - \Gamma}{K_H^M} \tag{23}$$

On multiplying by $(X_M TN)/TC$, this equation is changed to

$$\frac{(TN)\,X_M}{(TC)\,\bar{X}_M} = \frac{\Gamma}{K_H^M}\frac{TN}{TC} + \frac{(TN)\,X_M}{TC}\frac{K_H^M - \Gamma}{K_H^M} \qquad (24)$$

where $(TN)X_M$ is the equilibrium concentration of M^+ in solution and $(TC)\bar{X}_M$ is the equilibrium concentration of M^+ in exchanger phase. They are expressed in terms of C_M and Q_M, respectively, and Eq.(24) is represented by:

$$\frac{C_M}{Q_M} = \frac{\Gamma}{K_H^M}\frac{TN}{TC} + \frac{K_H^M - \Gamma}{(TC)\,K_H^M}\,C_M \qquad (25)$$

At infinitesimal exchange, K_H^M is approximately constant. Therefore, plot of C_M/Q_M vs. C_M will give a straight line with a constant slope of $(K_H^M - \Gamma) / \{(TC)K_H^M\}$. This was the Langmuir isotherm to be derived, which was used in the form:[19,20]

$$Q_M = \frac{K\,Q_{max}C_M}{1 + KC_M} \quad or \quad \frac{C_M}{Q_M} = \frac{1}{K\,Q_{max}} + \frac{C_M}{Q_{max}} \qquad (26)$$

In the above treatment, the chemical meanings of the Langmuir constant K and other quantity have been clearly given:

$$K = \frac{K_H^M}{\Gamma(TN)} \quad and \quad Q_{max} = TC \quad or \quad \frac{(TC)K_H^M}{K_H^M - \Gamma} \qquad (27)$$

The Γ value is nearly equal to unity in case of mono-monovalent exchange. Hence, Q_{max} in the third equation in Eq.(27) is equal to TC when K_H^M is very large and Γ is negligible.

(2) case of n=2

The selectivity coefficient is given by

$$K_H^M = \frac{\bar{X}_M\,X_H^2}{\bar{X}_H^2\,X_M}\,\Gamma\eta \quad or \quad \frac{K_H^M}{\Gamma\eta} = \frac{\bar{X}_M\,X_H^2}{\bar{X}_H^2\,X_M} = m \qquad (28)$$

Equation (5) can be used to give

$$\bar{X}_M\,(1-X_M)^2 = m(1-\bar{X})^2X_M \quad or \quad (1-X_M)\left(\frac{1}{X_M} - 1\right) = m(1-\bar{X}_M)\left(\frac{1}{\bar{X}_M} - 1\right) \qquad (29)$$

In the infinitesimal loading and low concentration of exchanging ion,

$$\frac{1}{X_M} \ , \ \frac{1}{\bar{X}_M} > 1$$

Equation (29) can be simplified to:

$$\frac{1-X_M}{X_M} = m\frac{1-\bar{X}_M}{\bar{X}_M} \quad or \quad \frac{m}{\bar{X}_M} = \frac{1}{X_M} + (m-1) \tag{30}$$

By multiplying by 1/{(TN)(TC)}, we get:

$$\frac{m}{(TN)(TC)\bar{X}_M} = \frac{1}{(TN)(TC)X_M} + \frac{m-1}{(TN)(TC)} \tag{31}$$

Because $(TC)\bar{X}_M=Q_M$ and $(TN)X_M=C_M$, finally the following equation results.

$$\frac{m}{TN}\frac{1}{Q_M} = \frac{1}{TC}\frac{1}{C_M} + \frac{m-1}{(TN)(TC)} \tag{32}$$

The m value is nearly constant, because the selectivity constant K_H^M and Γ are constant in small X_M and $\bar{X}_M$ values. Thus, the Langmuir equation has been derived. The similar procedure for the case of n=3 provides the Langmuir-type equation.

Thus, the Langmuir-type equation at infinitesimal exchange has been demonstrated to be an expression of the selectivity coefficient of Eq.(8). The Kielland plot should be based on for the basic and entire expression of the ion exchange on inorganic ion exchangers.

It is known that TiSbA can be prepared at different antimony and titanium ratios (Sb/Ti) of 0.3~1. The normalization for TiSbA is based on the assumption that one antimony gives one hydrogen ion available for ion exchange. Thus, the theoretical capacity of 3.02 meq/g is calculated from the experimental formula of $0.343Sb_2O_5 \cdot TiO_2 \cdot 2.00H_2O$.

3. EXPERIMENTAL

The TiSbA in H^+ form was immersed in a mixed solution of varying ratio of the metal nitrate / nitric acid in a sealed glass tube with intermittent shaking at 30±0.5, 45±0.5 and 60±0.5°C. The ratio, (volume of mixed solution) / (g of TiSbA), was kept in 100 (cm^3/g). The total normality in mixed solution was adjusted to 0.2N (1N = 1 normal). The equilibrium concentrations in the solid phase and in solution phase were deduced from the change of M^{3+} and H^+ concentration relative to the initial concentration of the solution. The concentration of metal ions in the solutions was determined by inductively coupled plasma atomic emission spectroscopy (ICP-AES). The H^+ concentration was determined by titration with 0.1mol dm^{-3} standard sodium hydroxide solution.

4. RESULTS AND DISCUSSION

4-1 Kielland plot

It has been known that the selectivity on inorganic ion exchangers is much dependent on the concentration of metal ions in the exchanger phase because of their rigid structure mentioned above. It is known that large steric effect may arise in a rigid exchanger which undergoes little swelling or shrinkage, if there is a large difference in the ionic crystal radii of the two exchanging cations.

Among the ion exchange system of trivalent metal ions / hydrogen ions, i.e. Al^{3+}, Ga^{3+}, In^{3+}, Y^{3+}, La^{3+}, Nd^{3+}, Eu^{3+} and Yb^{3+} / H^+, were selected in order to interpretation of the selectivity for trivalent metal ions. The Kielland plot appear composed of two straight lines with a break point at $\bar{X}_M$=0.005-0.01 for metal ions / H^+ exchange systems studied (Figs.4-2 a,b,c). It suggests two sort of exchange sites available for the trivalent metal ions. The log K_H^M values decreased gradually with increasing $\bar{X}_M$, indicating the steric effect depends on the exchanging metal ion. The kielland plot of different trivalent metal ions / H^+ exchange systems at 30°C are summarized in Fig.4-3. Moving the axis of abscissa from left to right up to $\bar{X}_M$=0.16 in Fig.4-3, the different selectivity can be found in the different range of $\bar{X}_M$. The selectivity was $Al^{3+} < Y^{3+} < Yb^{3+} < Ga^{3+} < Eu^{3+} < Nd^{3+} < La^{3+} < In^{3+}$ for range of $\bar{X}_M$= 0 to 0.02 and $Al^{3+} < Y^{3+} < Yb^{3+} < Eu^{3+} < La^{3+} < Nd^{3+} < Ga^{3+} < In^{3+}$ for range of $\bar{X}_M > 0.02$.

In general, when small cations in inorganic ion exchangers are exchanged with large cations in solution, the ingoing ions are initially preferred and become progressively less preferred with increasing loading, because the large space are occupied by cations and cations repel each other. This extent can be evaluated by the comparison of numerical values of Kielland coefficient $|C_m|$, i.e. a large negative value of Kielland coefficient indicates large steric effect.[21)]

The $|C_m|$, which is referred to Kielland coefficient are listed in Table 4-1. This shows that group 13 metal ions with a small effective ionic radius[22)] enter the exchanger with small steric hindrance in comparison with rare earth metal ions. This difference of the steric effect brings two different selectivity series against EIR for group 13 metal ions and rare earth metal ions. The region with the large $|C_m|$ value is limited to a small extent of exchange compared with that of Li^+ which showed a break point at $\bar{X}_M$=0.025.[23)] This is due to that the trivalent metal ions are much strongly hydrated in

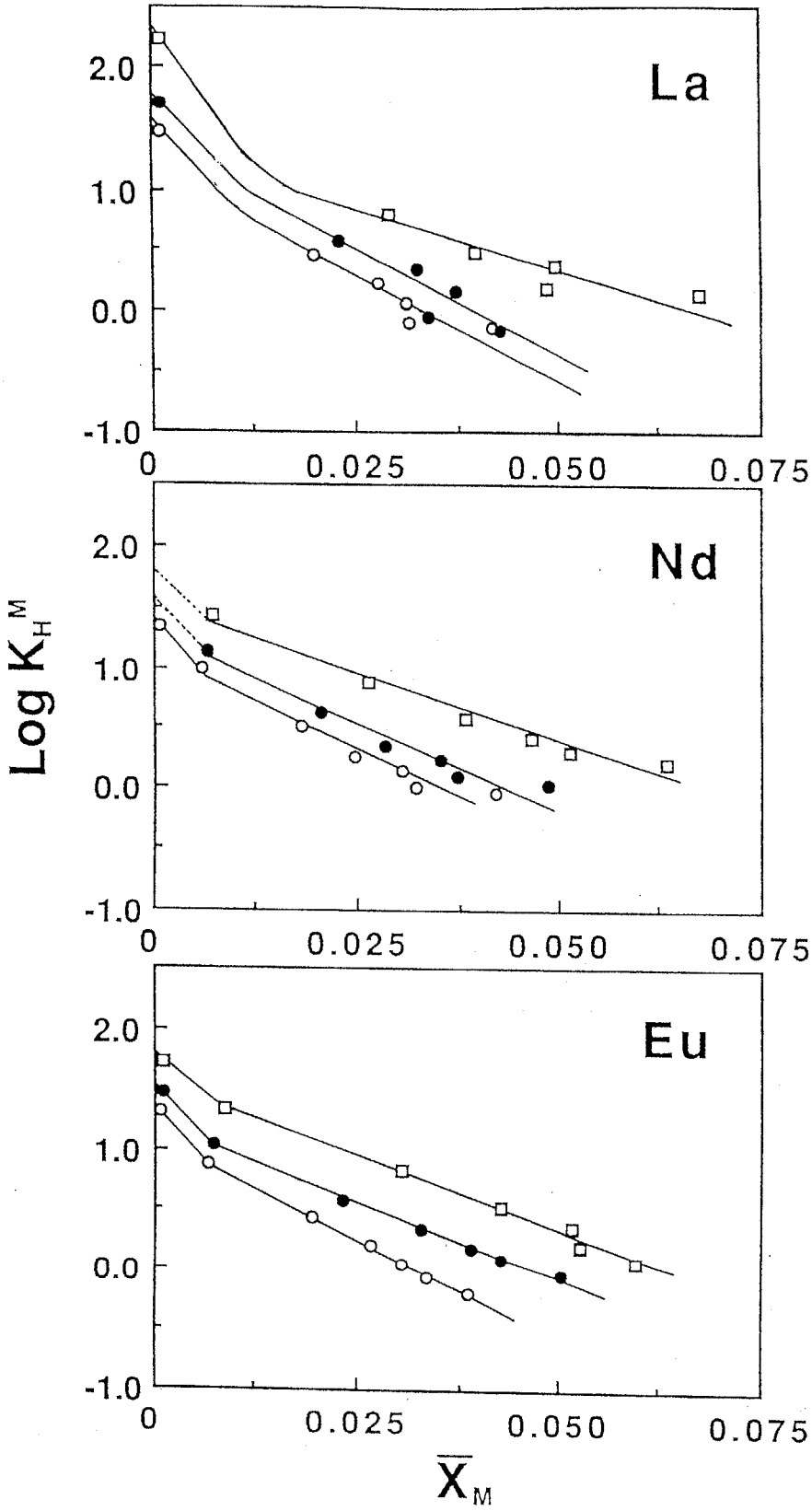

Fig.4-2 (a) Kielland Plots of La^{3+}, Nd^{3+} and Eu^{3+} / H^+ Exchange on TiSbA

Total Normality, 0.2N; Temp., ○:30, ●:45 and □:60°C

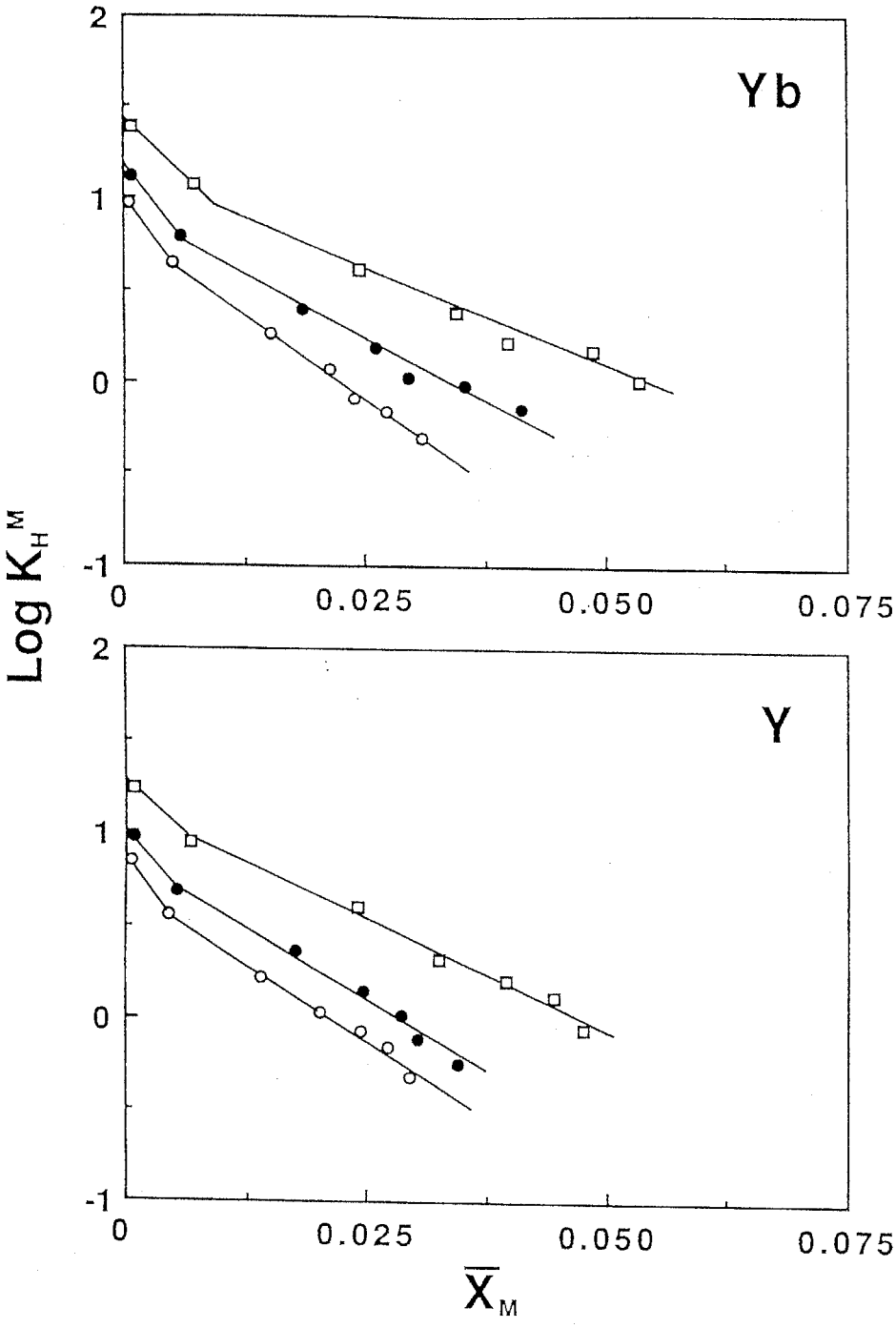

Fig.4-2 (b) Kielland Plots of Yb^{3+} and Y^{3+} / H^+ Exchange on TiSbA

Total Normality, 0.2N; Temp., ○:30, ●:45 and □:60°C

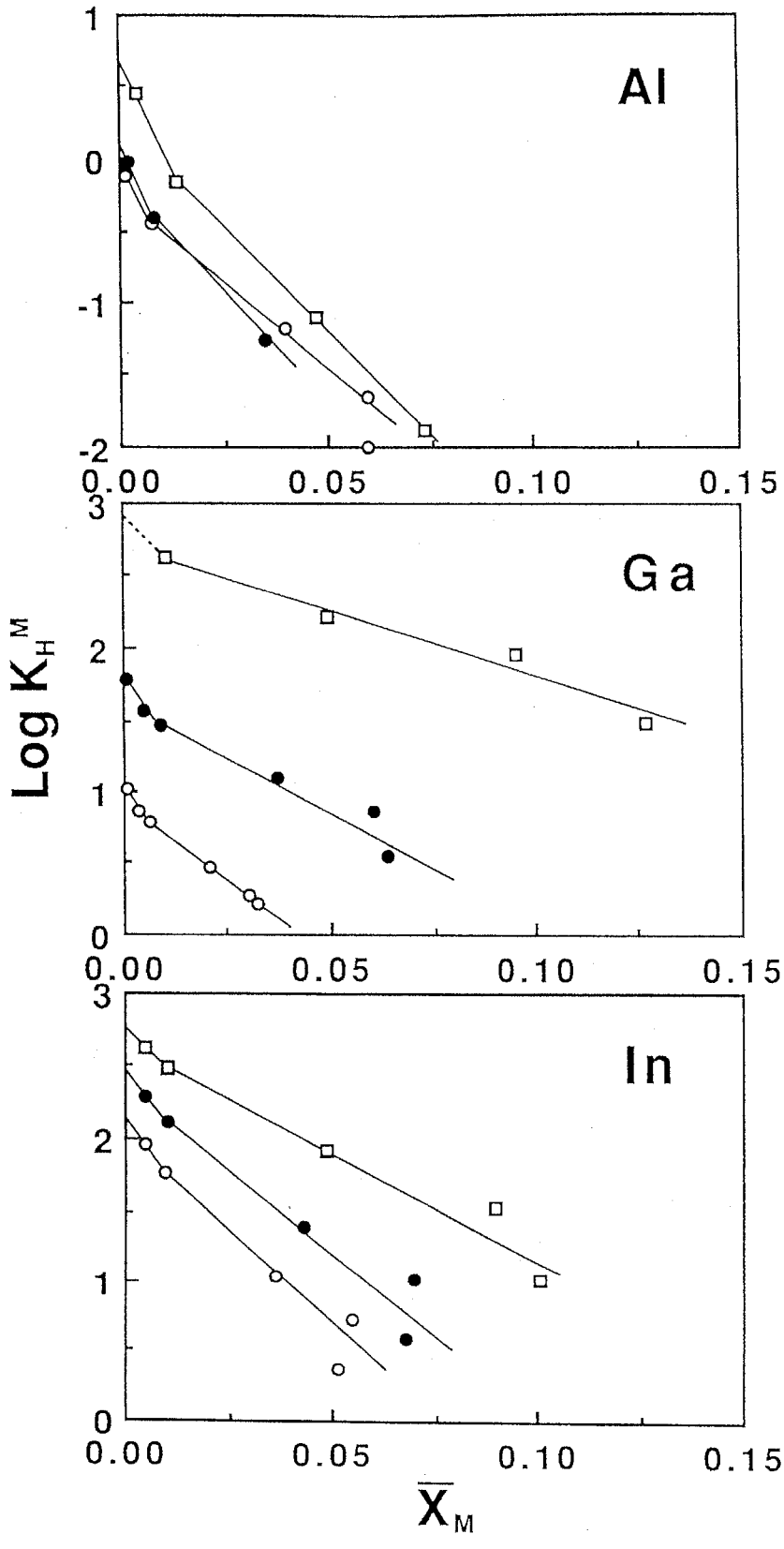

Fig.4-2 (c) Kielland Plots of Al^{3+}, Ga^{3+} and In^{3+} / H^+ Exchange on TiSbA
Total Normality, 0.2N; Temp., ○:30, ●:45 and □:60°C

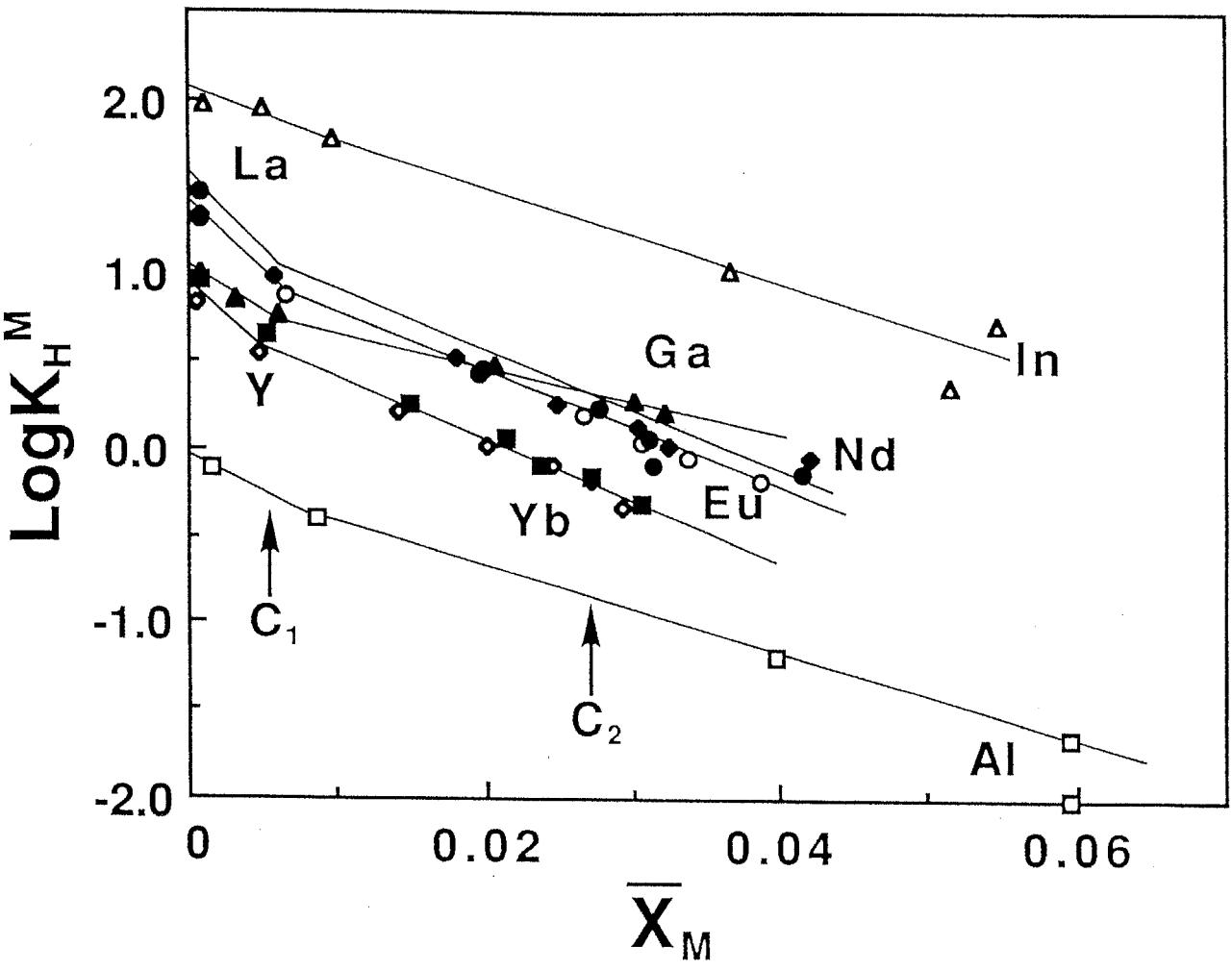

Fig.4-3 The Summarized Kielland Plots of M^{3+}/H^{+} Exchange on TiSbA at 30°C
Total Normality, 0.2N

Table 4-1 Kielland Coefficient on Ion Exchange Reaction of M^{3+}/H^{+} on TiSbA at 30°C.

	Al	Ga	In	Y	La	Nd	Eu	Yb
C_1	-46.7	-52.6	-35.2	-107		-72.9	-72.9	-107
C_2	-12.1	-10.3	-11.2	-17.4	-17.1	-17.1	-17.1	-18.5

comparison with Li^+ and retain the large dimension.

4-2 Hypothetical thermodynamic data

The thermodynamic equilibrium constant, K, can be evaluated from eq.(10) by integrating the continuous function between ln K_H^M vs. $\bar{X}_M$ over the entire range of $\bar{X}_M$ from 0 to 1. However, $\bar{X}_M$ could not reach to unity for trivalent metal ions on TiSbA because of the steric effect. In this study, the hypothetical thermodynamic constant K_{ideal} for the ideal exchange was calculated by using Eq.(17) assuming that C_m equals to zero. The ΔG^o_{ideal} is defined by Eq.(19).

The ΔH^o_{ideal} values can be regarded as constant, because van't Hoff's plots, $(K_H^M)_{X_M,\bar{X}_M \to 0}$ vs. 1/T, showed good linearity over the entire range of temperature studied (Fig.4-4). The ΔG^o_{ideal}, values at 298 K were calculated by extrapolating the determined $(\log K_H^M)_{X_M,\bar{X}_M \to 0}$ values to 25°C. The selectivity for infinitesimal concentration was increased as follows: $Al^{3+} < Y^{3+} < Yb^{3+} < Eu^{3+} = Nd^{3+} < La^{3+} < In^{3+} = Ga^{3+}$ at 60°C. The ΔG^o_{ideal} values at 25°C were calculated by extrapolating the determined $(\log K_H^M)_{X_M,\bar{X}_M \to 0}$ values to 25°C. The calculated ΔG^o_{ideal}, ΔH^o_{ideal} and ΔS^o_{ideal} values at 25°C were summarized in Table 4-2. The rare earth metal ions except for La^{3+} have the similar values of ΔH^o_{ideal} and ΔS^o_{ideal}. It can be considered that rare earth metal ions take similar behavior each other on TiSbA.

The ion exchange reaction (1) can be separated into the hydration ($-\Delta Y_{hyd}$) and ion-exchange processes (ΔY_{exch}) as follows;

$$-\Delta Y_{hyd}: \quad \frac{1}{3} M^{3+}(aq.) + H^+(gas) \rightleftarrows \frac{1}{3} M^{3+}(gas) + H^+(aq.)$$

$$\Delta Y_{ex}: \quad \frac{1}{3} M^{3+}(gas) + \overline{H^+} \rightleftarrows \frac{1}{3} \overline{M^{3+}} + H^+(gas)$$

where the Y represents thermodynamic functions such as G, H and S. The values of ΔY^o contribute to the difference in the thermodynamic functions of ΔY^o_{exch} and ΔY^o_{hyd}. ΔY^o_{hyd} is based on the $\Delta Y^o_{hyd}=0$ of the reaction; $H^+(gas) \rightarrow H^+(aq)$. The calculated values of ΔY^o, ΔY^o_{hyd} and ΔY^o_{exch} were summarized on Table 4-2.[24)]

Large values of ΔH^o_{ideal} and ΔS^o_{ideal} were found on the Ga^{3+} / H^+ exchange system, as compared with those of other systems studied. The ΔS^o_{exch} showed positive values except for Al^{3+} and Y^{3+}. An extremely high value was observed on the Ga^{3+}, In^{3+} and

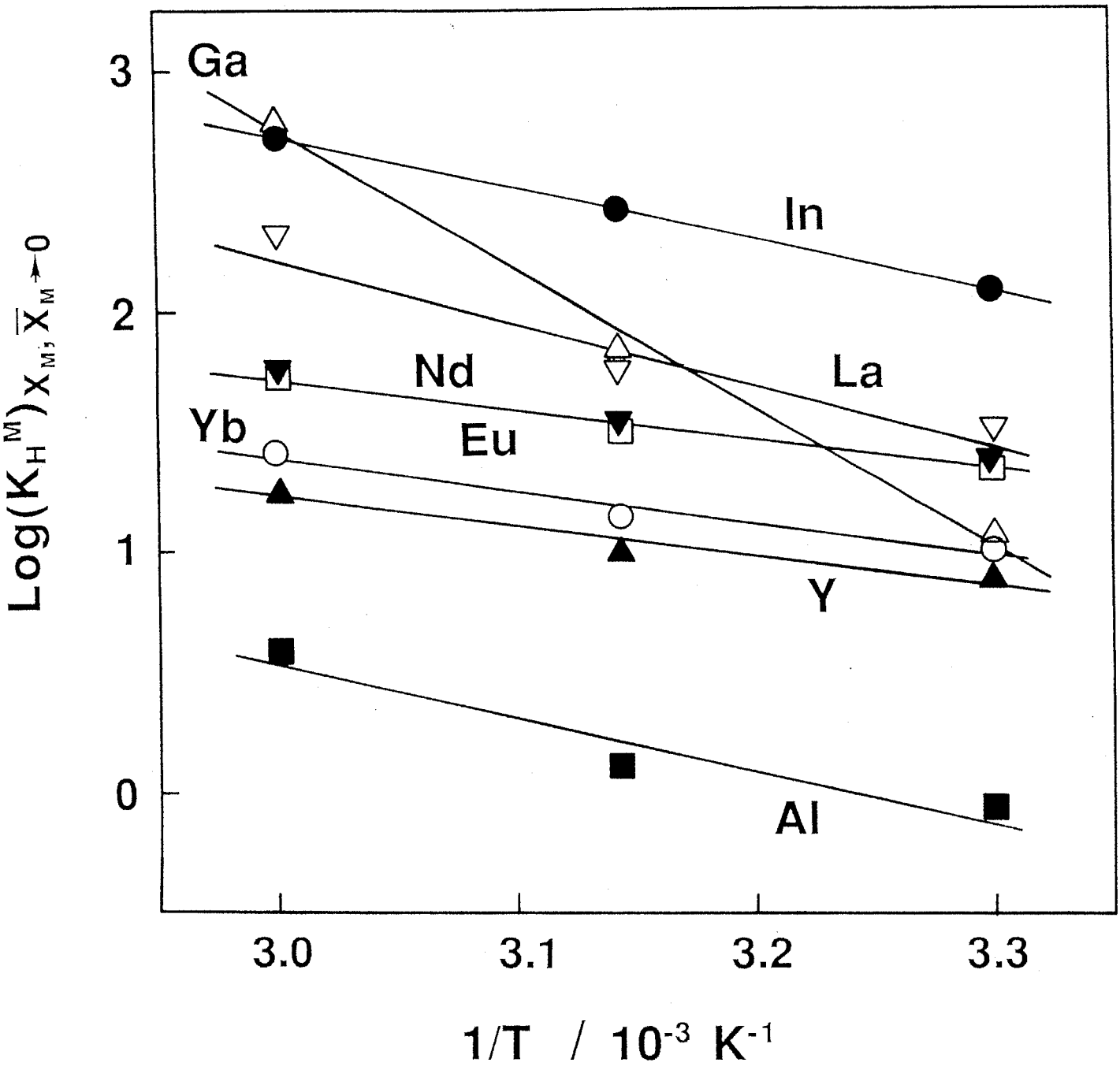

Fig.4-4 Van't Hoff Plots of $\ln(K_H{}^M)_{X_M,X_M\to 0}$ on TiSbA

Table 4-2 Hypothetical Thermodynamic Data of Ion Exchange Reaction of M^{3+}/H^{+} on TiSbA at 25°C.

	$\Delta G°_{ideal}$ kJ mol^{-1}	$\Delta H°_{ideal}$	$\Delta H°_{hyd}$* kJ mol^{-1}	$\Delta H°_{exch}$	$\Delta S°_{ideal}$	$\Delta S°_{hyd}$* J $K^{-1}mol^{-1}$	$\Delta S°_{exch}$
Al	6.31	41.8	-1406	-1364	119	-144.2	-25.2
Ga	0.904	111	-1400	-1289	370	-156.6	213
In	-6.34	40.2	-818	-778	156	10.40	166
Y	0.419	23.7	-285.1	-261	78.3	-87.20	-8.9
La	-2.53	51.5	-3.4	48.1	181	-55.34	126
Nd	-2.48	23.0	-138	-115	85.6	-63.73	21.9
Eu	-2.26	25.0	-226	24	91.4	-80.50	10.9
Yb	-0.290	25.4	-43.2	-17.8	86.1	-72.78	13.3

* Ref. 24.

La^{3+}/ H^+ exchange systems.

If the ΔS^o is zero, where the value of ΔS^o_{exch} is equal to that of ΔS^o_{hyd}, this suggests that the exchanging cation has the same hydration structure as that in aqueous solution. The positive value of ΔS^o_{exch} may indicate that degree of freedom of metal ion increases in the cavity of TiSbA. Such an increase of ΔS^o_{exch} may occur from dehydration of metal ions or net transfer of water molecules from solid phase to aqueous phase. In the less hydrated cations, the degree of freedom may increase by the transfer of some water molecules from TiSbA cage to the aqueous phase. On the other hand, Al^{3+} and Y^{3+} with small effective ionic radii are strongly hydrated in comparison with other cations, and so ΔS^o_{exch} has a negative value.

4-3 Langmuir plot

The Langmuir plot was exemplified by the Eu^{3+}/H^+ exchange in Fig.4-5. It is not a straight line, but concave upper. The K_H^M is not constant at the $\bar{X}_M$ values studied and steeply increases even at $\bar{X}_M$<0.005. The Langmuir plot is an expression of the mass action law, and depends on the equilibrium concentration of exchanging ions, as has been made clear in Eq.(27). The two-step process is hidden in this plot. Extended selectivity studies in the low $\bar{X}_M$ region are required for delineating the two types of exchange in the Kielland plot and to determine the thermodynamic constants of these exchangers. Therefore, the thermodynamic quantities are not reported here.

4-4 Predictive evaluation

The concentration dependence of Kd values on the concentration of Eu^{3+} ions was calculated from their Kielland plots (Fig.4-6). The full lines show the calculated Kd values with a two-site model and the dotted lines show the calculated Kd values with a single-site model. In the latter, the site is assumed to be homogeneous in all range of $\bar{X}_M$. The empirical Kd values have fallen on the calculated line with the two site model.

The selectivity coefficient at the infinitesimal exchange $(K_H^M)_{X_M,\bar{X}_M\to 0}$ was evaluated from the Kielland plot. The Kd value at the infinitesimal exchange $(Kd)_{X_M,\bar{X}_M\to 0}$ were calculated, using Eq.(16). They are summarized in Table 4-3 for the rare earth metal ions. A large separation factor for La-Yb pair is marked on the TiSbA compared with those on AG50W-X8.[25)]

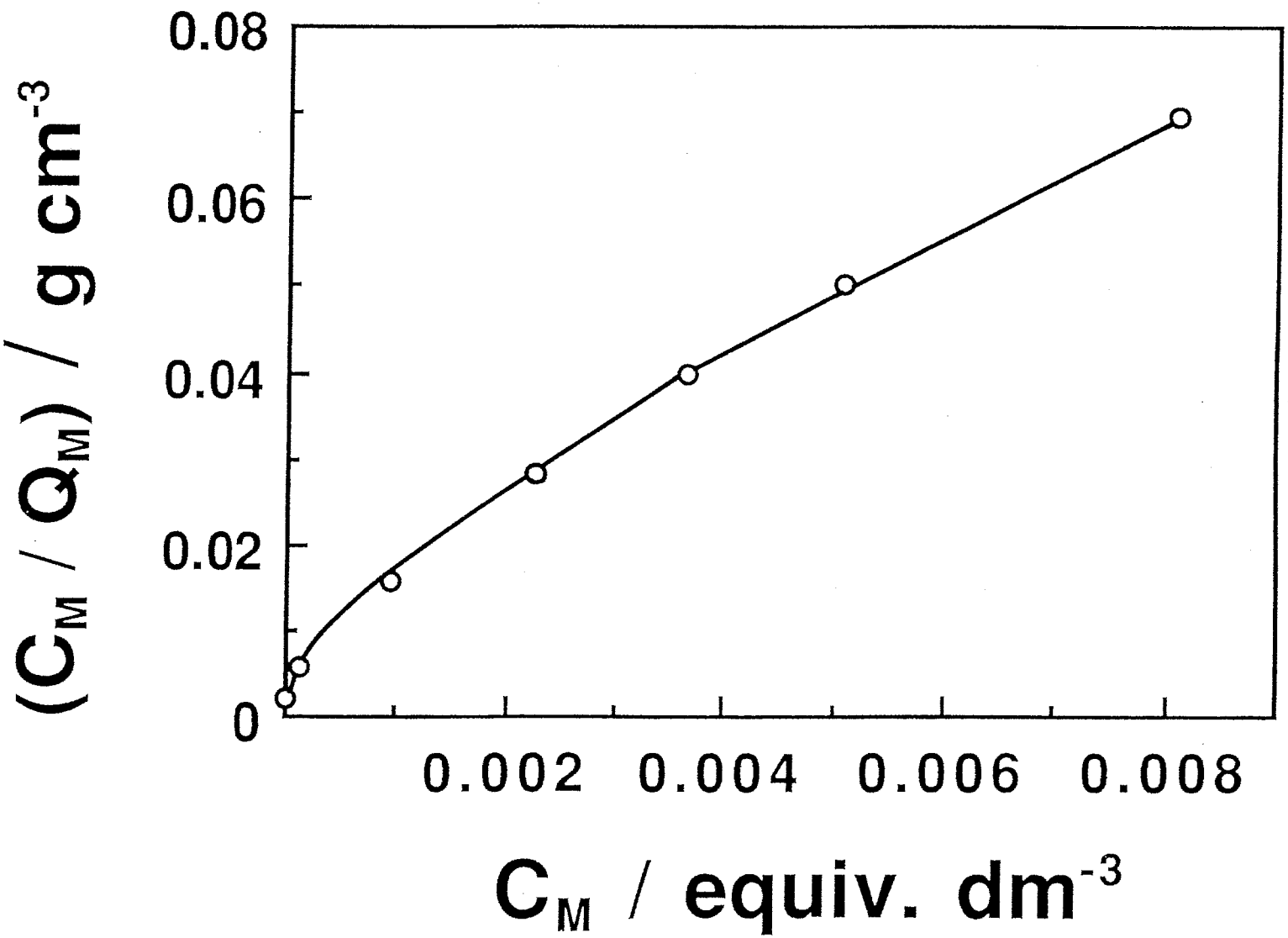

Fig.4-5 Langmuir Plot of Eu^{3+}/H^+ Exchange on TiSbA at 30°C
Total Normality, 0.2N; TiSbA, 0.10g; Total Vol., 10.0cm^3

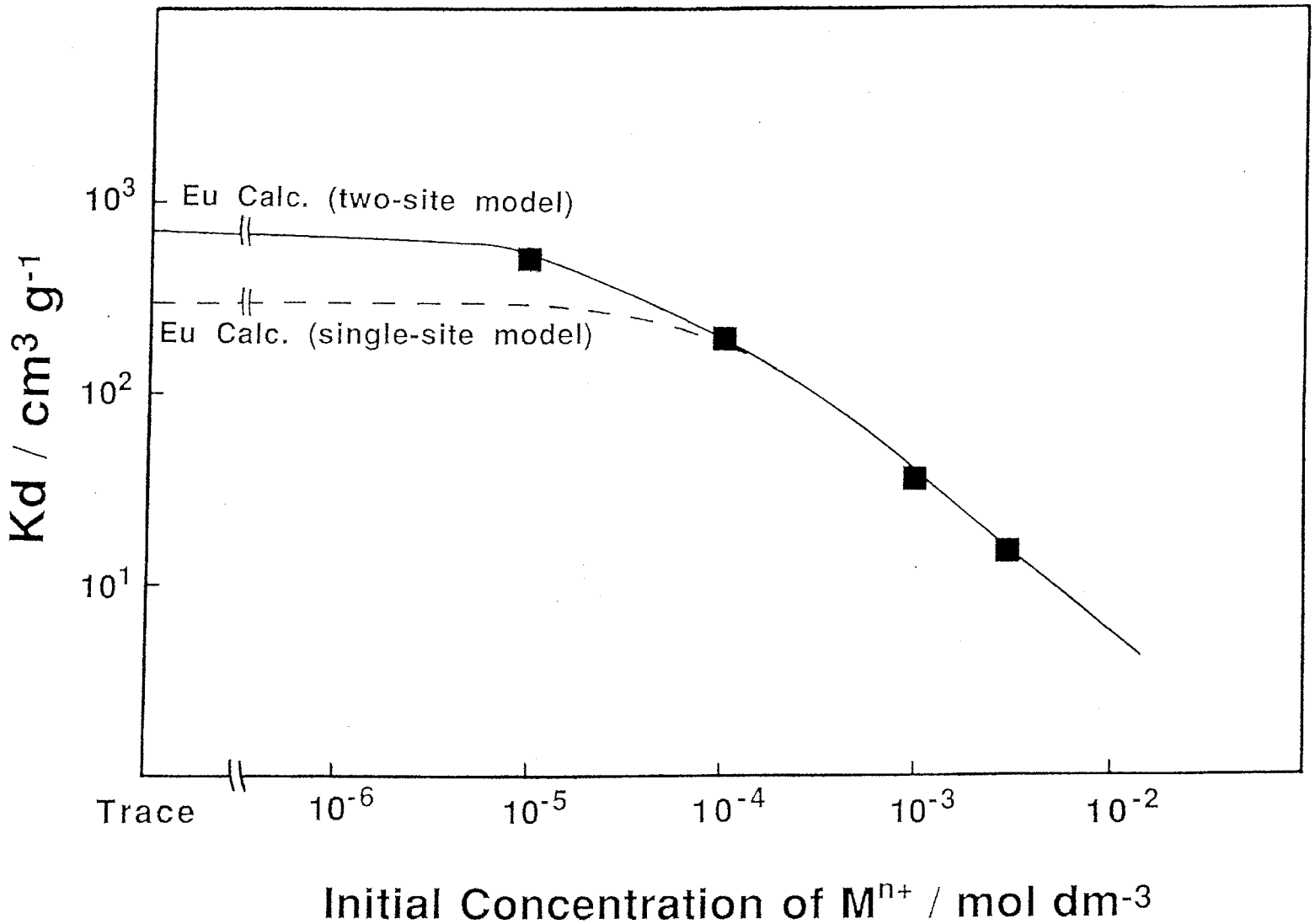

Fig.4-6 Calculated Kd Values as a Function of the Initial Concentration of Exchanging Ion
Empirical Value ■

Table 4-3 Selectivity Coefficients, Kd Values and Separation Factors (α_N^M) at Infinitesimal Exchange for Rare Earth Metal Ions on TiSbA.

TiSbA	Y	Yb	Eu	Nd	La
$(K_H^M)_{X_M,\bar{X}_M\to 0}$	9.0_4	$1.3_8\times10^1$	$2.8_2\times10^1$	$2.8_2\times10^1$	$3.9_8\times10^1$
$(K_d)_{X_M,\bar{X}_M\to 0}$	$2.2_4\times10^2$	$3.3_9\times10^2$	$6.9_2\times10^2$	$6.9_2\times10^2$	$9.7_7\times10^2$
α_N^M		1.5	2.0	1.0	1.4

BIO-RAD AG50W-X8	Y	Yb	La
$(K_H^M)_{X_M,\bar{X}_M\to 0}$	$5.6_3\times10^3$	$6.7_2\times10^3$	$8.0_7\times10^3$
$(K_d)_{X_M,\bar{X}_M\to 0}$	$3.5_8\times10^1$	$4.1_3\times10^1$	$4.7_3\times10^1$
α_N^M		1.2	1.1

Total normality: 0.2N for TiSbA and 2N for AG50W-X8.

5. REFERENCES

1. M. Abe, R. Chitrakar, M. Tsuji, and K. Fukumoto, Solvent Extr. Ion Exch., *3,* 1988 (1985).
2. R. Chitrakar and M. Abe, Analyst, *111,* 339 (1986).
3. M. Tsuji, H. Kaneko, M. Abe, Y. Morita and M. Kubota, Radiochim. Acta, (in press).
4. H. Kaneko, M. Tsuji, M. Abe, Y. Morita and M. Kubota, J. Nucl. Sci. Technol., *34,* 988 (1992).
5. M. Tsuji and S. Komarneni, J. Mater. Res., *4,* 698 (1989).
6. S. Komarneni and M. Tsuji, J. Am. Ceram. Soc., *72,* 1668 (1989).
7. M. Tsuji and M. Abe, Solvent Extr. Ion Exch., *2,* 253 (1984).
8. M. Tsuji and M. Abe, Radioisotopes, *33,* 218 (1984).
9. M. Tsuji and M. Abe, Bull. Chem. Soc. Jpn., *58,* 1109 (1985).
10. K. Ooi, Y. Miyai and S. Kudoh, Sep. Sci. Technol., *21,* 755 (1986).
11. M. Tsuji, S. Komarneni, Y. Tamaura and M. Abe, Mater. Res. Bull., *27,* 741 (1992).
12. M. Tsuji and S. Komarneni, Sep. Sci. Technol., *26,* 647 (1991).
13. M. Tsuji and S. Komarneni, Sep. Sci. Technol., *27,* 813 (1992).
14. D. W. Breck, Zeolite Molecular Sieves, Structure, Chemistry and Use, John Wiley and Sons, New York, 1974, P.532.
15. G. L. Gaines, Jr. and H. C. Thomas, J. Chem. Phys., *21,* 714 (1953).
16. R. M. Barrer and J. Klinowski, J. Chem. Soc., Faraday Trans. 1, *70,* 2080 (1974).
17. R. M. Barrer, in *Natural Zeolites, Occurrence, Properties, Use*, edited by L. B. Sand and F. A. Mumpton, Pergamon, New York, 1978, p.385.
18. E. Glueckauf, Nature, *163*, 414 (1949).
19. H. Mimura and T. Kanno, J. Nucl. Sci. Technol., *24,* 284 (1985).
20. H. Mimura, F. Tachibana and K. Akiba, Proc. 3rd Int. Conf. Nucl. Fuel Reprocessing Waste Management (RECOD'91), Apr.14-18, 1991, Sendai, Japan, Vol.II, p.796.
21. J. Kielland, J. Soc. Chem. Ind., 232T (1935).
22. R. D. Shannon and C. T. Prewitt, Acta Cryst., *B25,* 925 (1969).
23. M. Abe, Y. Kanzaki and R. Chitrakar, J. Phys. Chem., *91,* 2997 (1987).
24. Y. Marcus, Ion Solvation, John Wiley and Sons Ltd., Table 4.5 in p 79, New York, 1985.

25. F. W. E. Strelow, R. Rethemeyer and C. J. C. Bothma, Anal. Chem., *37*, 106 (1965).

CHAPTER 5

Selective Exchange Am^{3+} and Pu^{4+} on Synthetic Inorganic Ion Exchangers

1. INTRODUCTION

Separation of long-lived radionuclides, e.g., ^{137}Cs and ^{90}Sr, has been studied in neutral media using clay minerals,[1] zeolites[2-4] and topotactically leached phlogopite mica.[5] The last material has been reported to be highly selective for Cs^+. These are naturally occurring cation exchangers that have been mostly directed toward use in environmental decontamination and in the disposal of low-level radioactive wastes.

Much attention has recently been directed toward separation of α-emitting transuranium (TRU) ions from high-level nuclear waste (HLW).[6-10] The separation of TRU ions from HLW involves the following aspects:

(1) moderately concentrated HNO_3

(2) intense radiation field

(3) elevated temperatures associated with the intense radiation field

(4) coexisting bulk components with different valencies.

Hence, a high selectivity towards TRU ions is required for effective separation from HLW as well as for radiation and thermal stabilities.

Solvent extraction methods[7,8,11-13] have been mostly used for the chemical separation of TRU from HLW. The extractants and solvents are deteriorated by radiolysis in the intense radiation field. On the other hand, inorganic ion exchangers have higher radiation and thermal stabilities. Their use for the separation of radioactive elements from HLW is advantageous at least with respect to these stabilities.

The above-mentioned aluminosilicate-type ion sieves are not stable in acidic media of pH < 1-2. Synthetic inorganic ion exchangers have high selectivity for certain elements in relatively concentrated HNO_3, as well as higher radiation and thermal stabilities in comparison with organic extractants and commercial ion-exchange resins.[14-17]

The objective of the present work is to study the selectivity for Am^{3+} and Pu^{4+} on cation exchange materials which are chemically stable in realatively concentrared HNO_3. And the ion exchange property of Am^{3+} was compared with those of other trivalent ions on TiSbA.

2. EXPERIMENTAL

2-1 Preparation of ion exchangers

Ion exchangers used in this study were prepared according to references. The procedures are described briefly as follows:

(a) Crystalline Antimonic(V) Acid (C-SbA):[18] A precipitate was allowed to form by hydrolysis of 4mol dm^{-3} $SbCl_5$ solution prepared by prehydrolysis (1+1 on a volume basis), and then aged in the mother solution at 40°C with intermittent shaking for over 20 days in order to enhance crystallization. The product was washed with cold deionized water to prevent peptization until it was free from Cl^-. The washing solution was separated from the solid by a centrifuge (about 10,000 rpm). The washed product was dried at room temperature, ground and sieved to obtain 100~200 mesh-sized fraction. Any adhering small particles were removed by rewashing with deionized water.

(b) Tin(IV) Antimonate (SnSbA):[19] An aliquot of 4mol dm^{-3} $SbCl_5$ solution prepared by prehydrolysis as described above was mixed with a requisite amount of 4mol dm^{-3} $SnCl_4$ solution at 60°C. The mixed solution was then poured into 25-fold volume of deionized water at 60°C to form a precipitate. The precipitate was aged in the mother solution for 4 days followed by thorough washing with deionized water to remove a large part of the resultant HCl until pH> 1.5 as above. The washed product was dried at 60°C, ground and sieved to obtain 100~200 mesh-sized fraction.

(c) Titanium(IV) Antimonate (TiSbA): TiSbA used in this study were prepared according to the manner of the preparation in chapter 2.

(d) Cryptomelane-type Hydrous Manganese Dioxide (CRYMO):[20] A precipitate was allowed to form by adding 0.5mol dm^{-3} $KMnO_4$ containing 1mol dm^{-3} H_2SO_4 to a mixed solution of 1mol dm^{-3} $MnSO_4$ and 1mol dm^{-3} H_2SO_4 at 60°C. It was aged in the mother solution overnight and washed with 6mol dm^{-3} HNO_3 (0.5dm^3), followed by thorough washing with water. The washing solution was separated by a centrifuge (about 10,000rpm). The washed product was dried at 65~75°C for 3 days, ground and sieved to obtain 100~200 mesh-sized fraction. H^+ was exchanged for K^+, which was incorporated into the crystal structure: the dried and sieved material was packed in a glass column (20cm × 1.0cm I.D.) and concentrated HNO_3 was percolated through the column at room temperature until the concentration of K^+ in the effluent was lower than 10^{-4}mol dm^{-3}. The treated material was washed thoroughly and air-dried at room

temperature.

2-2 Selectivity Study

The above exchanger (0.200g) in the H^+ form was equilibrated with $20cm^3$ of the mixed solution containing a TRU element and HNO_3 with intermittent stirring at 30°C. ^{237}Np and ^{241}Am were determined by γ-spectrometry and Pu by α-counting. The uptake was estimated from the difference between the initial and the equilibrated concentrations. The distribution coefficient (Kd) was calculated using the same equation in Chapter3. The Kd values of Pu^{4+} and Am^{3+} in simulated high level nuclear waste were also determined in the similar manner.

2-3 Chemicals

$^{241}Am^{3+}$ was used as supplied from Amersham International. $^{237}NpO_2^+$ was prepared by dissolving oxide and purifying with di-isodecyl phosphoric acid (DIDPA).[21] Pu was extracted with tributyl phosphate (TBP) from a high-level nuclear waste. It was chemically converted to Pu^{4+}, followed by purification using an anion-exchange chromatography.

DIDPA and $SbCl_5$ were supplied by Daihachi Chemical Ind. Co. and Yotsuhata Chemical Co., and used without further purification. Other chemicals were of analytical grade from Wako Pure Chemical Co. Ltd. (Japan).

3. RESULTS AND DISCUSSION

3-1 Ion exchanger

X-Ray diffraction patterns and TG-DTA profiles of the synthetic materials showed good agreement with data reported previously.18-20,22,23) The chemical composition and crystallographic data are represented in Table 5-1.

3-2 Time dependence for adsorption

The relative concentration of actinides in the solution was plotted as a function of time (Fig.5-1). The rate of adsorption for each element showed a similar trend on different ion exchangers investigated. A relatively low rate of adsorption was observed on SnSbA. The equilibrium was attained within two weeks. Adsorption rate on the commercial strong acid-type cation exchanger (Dowex 50W-X8) has been believed to be faster than that on inorganic ion exchangers. But no clear difference between them was observed as far as the adsorption rate of actinides studied under the present conditions was concerned.

But large difference between them was not observed as long as the adsorption rate of actinides studied in the present conditions was concerned.

The ion-exchange rate in the initial stage was affected by the shaking mode on both ion exchangers (Fig.5-2). However, equilibration time was approximately the same for each ion exchanger.

3-3 Selectivity study

The Kd value was often used for the expression of the ion exchange selectivity. However, it is an empirical parameter and does not allow the general expression of the selectivity. It is much better to use the corrected selectivity coefficient K_H^M at the specified exchange $\overline{X}_M$ on the Kielland plot for general comparison and the discussion of ion selectivity on an ion exchanger. It varies strongly depending upon the fractional exchange in an inorganic ion exchanger in comparison with the organic ion exchanger. It is given by the linear relation for the single-site exchanger:

$$\log K_H^M = (\log K_H^M)_{X_M,\ \bar{X}_M \to 0} + 2C\,\bar{X}_M$$

The 2C value is negative and called the Kielland coefficient. A $|C|$ value is small in

Table 5-1 Chemical composition and crystal system of synthetic inorganic ion exchangers.

ion exchanger	chemical composition	crystal system
C-SbA	$Sb_2O_5 \cdot 4H_2O$	cubic
SnSbA	$1.1SnO_2 \cdot Sb_2O_5 \cdot 4.9H_2O$	tetragonal
TiSbA	$3.1TiO2 \cdot Sb_2O_5 \cdot 4.9H_2O$	tetragonal
TiSbA(TS1)	$1.8TiO2 \cdot Sb_2O_5 \cdot 4.8H_2O$	tetragonal
TiSbA(TS2)	$3.2TiO2 \cdot Sb_2O_5 \cdot 4.1H_2O$	tetragonal
CRYMO	$MnO_2 \cdot 0.3H_2O$	tetragonal

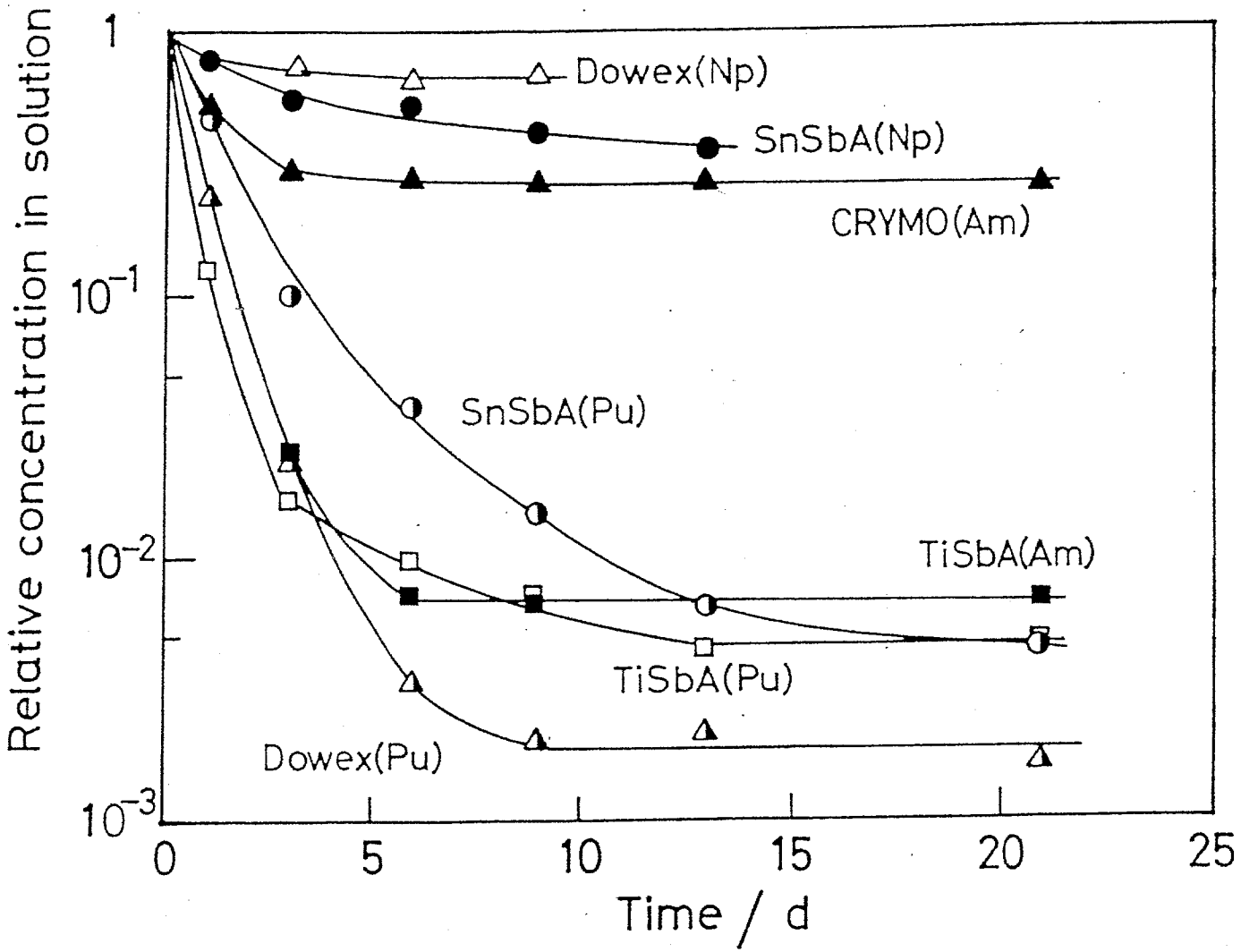

Fig.5-1 Time Dependence for Adsorption of TRU Ions on Synthetic Inorganic Ion Exchangers

Exchangers, 0.200g; Solution, 5.3×10^{-5} M (M = mol dm^{-3}) for NpO_2^+, 2.1×10^{-9}M for Am^{3+}, 1.3×10^{-8}M for Pu^{4+} in 0.2M HNO_3; Total vol. of solution, 20cm^3; Temp., ca.15°C

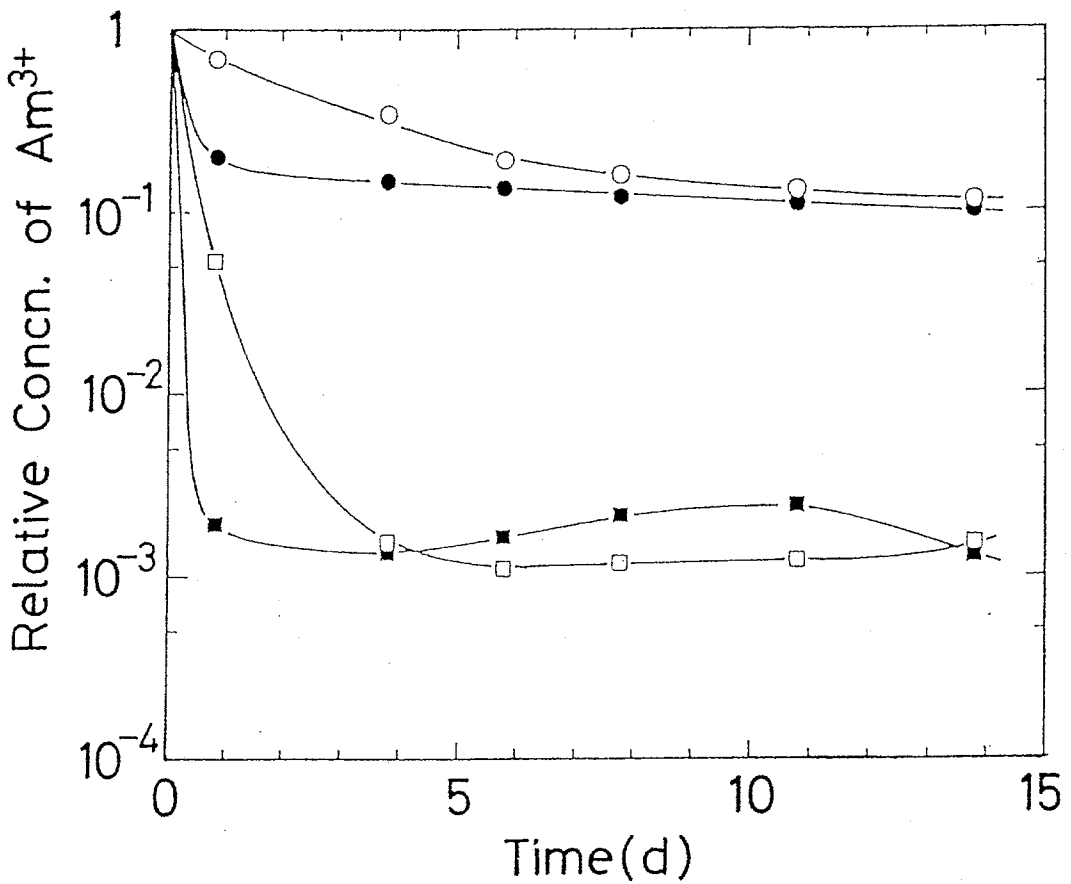

Fig.5-2 Effect of Shaking Modes on Adsorption of Am^{3+} on TS1 and Organic Ion Exchangers
Exchangers,0.200g; Solution, 2.1×10^{-9}M for Am^{3+} in 0.2M HNO_3; Total vol. of solution, $20cm^3$; Temp., 30°C; ○ ,● :TS1, □ ,■ :Dowex50W-X8, Open marks: intermittent shaking, Closed marks: continuous shaking

organic ion exchange resin and very large in a synthetic inorganic ion exchanger: For instance, -20.1 for Ce^{3+}; -18 for Sm^{3+}; -48 for Sc^{3+} on C-SbA.[24)]

The Kd values for Pu^{4+}, Am^{3+} and NpO_2^+ were compared as a function of HNO_3 because he Kielland plot could not be determined due to limited concentration of those nuclides available (Figs.5-3 a~e). High selectivity toward Pu^{4+} can be stressed on C-SbA, SnSbA, TiSbA and Dowex 50W-X8, while low selectivity for Pu^{4+} was observed on CRYMO. The selectivity on these four exchangers increased in the order of NpO_2^+ < Am^{3+} < Pu^{4+}, but was reversed on CRYMO, giving the order of NpO_2^+ < Pu^{4+} < Am^{3+} in the region of 0.2 ~ 1mol dm^{-3} HNO_3. The plot for Pu^{4+} gave a straight line in the concentration range studied, except for the low concentration region of HNO_3. This may be due to hydrolysis and/or disproportionation of Pu^{4+} in nitric acid solutions of low concentration:[25)]

$$Pu^{4+} + 2H_2O = 2Pu^{3+} + PuO_2^{2+} + 4H^+$$

$$Pu^{4+} + H_2O = PuOH^{3+} + H^+$$

The slope of the straight line for Am^{3+} showed -4.7 on C-SbA, -3.4 on SnSbA, -2.8 on TiSbA and -2.5 on CRYMO, indicating that the ion-exchange process is predominant for adsorption of these ions.

The selectivity for NpO_2^+ is low (Kd < 10) on C-SbA, TiSbA and CRYMO, in contrast with the high selectivity for Pu^{4+} and Am^{3+} on these ion exchangers. This can be ascribed to low charge and large dimension of NpO_2^+. This large difference in selectivity will make it possible to separate NpO_2^+ from Pu^{4+} and Am^{3+} using these ion exchangers. SnSbA and Dowex 50W-X8 (Figs.5-3 b and e) showed larger Kd values for NpO_2^+ than other three ion exchangers. The log-log plot of Kd vs [HNO_3] showed a straight line except for 2mol dm^{-3} HNO_3. The slope of the straight line was -1, clearly indicating the ion-exchange process.

Higher Kd values than those estimated from the slope were observed for NpO_2^+ in 2mol dm^{-3} HNO_3. It is known to be disproportionate:

$$2NpO_2^+ = Np^{4+} + NpO_2^{2+}.$$

Np^{4+} may be selectively exchanged by SnSbA and TiSbA, as suggested by the results for Pu^{4+}. Hence, a formation of Np^{4+} by the above disproportionation of NpO_2^+ will have contributed to the increase in the Kd value in 2mol dm^{-3} HNO_3.

Kd values for the TRU elements were compared in 1mol dm^{-3} HNO_3 (Table 5-2).

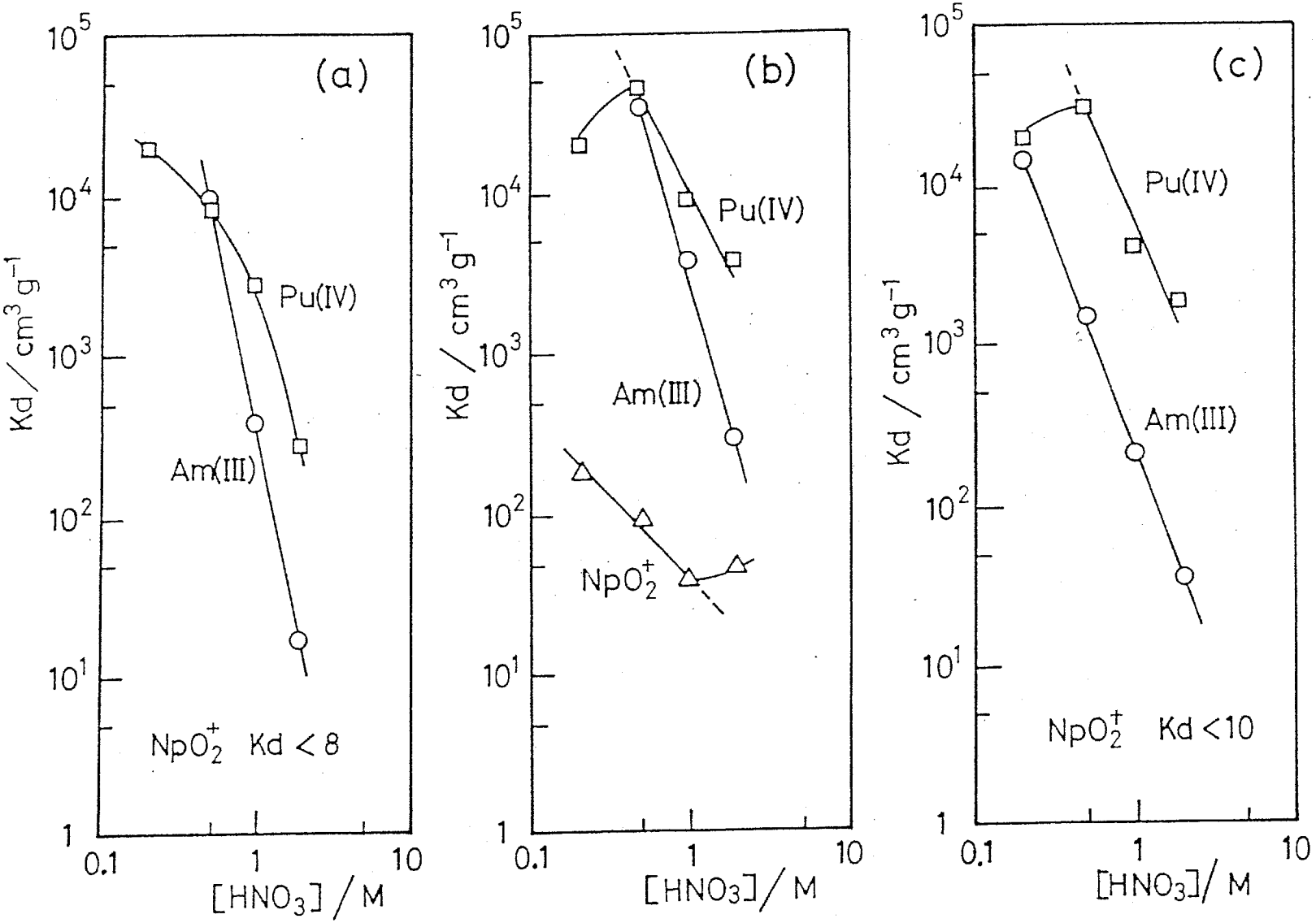

Fig.5-3 Plot of Kd vs. Concentration of HNO_3 in log-log scale for TRU ions on C-SbA(a), SnSbA(b), TiSbA(c), CRYMO(d) and Dowex 50W-X8(e)

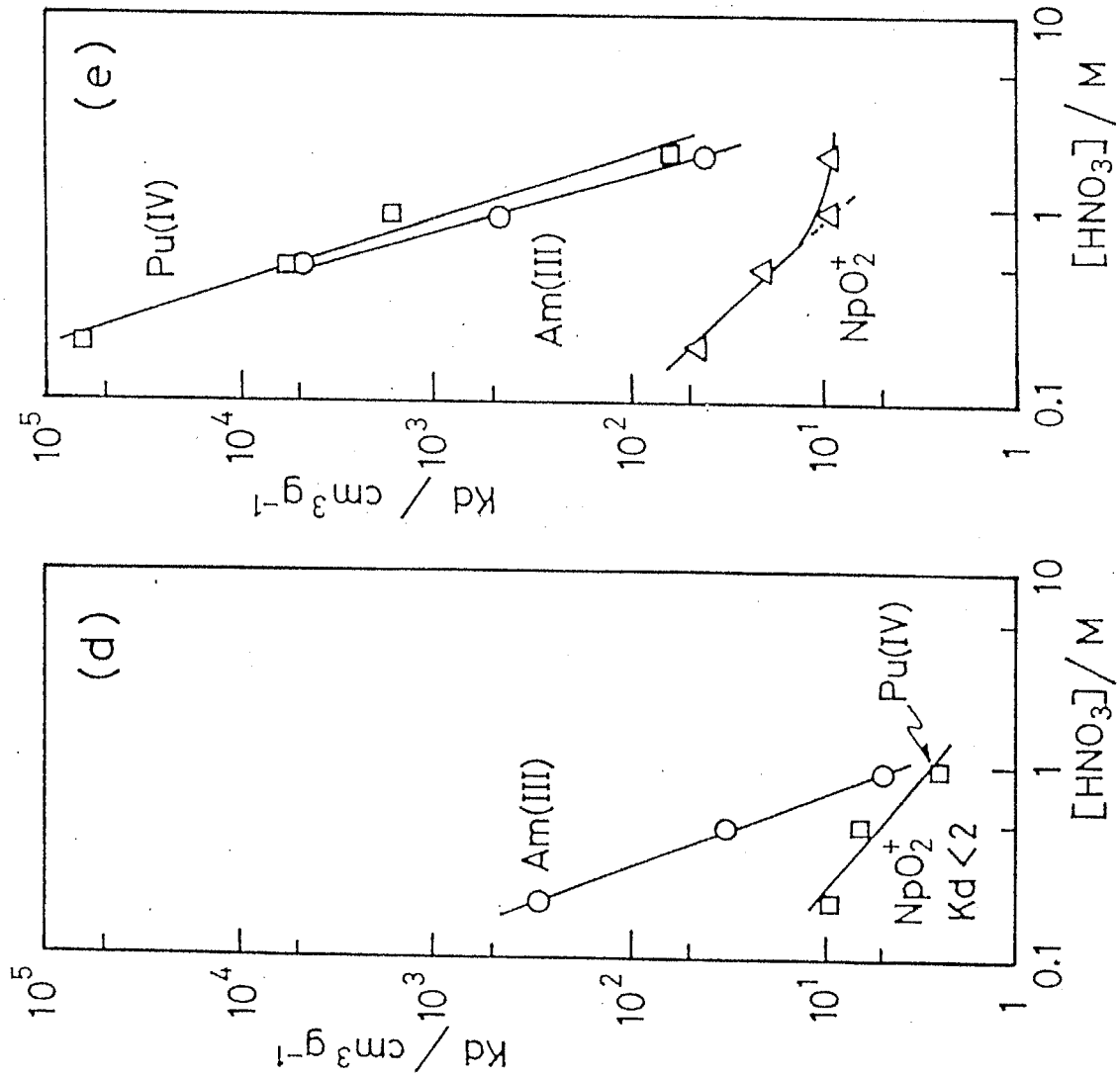
(e)
Pu(IV)
Am(III)
NpO_2^+
Kd / $cm^3 g^{-1}$
10^5
10^4
10^3
10^2
10^1
1
0.1
1
10
$[HNO_3]$ / M
(d)
Am(III)
Pu(IV)
NpO_2^+
Kd < 2
Kd / $cm^3 g^{-1}$
10^5
10^4
10^3
10^2
10^1
1
0.1
1
10
$[HNO_3]$ / M

Table 5-2 Distribution coefficients (Kd) and separation factors (α)* for Pu^{4+}, Am^{3+} and NpO_2^+ in 1M HNO_3 on selected inorganic ion exchangers.

exchanger	parameters	NpO_2^+	Am^{3+}	Pu^{4+}
C-SbA	Kd	< 8	$3.3_0 \times 10^2$	$2.4_0 \times 10^3$
	α	> 41	7.3	
SnSbA	Kd	3.9x10	$3.1_0 \times 10^3$	$1.0_8 \times 10^4$
	α	> 79	3.5	
TiSbA	Kd	< 10	$1.9_2 \times 10^2$	$6.0_0 \times 10^3$
	α	> 19	31	
Dowex50W-X8	Kd	9.3	$3.8_0 \times 10^3$	5.9×10^2
	α	40	1.6	
CSbA**	Kd	2.920x10	2.800×10^3	1.340×10^4
	α	95.8	4.78	
ZrP**	Kd	1.170x10	2.710x10	2.160×10^2
	α	2.31	7.97	
TiP**	Kd	< 1	1.060x10	2.890×10^3
	α	> 10	272	

* defined by the ratio of Kd values for neighboring ion pair
** Ref.10 CSbA: polyanS, ZrP: zirconium phosphate,
TiP: titanium phosphate.

Reference Kd values for other inorganic ion exchangers[10] were included for comparison. The synthetic inorganic ion exchangers showed a larger separation factor and larger Kd values for Pu^{4+} and Am^{3+} than the strongly acidic cation exchanger Dowex 50W-X8. Other reported inorganic ion exchangers, e.g., polyantimonic acid (CSbA), zirconium phosphate (ZrP), and titanium phosphate (TiP), showed large Kd values for Pu^{4+} and Am^{3+} in 1mol dm^{-3} HNO_3, while low Kd values were observed for NpO_2^+. However, the linearity for log-log plot of Kd vs [HNO_3] has not been mentioned,[10] possibly due to its complicated adsorption mechanism.

The Kd value of Am^{3+} on C-SbA was plotted against the effective ionic radius (EIR)[26] to compare the selectivity along with other trivalent cations (Fig.5-4). Kd values for lanthanides and other trivalent cations were determined in the initial concentration of 10-4mol dm^{-3}. A Kd value of Am^{3+} has fallen on the Kd curve of the lanthanide group, possibly due to the similarity of electronic structure ($s^2p^6f^n$ type). Other groups of cations showed a different dependence on the EIR. The concentration dependence of Kd value for Am^{3+} is to be determined for exact comparison of the selectivity.

Kd values extrapolated to 0.1mol dm^{-3} HNO_3 were plotted as a function of EIR for Am^{3+} and some lanthanide ions to allow comparison of the selectivity on SnSbA (Fig.5-5) and TiSbA (Fig.5-6). The log-log plots of Kd for La^{3+} and Yb^{3+} on SnSbA and TiSbA vs. [HNO_3] showed a straight line with a slope of -3, which indicates the ion-exchange process (Fig.5-7). Here Am^{3+} showed larger selectivity than lanthanide ions. The crystal ionic radius of Am^{3+} 0.975 is closer to that of Nd^{3+} 0.983 (Fig.5-8). However, they will not be exchanged as completely dehydrated ions. Then, the hydrated radius was compared between Am^{3+} and lanthanides. The hydrated Am^{3+} radius has been reported to be 4.52 which parallels its lanthanide homolog Eu^{3+}.[27] Kd values as a function of the initial concentration of the exchanging ions or the Kielland plot are needed to allow exact comparison of ion-exchange selectivity between Am^{3+}/H^+ and Ln^{3+}/H^+ exchange systems.

Other factor affecting Kd values is the concentration of exchanging ions. Both ion exchangers showed a concentration dependence (Fig.5-9). It does not allow precise extrapolation to such low concentration for lanthanides ions which was used for Am^{3+}. However, the Kd value of La^{3+} and Nd^{3+} seems lower than that of Am^{3+}. This is to be studied in higher concentration.

The extended selectivity study on the inorganic ion exchangers has been carried out

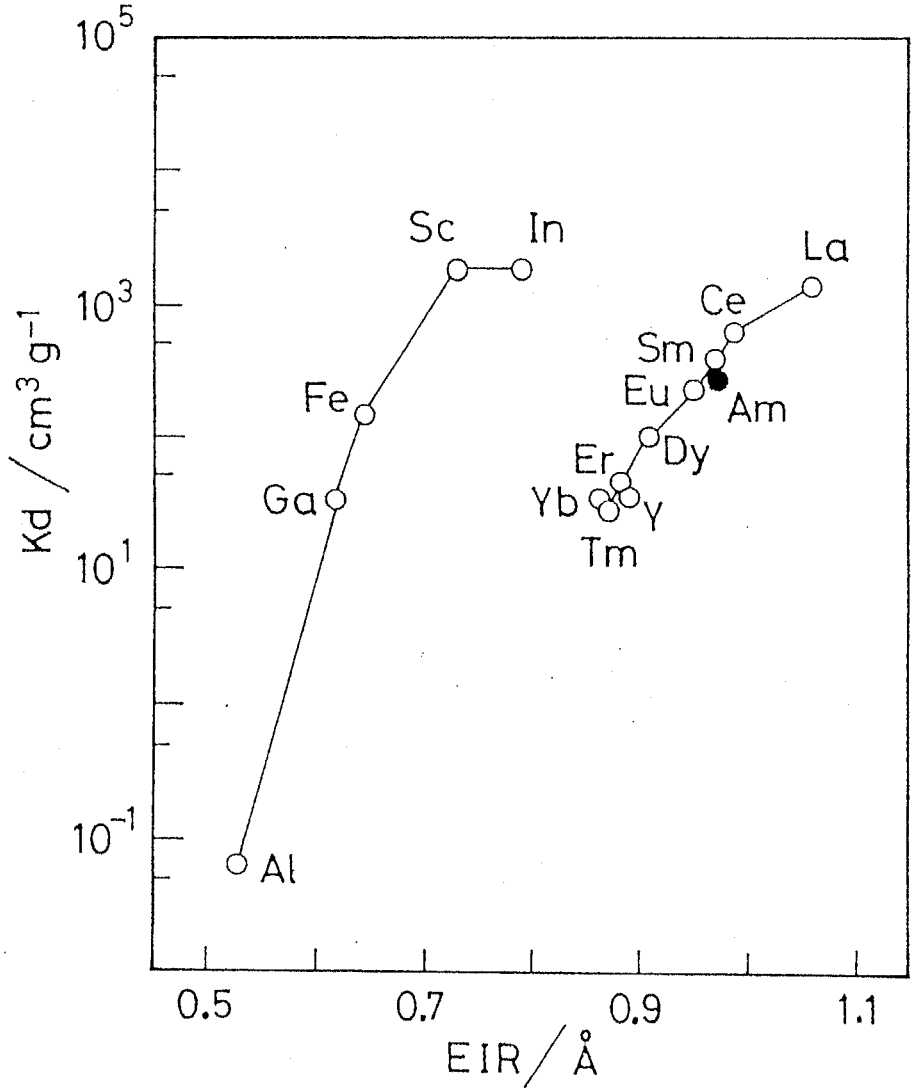

Fig.5-4 Change in Kd of Am^{3+} and trivalent metal ions with effective ionic radius (EIR) on C-SbA in 1M HNO_3

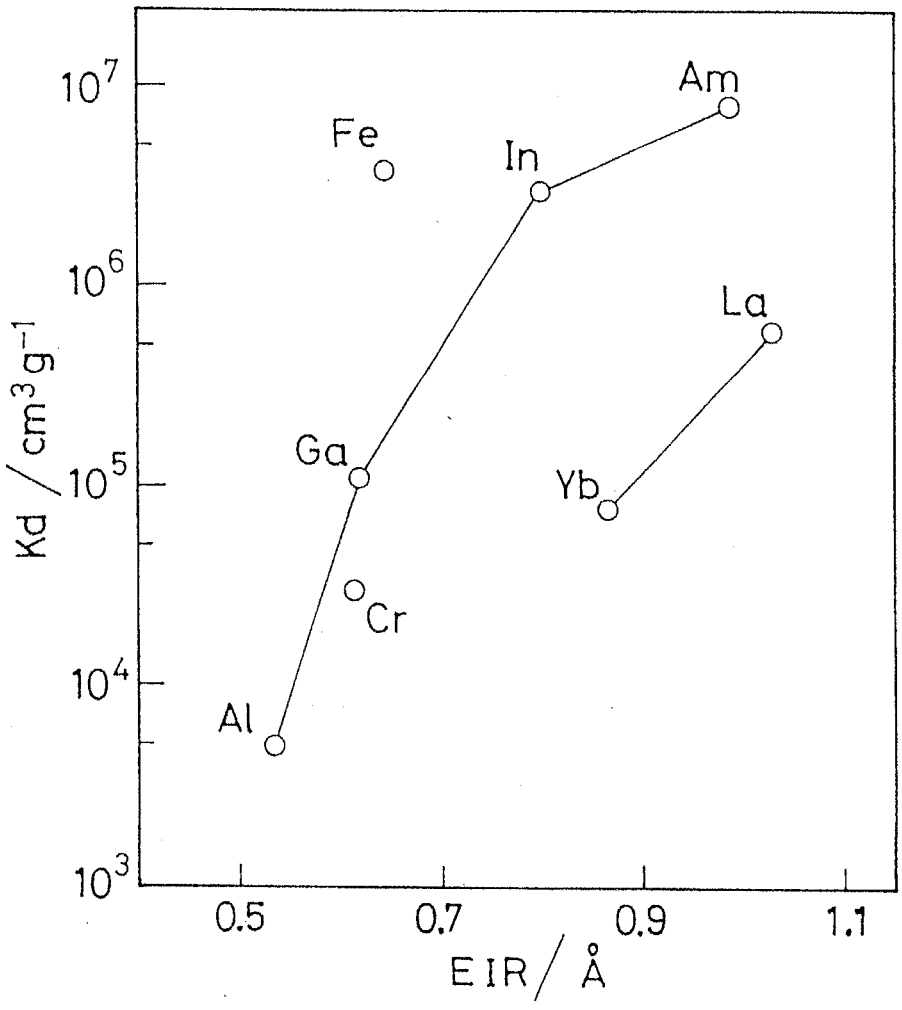

Fig.5-5 Change in Kd of Am^{3+} and trivalent metal ions with effective ionic radius (EIR) on SnSbA in 0.1M HNO_3

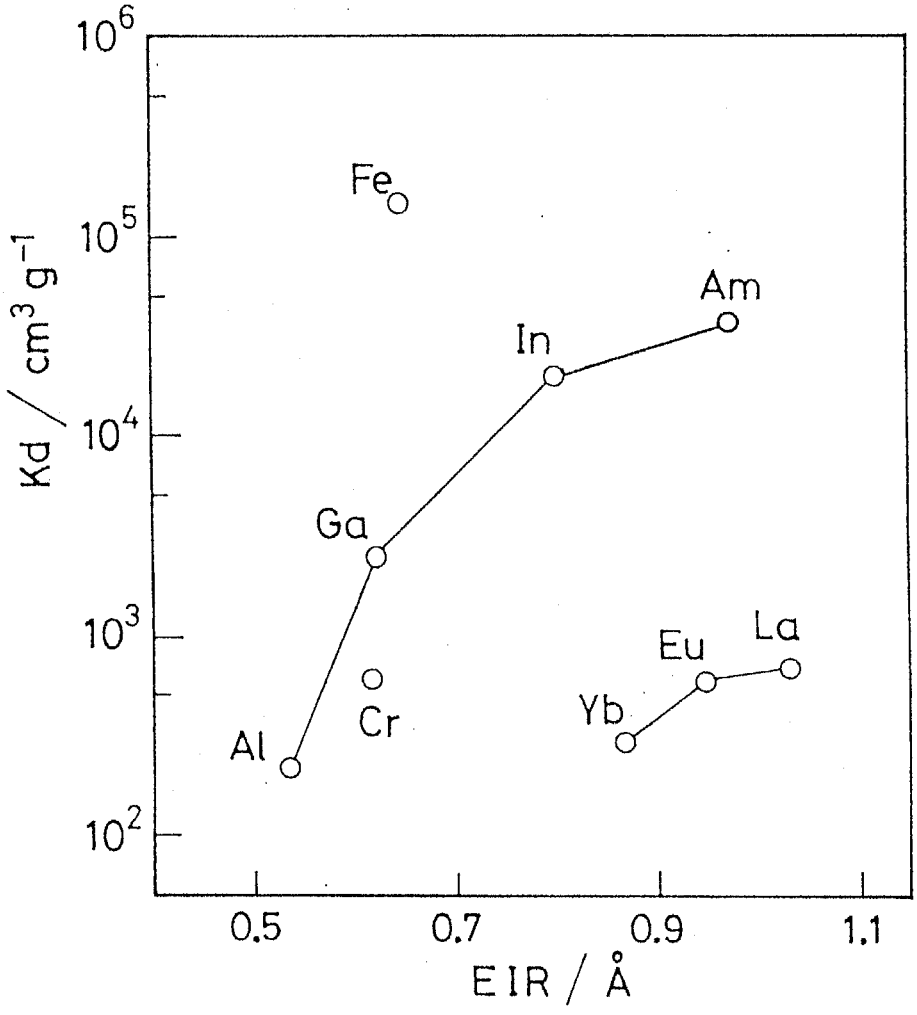

Fig.5-6 Change in Kd of Am^{3+} and trivalent metal ions with effective ionic radius (EIR) on TiSbA in 0.1M HNO_3

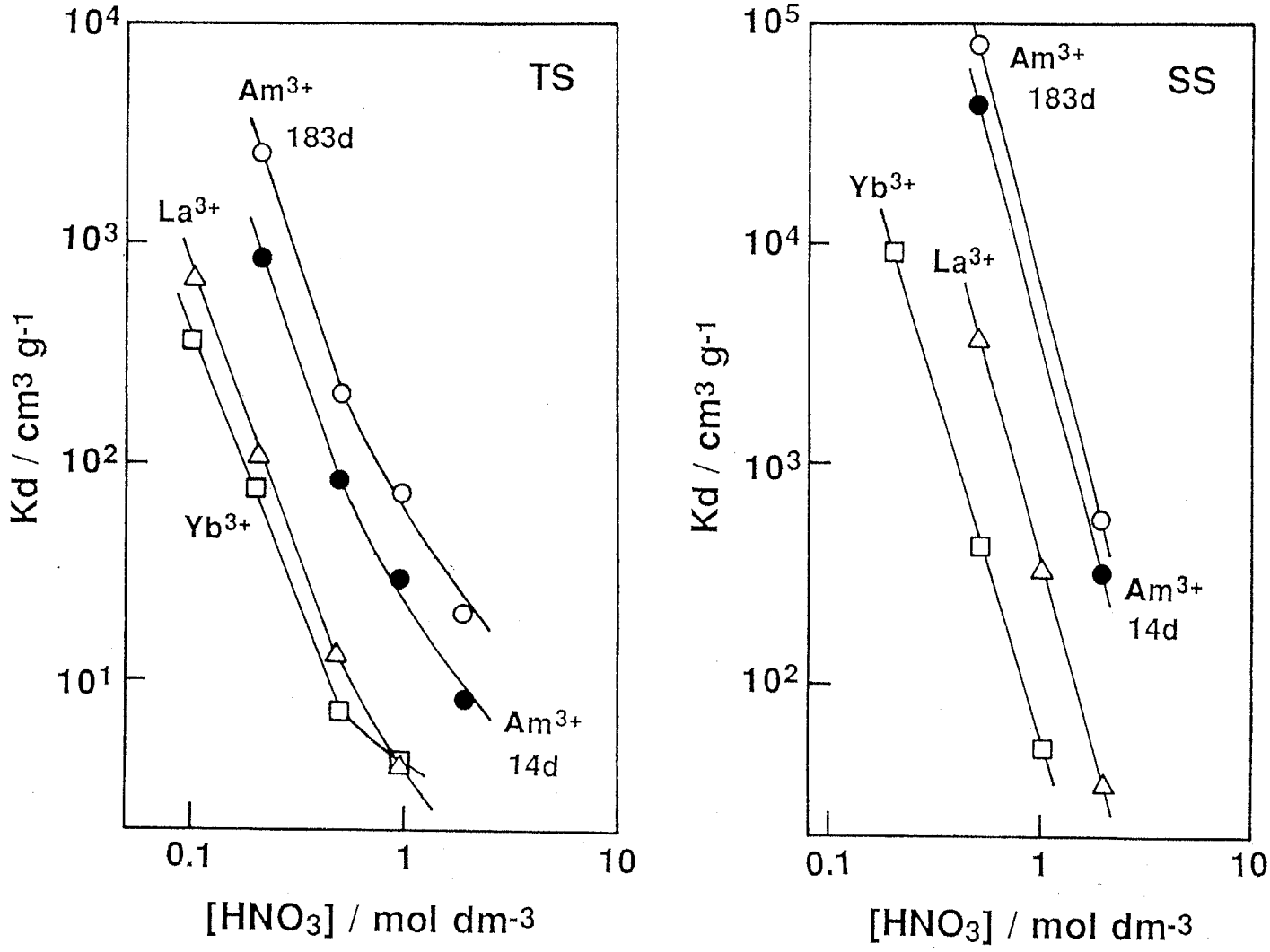

Fig.5-7 Plot of Kd of Am^{3+} and Lanthanide Ions in log-log Scale Numerals show Equilibration Time

Weight of exchanger, 0.10g; Total vol. of soln., $10cm^3$; Initial concn.: 2.1×10^{-9}M for Am^{3+}, 1×10^{-4}M for La^{3+} and Yb^{3+}; Temp., 30°C; □, △, ○, ● forward process on exchanger TS1 or SS, ◑: reverse process on TS1, ■ : reverse process on SS

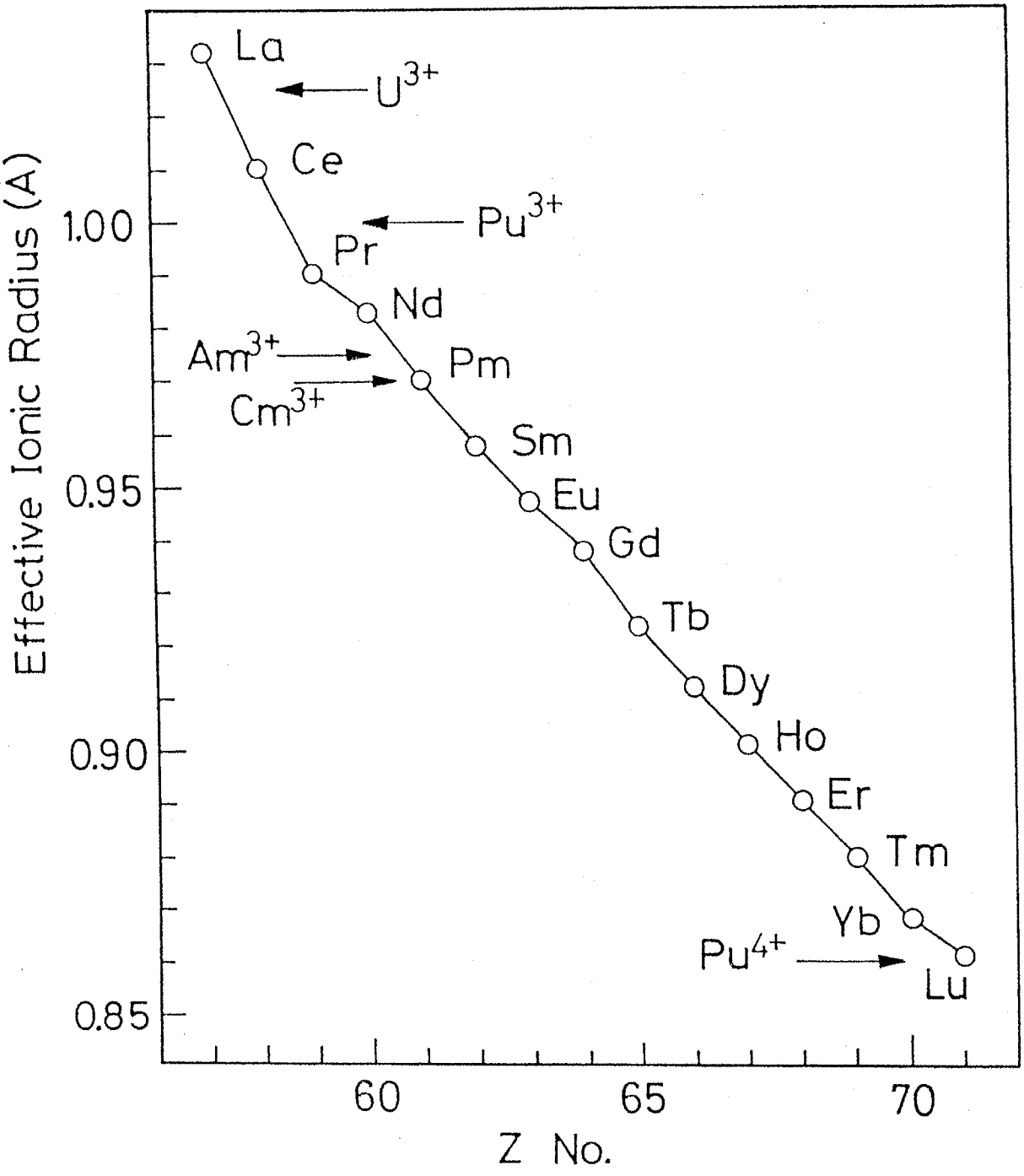

Fig.5-8 Effective Ionic Radius of Trivalent Lanthanides and Relevant TRU Ions as a Function of Atomic Number

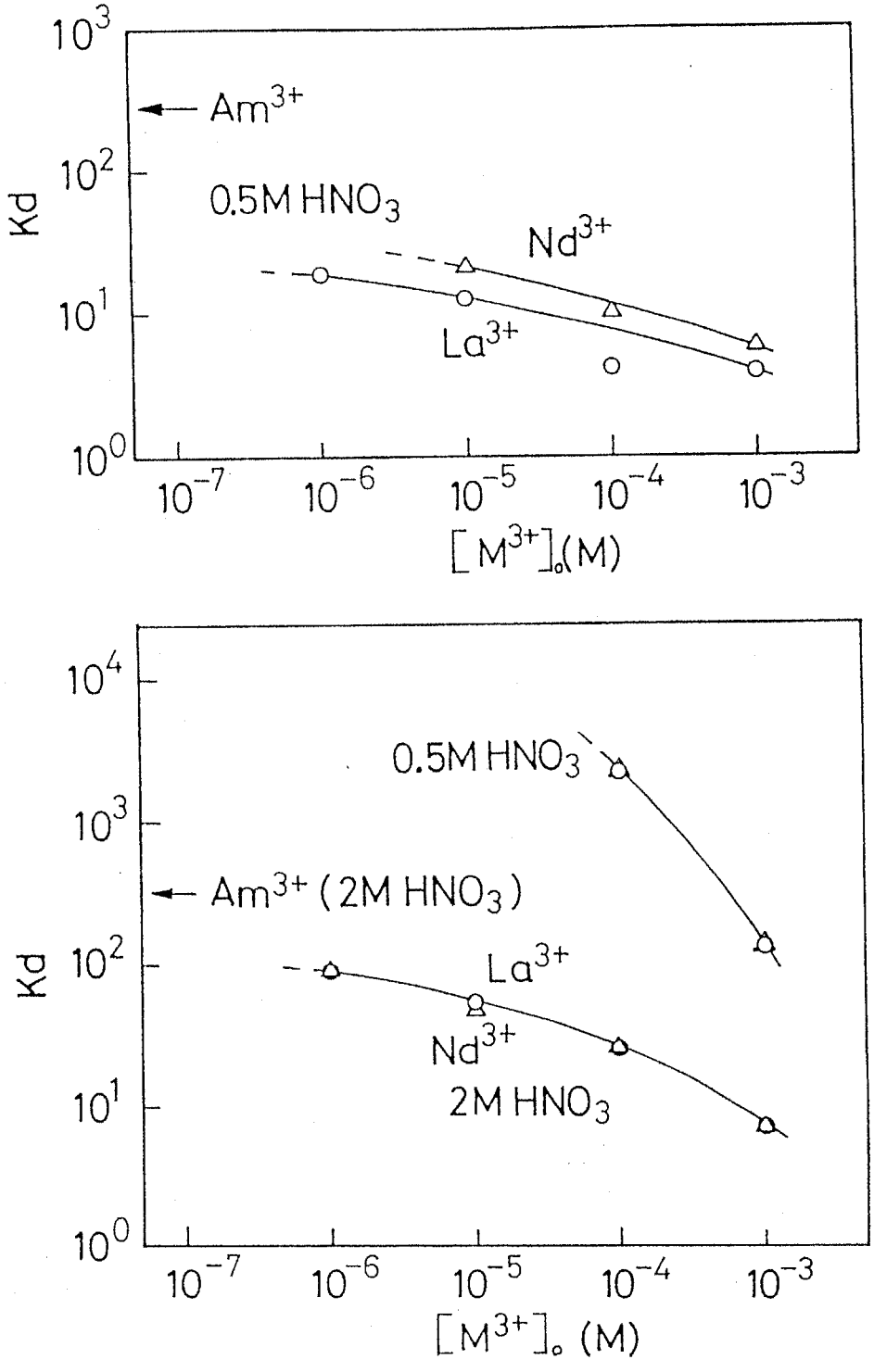

Fig.5-9 Concentration Dependence of Kd for La^{3+} or Nd^{3+} on TS1(top) or SS(bottom)
Weight of exchanger, 0.10g; Total vol. of soln., 10cm^3; Temp., 30°C

in a simulated high level waste containing 0.5mol dm^{-3} and 1.9mol dm^{-3} HNO_3 (Tables 5-3, 4, 5 and 6). Pu^{4+} and Am^{3+} were spiked in the simulated solution A or B at 1.3x10-8 mol dm^{-3} and 2.1x10-9 mol dm^{-3}, respectively, as indicated in Table 5-3. Kd values of Am^{3+} on SnSbA and TiSbA decreased due to strong interfereces by other metal ions especially Na^{+}, Fe^{3+}, Sr^{2+}, and Ba^{2+}, but those of Pu^{4+} still remained large in 0.5mol dm^{-3} HNO_3. The latter values decreased in the simulated solution at 1.9mol dm^{-3} HNO_3.

In conclusion, TiSbA and SnSbA inorganic ion exchangers have been demonstrated to show high selectivity for Pu^{4+} and Am^{3+} and low selectivity for NpO_2^{+} in moderately concentrated HNO_3. They indicated nearly the same adsorption rate as a commercial strongly acidic cation exchange resin. These antimonate cation exchangers will be of potential use for the backend chemistry in the nuclear fuel cycle.

Table 5-3 Concentration of Constituents in Simulated High-level Waste.

Constituent	Concentration / mol dm^{-3} A	B
H^+	0.5	1.9
Na^+	0.057	0.058
Cr^{3+}	0.0069	0.0069
Fe^{3+}	0.029	0.029
Ni^{2+}	0.0045	0.0046
Rb^+	0.0056	0.0056
Sr^{2+}	0.012	0.013
Cs^+	0.028	0.028
Ba^{2+}	0.016	0.016
Ru^{3+}	0.026	0.026
Rh^{3+}	0.0060	0.0061
Pd^{2+}	0.014	0.014
Zr(IV)	---	0.052
Mo(VI)	---	0.052
Te(IV)	---	0.0052
Nd^{3+}	0.096	0.097
Pu^{4+}	1.3×10^{-8}	1.3×10^{-8}
Am^{3+}	2.1×10^{-9}	2.1×10^{-9}

Table 5-4 Kd Values of Pu^{4+} and Am^{3+} in HNO_3 and Simulated Nuclear Waste Solution.

HNO_3 / mol dm^{-3}	DR*	Am			Pu		
		SnSbA	TS1	TS2	SnSbA	TS1	TS2
0.5	0	4.4×10^4	1.3×10^2	1.5×10^2	6.4×10^4	2.7×10^3	1.2×10^3
	0.05	45	5.8	4.3	1.0×10^4	7.0×10^3	1.2×10^4
	0.2	17	6.3	<1	3.1×10^3	2.0×10^3	8.3×10^3
	1.0	16	<1	11	3.5×10^2	1.0×10^3	3.0×10^3
1.9	0	3.4×10^2	8.1	8.9	1.0×10^3	2.3×10^2	1.7×10^2
	0.05	9.2	3.4	<1	33	59	60
	0.2	2.7	<1	<1	<1	9.8	4.3
	1.0	5.2	3.2	4.0	33	19	18

* dilution ratio to the concentration of Table 5-3.

Table 5-5 Kd values for various cations in simulated nuclear waste solution in 0.5M HNO_3.

	SnSbA			TS1			TS2		
DR*	0.05	0.2	1.0	0.05	0.2	1.0	0.05	0.2	1.0
Na	63	4.1	<1	<1	<1	<1	<1	<1	<1
Cr	<1	<1	NA	<1	<1	NA	<1	<1	NA
Fe	200	46	4.7	49	21	2.7	59	26	5.3
Ni	11	4.7	<1	<1	2.0	<1	<1	<1	<1
Rb	4.7	4.8	<1	4.8	5.3	<1	<1	3.8	<1
Sr	290	120	14	<1	1.3	<1	<1	1.1	<1
Cs	13	5.2	<1	36	16	<1	19	9.6	<1
Ba	34	12	<1	22	8.2	<1	8.8	4.1	<1
Ru	7.4	4.9	<1	17	6.2	<1	10	5.0	<1
Rh	<1	NA	NA	<1	NA	NA	<1	NA	NA
Pd	<1	NA	NA	<1	NA	NA	<1	NA	NA
Nd	19	7.2	<1	4.3	2.9	<1	2.5	1.6	<1
Am	45	17	16	5.8	6.3	<1	4.3	<1	11
Pu	10000	3100	350	7000	2000	1000	12000	8300	3000

* dilution ratio to the concentration of Table 5-3.
NA: not analyzed.

Table 5-6 **Kd values for various cations in simulated nuclear waste solution in 1.9M HNO_3.**

	SnSbA			TS1			TS2		
DR*	0.05	0.2	1.0	0.05	0.2	1.0	0.05	0.2	1.0
Na	46	7.6	<1	<1	<1	<1	<1	<1	<1
Cr	2.7	<1	<1	<1	<1	<1	<1	<1	<1
Fe	20	5.7	1.3	<1	<1	<1	<1	<1	<1
Ni	3.3	<1	<1	<1	<1	<1	<1	<1	<1
Rb	5.0	<1	<1	3.3	<1	<1	<1	<1	<1
Sr	17	3.0	<1	<1	<1	<1	<1	<1	<1
Cs	8.6	4.0	<1	12	7.8	<1	7.8	5.0	<1
Ba	7.6	3.2	<1	3.8	<1	<1	<1	<1	<1
Ru	<1	NA	NA	<1	NA	NA	<1	NA	NA
Rh	<1	NA	NA	<1	NA	NA	<1	NA	NA
Pd	<1	NA	NA	<1	NA	NA	<1	NA	NA
Zr	360	2.4	7.2	400	51	7.0	460	53	5.0
Mo	570	75	38	240	53	9.5	740	92	13
Te	56	<1	<1	2.7	2.0	<1	6.4	4.4	<1
Nd	<1	NA	NA	<1	NA	NA	<1	NA	NA
Am	9.2	2.7	5.2	3.4	<1	3.2	<1	<1	4.0
Pu	33	<1	33	59	9.8	19	60	4.3	18

* dilution ratio to the concentration of Table 5-3.
NA: not analyzed.

4. REFERENCES

1. T. Tamura, Proc. Intl. Clay Conf., *1,* 425 (1966); idem, Nucl. Safety, *5,* 262, 267 (1968).
2. E. D. Collins, D. O. Campbell, L. J. King and J. B. Knauer, IAEA-TECDOC-337, 1985, p.43.
3. H. Mimura and T. Kanno, J. Nucl. Sci. Technol., *22,* 234 (1985); idem, IAEA-TECHDOC-337, 1985, p.237.
4. H. Mimura, F. Tachibana and K. Akiba, Proc. 3rd Int. Conf. Nucl. Fuel Reprocessing Waste Management (RECOD '91), April 14-18, 1991, Sendai, Japan, Vol. 1.
5. S. Komarneni and R. Roy, Science, *239,* 1286 (1988).
6. S. Ahrland, I. Grenthe and B. Noren, Acta Chem. Scand., *14,* 1059, 1077 (1960).
7. E. P. Horwitz, D. G. Kalina, H. Diamond, G. F. Vandegrift and W. W. Schultz, Solvent Extr. Ion Exch., *3,* 75 (1985).
8. M. Kubota, S. Dojiri, I. Yamaguchi, Y. Morita, I. Yamagishi, T. Kobayashi and S. Tani, Proc. 1989 Joint Int. Waste Management Conf., Vol.2, p.537 (1989).
9. T. Inoue, M. Sakata, H. Miyashiro, T. Matsumura, A. Sasahara and N. Yoshiki, Nucl. Technol., *93,* 206 (1991).
10. E. W. Hooper, IAEA-TECHDOC-337, 1985.
11. IAEA, Technical Report Series No.214 (STI-DOC-10-214) (1982).
12. G. Persson, S. Wingefors, J. O. Liljenzin and I. Svantesson, Radiochim. Acta, *35,* 163 (1984).
13. Y. Morita, S. Tani and M. Kubota, Proc. 3rd Int. Conf. Nucl. Fuel Reprocessing Waste Management (RECOD '91), April 14-18, 1991, Sendai, Japan, Vol.1, p.348.
14. V. Veselý and V. Pekárek, Talanta, *19,* 219 (1972).
15. V. Pekárek, and V. Veselý, Talanta, *19,* 1245 (1972).
16. M. Abe, Bunseki Kagaku, *23,* 1254, 1561 (1974).
17. M. Abe and K. Sudoh, J. Inorg. Nucl. Chem., *43,* 2537 (1981).
18. M. Abe and T. Ito, Chem. Soc. Jpn., *41,* 333 (1968).
19. M. Abe and K. Hayashi, Solvent Extr. Ion Exch., *1,* 97 (1983).
20. M. Tsuji and M. Abe, Solvent Extr. Ion Exch., *2,* 253 (1984).
21. Y. Morita and M. Kubota, Solvent Extr. Ion Exch., *8,* 529 (1990).
22. M. Abe and M. Tsuji, Chem. Lett., 1561 (1983).

23. M. Abe, R. Chitrakar, M. Tsuji and K. Fukumoto, Solvent Extr. Ion Exch., *3,* 149 (1985).
24. M. Abe, M. Hirata and M. Tsuji, Bull. Chem. Soc. Jpn., *62,* 3801 (1989).
25. L. M. Toth, J. T. Bell and H. A. Friedman, Radiochim. Acta, *49,* 193 (1990).
26. R. D. Shannon and C. T. Prewitt, Acta Crystallogr., Sect.B *25,* 925 (1969).
27. J. J. Katz, G. T. Seaborg and L. R. Morss, The Chemistry of the Actinides Elements, 2nd ed., Chapman and Hall, New York 1986, p.912.

[List of Publications]

1. H. Kaneko, M. Tsuji, M. Abe, Y. Morita and M. Kubota,
   "Selective exchange of Pu^{4+} and Am^{3+} by titanium and tin antimonates cation exchangers", J. Nucl. Sci. Technol., *29,* 988 (1992).
2. H. Kaneko, M. Abe, M. Tsuji and Y. Tamaura,
   "Ion-exchange selectivity and chromatographic separation of trivalent metals on titanium antimonate", Chromatographia, in press.
3. M. Tsuji, H. Kaneko, M. Abe, Y. Morita and M. Kubota,
   "Synthetic inorganic ion exchangers showing high selectivity towards 5f elements", Radiochim. Acta, in press.
4. M. Tsuji, H. Kaneko and Y. Tamaura,
   "Predictive evaluation of ion-exchange selectivity on titanium antimonate cation exchanger", J. Chem. Soc. Faraday Trans., in press.
5. H. Kaneko, M. Tsuji and Y. Tamaura,
   "Thermodynamic study of M^{3+}/H^{+} exchange systems on titanium antimonate cation exchanger", Solvent Extr. Ion Exch., in press.

[List of Presentations]

1. アンチモン酸チタン陽イオン交換体による Al-Ga および Al-In の分離
   阿部、金子、辻　第３６回日本分析化学会年会　(1987)　熊本
2. アンチモン酸チタン陽イオン交換体の組成と Al-Ga および Al-In の分離能
   金子、阿部　第４回日本イオン交換研究発表会　(1988)　東京
3. アンチモン酸チタンにおける３価金属イオン交換反応の熱力学的考察
   金子、阿部、玉浦　第６４回日本化学会秋季年会　(1992)　新潟
4. 組成の異なるアンチモン酸チタンにおける M^{3+}/H^{+} イオン交換反応の熱力学的考察
   金子、阿部、辻、玉浦　第８回日本イオン交換研究発表会　(1992)　大阪

ACKNOWLEDGEMENT

The author offers his deep sense of gratitude from the cordial quintessence to Professor Yutaka Tamaura, Department of Chemistry, Research Center for Carbon Recycling & Utilization, Tokyo Institute of Technology, and Professor Mitsuo Abe (Emeritus Professor, Tokyo Institute of Technology), for their consistent guidance, supervision and discussion throughout the course of this study and help at different sectors during the stay in their laboratory. His sincere thanks to Dr. M. Tsuji for his immense help for various experiments, an encouraging attitude and the constructive criticism throughout this study. His sincere thanks to Prof. Y. Kanzaki, Showa College of Pharmaceutical Science, for his immense help for various experiments and an encouraging attitude throughout this study. His gratitudes are also to all other members of Abe-Laboratory, Tamaura-Laboratory and Center of Environmental Preservation for their cooperation and friendly behavior, especially to Mr. T. Yoshida, Mr. H. Watanabe, and Mrs. N. Hasegawa for their help. Taking this dissertation as an opportunity to thank many who had been kind enough to let me use their laboratory facilities or to spare their valuable time to contribute to my needs. Among these are, Prof. T. Yashima, Prof. M. Yoshida, Prof. M. Oguni, Prof. J. Hirabayashi, and Prof. K. Kitayama in Department of Chemistry, Prof. I. Ando in Department of High Polymer Engineering, Prof. K. Domen and J. Yoshimura in Research Laboratory of Resources Utilization, Dr. K. Asakura in Department of Chemistry, the University of Tokyo, Dr. M. Nomura and Dr. A. Koyama in Photon Factory, KEK.

March, 1993